ENCLOSURE 5

TENNESSEE VALLEY AUTHORITY
BROWNS FERRY NUCLEAR PLANT (BFN)
UNIT 1

TECHNICAL SPECIFICATIONS (TS) CHANGE TS-431
EXTENDED POWER UPRATE (EPU)

CDI REPORT NO. 09-25NP, "STRESS ASSESSMENT OF BROWNS FERRY NUCLEAR UNIT 1 STEAM DRYER TO 120% OLTP POWER LEVEL," REVISION 0

(NON-PROPRIETARY VERSION)

Attached is the non-proprietary version of CDI Report No. 09-25NP, "Stress Assessment of Browns Ferry Nuclear Unit 1 Steam Dryer to 120% OLTP Power Level."

This Document Does Not Contain Continuum Dynamics, Inc. Proprietary Information

CDI Report No. 09-25NP

Stress Assessment of Browns Ferry Nuclear Unit 1 Steam Dryer to 120% OLTP Power Level

Revision 0

Prepared by

Continuum Dynamics, Inc.
34 Lexington Avenue
Ewing, NJ 08618

Prepared under Purchase Order No. 00053157 for

TVA / Browns Ferry Nuclear Plant
Nuclear Plant Road, P. O. Box 2000 PAB-2M
Decatur, AL 35609

Approved by

Alan J. Bilanin

Reviewed by

Milton E. Teske

August 2009

This report complies with Continuum Dynamics, Inc. Nuclear Quality Assurance Program currently in effect.

Executive Summary

The finite element model and analysis methodology, used to assess stresses induced by the flow of steam through the steam dryer at Brown Ferry Nuclear Unit 1 (BFN1), are described and applied to obtain stresses at 120% Originally Licensed Thermal Power (OLTP) conditions also referred to here as the Extended Power Uprate (EPU) condition. The resulting stresses are assessed for compliance with the ASME B&PV Code, Section III, subsection NG, for the load combination corresponding to normal operation (the Level A Service Condition). The results presented herein pertain to the BFN1 steam dryer configuration with scheduled modifications that will be incorporated to improve stress margins prior to EPU operation. These modifications are described in Section 3.

The analysis is carried out in the frequency domain, which confers a number of useful computational advantages over a time-accurate transient analysis including the ability to assess the effects of frequency scalings in the loads without the need for additional finite element calculations. [[

[3]]] The analysis develops a series of unit stress solutions corresponding to the application of a unit pressure at a MSL at specified frequency, f. Each unit solution is obtained by first calculating the associated acoustic pressure field using a separate analysis that solves the damped Helmholtz equation within the steam dryer [1]. This pressure field is then applied to a finite element structural model of the steam dryer and the harmonic stress response at frequency, f, is calculated using the commercial ANSYS 10.0 finite element analysis software. This stress response constitutes the unit solution and is stored as a file for subsequent processing. Once all unit solutions have been computed, the stress response for any combination of MSL pressure spectrums (obtained by Fast Fourier Transform of the pressure histories in the MSLs) is determined by a simple matrix multiplication of these spectrums with the unit solutions.

The loads used to calculate the stresses account for all the end-to-end biases and uncertainties in the loads model [2] and finite element analysis. In addition, no low power-based noise filtering has been performed for the analyses contained herein. Results obtained from application of the methodology to the BFN1 steam dryer show that at nominal EPU operation (no frequency shifts) the minimum alternating stress ratio (SR-a) anywhere on the steam dryer, excluding secondary structural members, is SR-a=2.18. Moreover, to account for uncertainties in the modal frequency predictions of the finite element model, the stresses are also computed for loads that are shifted in the frequency domain by ±2.5%, ±5%, ±7.5% and ±10%. The minimum alternating stress ratio encountered at any frequency shift is found to be SR-a=2.03 occurring at the -2.5% shift. The stress ratio due to maximum stresses (SR-P) is SR-P=1.40 without frequency shifts and SR-P=1.27 when frequency shifts are considered.

These results exclude stresses associated with secondary structural members. When all structural parts are considered, including secondary structural members that are not needed for maintaining structural integrity, additional high stress locations emerge. All of these locations involve the T-bar originally required for transportation and assembly of the dryer. A separate analysis has been conducted to determine the stress condition and position retention capability of

the structure if the highest stressed nodes are removed from the model to simulate a conservatively postulated, localized failed condition. This analysis shows that limiting alternating stress ratio on the T-bar welds becomes SR-a=2.14 at EPU.

Given that the alternating stress ratio SR-a obtained using any of two EPU predictive stress methods remains above 2.03 at all frequency shifts together with the comparatively small dependence of SR-P upon acoustic loads, the current Unit 1 dryer qualifies for operation at EPU conditions with regard to stress evaluation.

Table of Contents

1. Introduction and Purpose

Plans to qualify the Browns Ferry nuclear plant for operation at 120% Original Licensed Thermal Power (OLTP) or Extended Power Uprate (EPU) operating condition require an assessment of the steam dryer stresses experienced under the increased loads. The steam dryer loads due to pressure fluctuations in the main steam lines (MSLs) are potentially damaging and the cyclic stresses from these loads can produce fatigue cracking if loads are sufficiently high. The industry has addressed this problem with physical modifications to the dryers, as well as a program to define steam dryer loads and their resulting stresses. The purpose of the stress analysis discussed here is to calculate the maximum and alternating stresses generated during EPU and determine the margins that exist when compared to stresses that comply with the ASME Code (ASME B&PV Code, Section III, subsection NG).

The stress analysis considered here pertains to the Browns Ferry Unit 1 (BFN1) steam dryer modified from its current configuration (at the time of submission of this report) to support EPU operation. As such, it incorporates scheduled design changes introduced to improve stress ratios at EPU including:

(i) addition of a half-pipe reinforcement on each steam dam to suppress vibration and reduce stresses;
(ii) removal of the old tie bar/lock gussets previously left in place to reinforce the steam dam with new gussets;
(iii) thinning of a section of the inner hood panel to alleviate local stresses;
(iv) addition of reinforcement plates on the outer vane bank end plates and also underneath the tie bars connecting the middle and outer vane banks where they land on the middle hoods;
(v) addition of stress relief holes at the bottom of drain channels and hood stiffeners to alleviate local weld stresses;
(vi) extension of the interior skirt/channel welds;
(vii) reinforcement of the outer gusset/steam dam weld; and
(viii) reinforcement of the top corner of the outer closure plate/middle hood junction. These are described further in Section 3.1. The scheduled final design of the steam dryer for EPU operation is analyzed herein.
(ix) reinforcement of the T-beam stitch weld at selected locations.

The stress analysis of the modified BFN1 steam dryer establishes whether the existing and planned modifications are adequate for sustaining structural integrity and preventing future weld cracking under planned EPU operating conditions. The load combination considered here corresponds to normal operation (the Level A Service Condition) and includes fluctuating pressure loads developed from BFN1 main steam line data, and weight. Level B service conditions, which include seismic loads, are not included in this evaluation. The fluctuating pressure loads, induced by the flowing steam, are predicted by processing main steam line (MSL) pipe strain gage measurements using a separate acoustic circuit analysis of the steam dome and main steam lines [4]. It is known that the MSL strain gage measurements also contain non-acoustic contributions, collectively referred to as 'plant noise' (e.g., pipe vibrations, operating machinery and measurement noise) which physically do not contribute to dryer

acoustic loads. In previous analyses [5] it was attempted to subtract this non-acoustic noise using low power measurements. To meet schedule however, no low power noise subtraction has been performed in the present analysis.

[[

(3)]] This approach also affords a number of additional computational advantages over transient simulations including: [[

(3)]] This last advantage is realized through the use of "unit" solutions representing the stress distribution resulting from the application of a unit fluctuating pressure at one of the MSLs at a particular frequency. [[(3)]]

This report describes the overall methodology used to obtain the unit solutions in the frequency domain and how to assemble them into a stress response for a given combination of pressure signals in the MSLs. This is followed by details of the BFN1 steam dryer finite element model including the elements used and overall resolution, treatment of connections between elements, the hydrodynamic model, the implementation of structural damping and key idealizations/assumptions inherent to the model. Post-processing procedures are also reviewed including the computation of maximum and alternating stress intensities, identification of high stress locations, adjustments to stress intensities at welds, and evaluation of stress ratios used to establish compliance with the ASME Code. The results in terms of stress intensity distributions and stress ratios are presented next, together with PSDs of the dominant stress components.

2. Methodology

2.1 Overview

Based on previous analysis undertaken at Quad Cities Units 1 and 2, the steam dryer can experience strong acoustic loads due to the fluctuating pressures in the MSLs connected to the steam dome containing the dryer. C.D.I. has developed an acoustic circuit model (ACM) that, given a collection of strain gage measurements [6] of the fluctuating pressures in the MSLs, predicts the acoustic pressure field anywhere inside the steam dome and on the steam dryer [1, 2, 4]. The ACM is formulated in frequency space and contains two major components that are directly relevant to the ensuing stress analysis of concern here. [[

[3]]]

[[

[3]]]

[[

[3]]

2.2 [[[3]]

[[

[3]]

[[

[3]]]

2.3 Computational Considerations

Focusing on the structural computational aspects of the overall approach, there are a number of numerical and computational considerations requiring attention. The first concerns the transfer of the acoustic forces onto the structure, particularly the spatial and frequency resolutions. The ANSYS finite element program inputs general distributed pressure differences using a table format. This consists of regular 3D rectangular (i.e., block) $n_x \times n_y \times n_z$ mesh where n_α is the number of mesh points in the i-th Cartesian direction and the pressure difference is provided at each mesh point (see Section 3.10). These tables are generated separately using a program that reads the loads provided from the ACM software, distributes these loads onto the finite element mesh using a combination of interpolation procedures on the surface and simple diffusion schemes off the surface (off-surface loads are required by ANSYS to ensure proper interpolation of forces), and written to ASCII files for input to ANSYS. A separate load file is written at each frequency for the real and imaginary component of the complex force.

The acoustic field is stored at 5 Hz intervals from 0 to 250 Hz. While a 5 Hz resolution is sufficient to capture frequency dependence of the acoustic field (i.e., the pressure at a point varies gradually with frequency), it is too coarse for representing the structural response especially at low frequencies. For 1% critical structural damping, one can show that the frequency spacing needed to resolve a damped resonant peak at natural frequency, f_n, to within 5% accuracy is $\Delta f = 0.0064 \times f_n$. Thus for f_n=10 Hz where the lowest structural response modes occur, a frequency interval of 0.064 Hz or less is required. In our calculations we require that 5% maximum error be maintained over the range from f_n=5 Hz to 250 Hz resulting in a finest frequency interval of 0.0321 Hz at the low frequency end (this adequately resolves all structural modes up to 250 Hz). Since there are no structural modes between 0 to 5 Hz, a 0.5 Hz spacing is used over this range with minimal (less than 5%) error. The unit load, $\hat{\mathbf{f}}_n(\omega, \mathbf{R})$, at any frequency, ω_k, is obtained by linear interpolation of the acoustic solutions at the two nearest frequencies, ω_i and ω_{i+1}, spaced 5 Hz apart. Linear interpolation is sufficient since the pressure load varies slowly over the 5 Hz range (linear interpolation of the structural response would not be acceptable over this range since it varies much more rapidly over the same interval).

Solution Management

[[

[3]]]

[[

[3]]]

Structural Damping

In harmonic analysis one has a broader selection of damping models than in transient simulations. A damping factor, z, of 1% critical damping is used in the structural analysis. In transient simulations, this damping can only be enforced exactly at two frequencies (where the damping model is "pinned"). Between these two frequencies the damping factor can by considerably smaller, for example 0.5% or less depending on the pinning frequencies. Outside the pinning frequencies, damping is higher. With harmonic analysis it is straightforward to enforce very close to 1% damping over the entire frequency range. In this damping model, the damping matrix, **D**, is set to

$$\mathbf{D} = \frac{2z}{\omega}\mathbf{K} \tag{7}$$

where **K** is the stiffness matrix and ω the forcing frequency. One can show that with this model the damping factor varies between 0.995% and 1.005% which is a much smaller variation than using the pinned model required in transient simulation.

Load Frequency Rescaling

One way to evaluate the sensitivity of the stress results to approximations in the structural modeling and applied loads is to rescale the frequency content of the applied loads. In this procedure the nominal frequencies, ω_k, are shifted to $(1+\lambda)\omega_k$, where the frequency shift, λ, ranges between $\pm 10\%$, and the response recomputed for the shifted loads. The objective of the frequency shifting can be explained by way of example. Suppose that in the actual dryer a strong structural-acoustic coupling exists at a particular frequency, ω^*. This means that the following conditions hold simultaneously: (i) the acoustic signal contains a significant signal at ω^*; (ii) the structural model contains a resonant mode of natural frequency, ω_n, that is near ω^*; and (iii) the associated structural mode shape is strongly coupled to the acoustic load (i.e., integrating the product of the mode shape and the surface pressure over the steam dryer surface produces a significant modal force). Suppose now that because of discretization errors and modeling idealizations that the predicted resonance frequency differs from ω^* by a small amount (e.g., 1.5%). Then condition (ii) will be violated and the response amplitude therefore significantly

diminished. By shifting the load frequencies one re-establishes condition (ii) when $(1+\lambda)\omega^*$ is near ω_n. The other two requirements also hold and a strong structural acoustic interaction is restored.

[[

(3)]]

Evaluation of Maximum and Alternating Stress Intensities

Once the unit solutions have been obtained, the most intensive computational steps in the generation of stress intensities are: (i) the FFTs to evaluate stress time histories from (5); and (ii) the calculation of alternating stress intensities. [[

(3)]]

The high computational penalty incurred in calculating the alternating stress intensities is due to the fact that this calculation involves comparing the stress tensors at every pair of points in the stress history. This comparison is necessary since in general the principal stress directions can vary during the response, thus for N samples in the stress history, there will be (N-1)N/2 such pairs or, for N=64K (the number required to accurately resolve the spectrum up to 250 Hz in 0.01 Hz intervals), 2.1×10^9 calculations per node each requiring the determination of the roots to a cubic polynomial. [[

(3)]]

3. Finite Element Model Description

A description of the ANSYS model of the Browns Ferry Unit 1 steam dryer follows.

3.1 Steam Dryer Geometry

A geometric representation of the Browns Ferry steam dryer was developed from available drawings (provided by TVA and included in the design record file, DRF-TVA-250B) within the Workbench module of ANSYS. The completed model is shown in Figure 1. This model includes the following modifications made to the Browns Ferry Unit 1 steam dryer on-site and additional modifications for EPU operation. These are as follows:

On-Site Modifications for Existing Dryer

(i) The 0.5 inch thick old outer hoods were cut away and replaced with 1 inch thick outer hoods.

(ii) Channel-shaped hood assemblies composed of 1 inch thick plates were added to the outer hoods.

(iii) The vertical hood supports located underneath the hood were cut away following the replacement with the thicker outer hood and exterior hood reinforcement assemblies.

(iv) The top tie rods were replaced with thicker new ones. The gussets on the top of the outer hoods supporting the steam dam plate were cut away to facilitate installation of the new tie bars and possibly alleviate local stresses.

(v) The cover plates were replaced by new ones that are 1 in thick.

(vi) The outermost sections (the parts between the upper support ring and outer vane bank) of the supporting beam spanning the dryer were removed.

(vii) Remove the thicker tie bars connecting to the inner hoods (i.e., those connecting the inner to inner hoods and those connecting the inner to middle hoods) and replace them with ones having tapered and flared ends to more evenly distribute loads at the end connections.

(viii) Similarly, replace the thicker tie bars connecting to the outer hoods with the modified ones having flared and tapered ends. However, rather than completely removing the existing tie bars, part of it is retained to support the lock gusset and restrain motion of the steam dam. The portion extending between the steam dam to the middle hood is removed.

(ix) Add three additional gussets to support each of the two steam dams.

Analysis of the existing dryer at EPU conditions without filtering using low power data showed significant stresses at additional locations that would result in alternating stress ratios at EPU below the target level of 2.0. Therefore, additional design modifications have been made to reduce these stresses to target levels. These modifications which will be implemented prior to EPU operation are as follows:

Additional Modifications for EPU Operation

(x) Add a half-pipe stiffener to the steam dam to suppress vibrations and associated stresses.

(xi) Thin a portion of the inclined section on the outer most panels of the inner hoods lying outside the closure plates by 0.1".

(xii) Replace the old tie bars/lock gussets previously left in place to support the steam dam by the same gussets used elsewhere on the steam dam.

(xiii) Create stress relief cutouts at the bottoms of the drain channels and hood stiffeners near the associated attachment welds to reduce localized stresses.

(xiv) Extend each interior drain channel/skirt weld by 2" (8 locations) for a total interior weld length of 3".

(xv) Thicken the previously undersized weld connecting the steam dam to the end gussets thus ensuring proper weld size and obviating the need for an undersize weld factor.

(xvi) Add a reinforcement strip on the end of the outer hood vane bank in the vicinity of the interior vertical vane bank plate.

(xvii) Add reinforcement plates on the middle hoods immediately underneath the tie bars connecting to the outer vane banks.

(xviii) Reinforce the top corner of the outer closure plate where it meets the middle hood.

(xix) Reinforcement of the T-beam/base plate stitch weld in the ranges: $21" < |x| < 24"$, $39.75" < |x| < 45"$ and $.70.75" < |x| < 86"$.

(xx) Addition of a reinforcement strip on the top cover plate where it meets the vertical outer hood.

All of these modifications are incorporated into the BFN1 steam dryer model used to generate the results presented in this report. The modified areas are shown in Figure 2 and Figure 3.

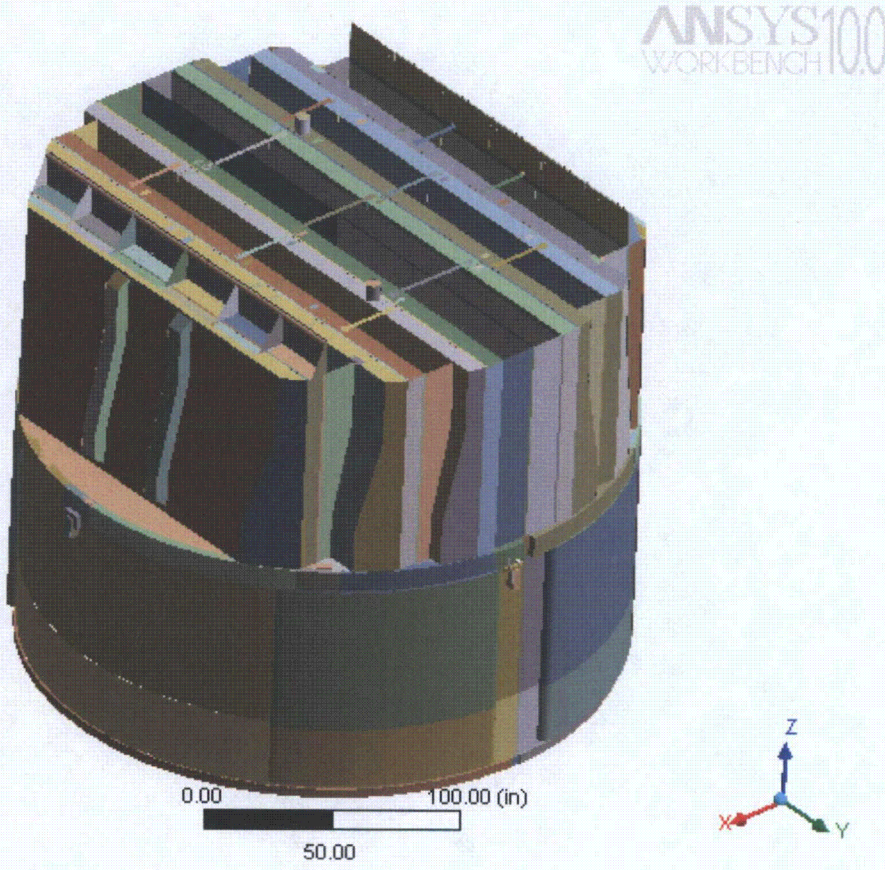

Figure 1. Overall geometry of the Browns Ferry Unit 1 steam dryer model.

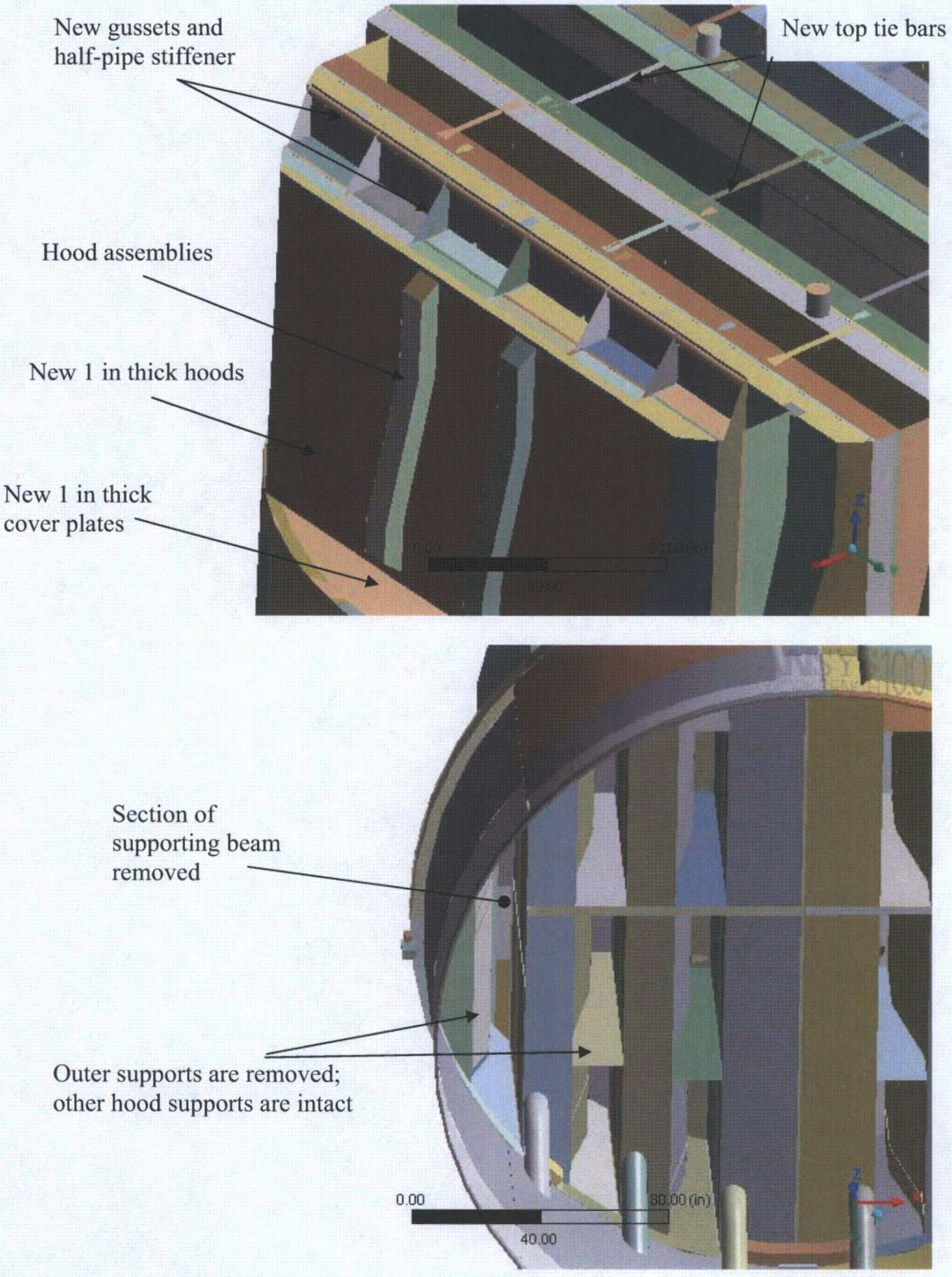

Figure 2. On-site modifications accounted for in the model and associated geometrical details.

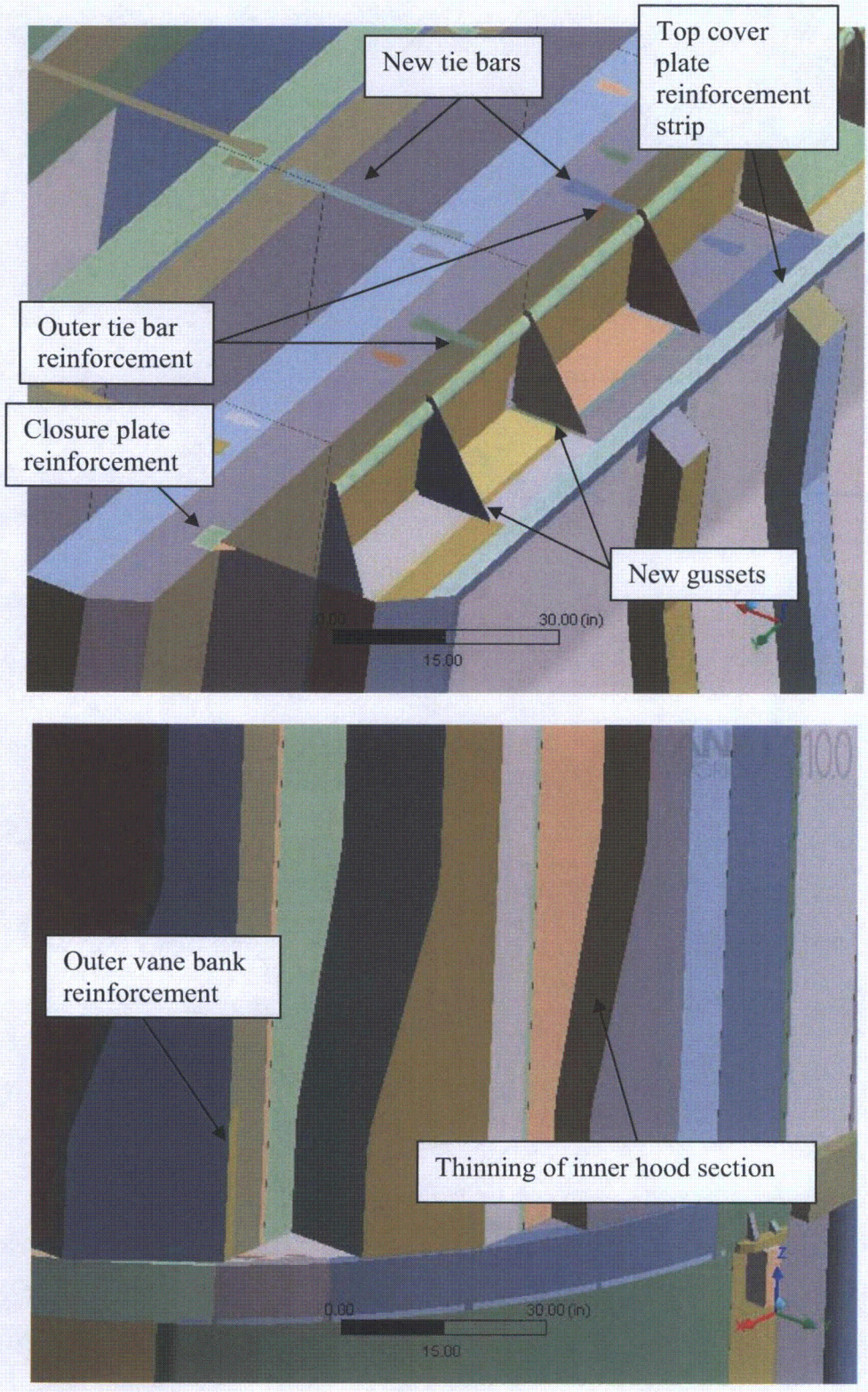

Figure 3. BFN1 modifications involving tie bars and additional steam dam gussets to improve stress margins.

3.2 Material Properties

The steam dryer is constructed from Type 304 stainless steel and has an operating temperature of 550°F. Properties used in the analysis are summarized below in Table 1.

Table 1. Material properties.

	Young's Modulus (10^6 psi)	Density (lbm/in^3)	Poisson's Ratio
structural steel	25.55	0.284	0.3
structural steel with added water inertia	25.55	1.055	0.3

The structural steel modulus is taken from Appendix A of the ASME Code for Type 304 Stainless Steel at an operating temperature 550°F. The effective properties of perforated plates and submerged parts are discussed in Sections 3.4 and 3.6. Note that the increased effective density for submerged components is only used in the harmonic analysis. When calculating the stress distribution due to the static dead weight load, the unmodified density of steel (0.284 lbm/in^3) is used throughout.

3.3 Model Simplifications

The following simplifications were made to achieve reasonable model size while maintaining good modeling fidelity for key structural properties:

- Perforated plates were approximated as continuous plates using modified elastic properties designed to match the static and modal behaviors of the perforated plates. The perforated plate structural modeling is summarized in Section 3.4 and Appendix C of [9].

- The drying vanes were replaced by point masses attached to the corresponding trough bottom plates and vane bank top covers. The bounding perforated plates, vane bank end plates, and vane bank top covers were explicitly modeled (see Section 3.5).

- The added mass properties of the lower part of the skirt below the reactor water level were obtained using a separate hydrodynamic analysis (see Section 3.6).

- [[

  (3)]]

- Four steam dryer support brackets that are located on the reactor vessel and spaced at 90° intervals were explicitly modeled (see Section 3.9).

- Most welds were replaced by node-to-node connections; interconnected parts share common nodes along the welds. In other locations the constraint equations between nodal degrees of freedom were introduced as described in Section 3.9.

3.4 Perforated Plate Model

The perforated plates were modeled as solid plates with adjusted elastic and dynamic properties. Properties of the perforated plates were assigned according to the type and size of perforation. Based on [11], for an equilateral square pattern with given hole size and spacing, the effective moduli of elasticity were found.

The adjusted properties for the perforated plates are shown in Table 2 as ratios to material properties of structural steel, provided in Table 1. Locations of perforated plates are classified by steam entry / exit vane bank side and vertical position.

Tests were carried out to verify that this representation of perforated plates by continuous ones with modified elastic properties preserves the modal properties of the structure. These tests are summarized in Appendix C of [9] and compare the predicted first modal frequency for a cantilevered perforated plate against an experimentally measured value. The prediction was obtained for a 40% open area plate (the maximum open area ratio of the perforated plates at BFN1, as seen in Table 2) using the analytical formula for a cantilevered plate and the modified Young's modulus and Poisson's ratio given by O'Donnell [11]. The measured and predicted frequencies are in close agreement, differing by less than 3%.

[[

$^{(3)}$]]

[[

[3]]]

Figure 4. [[[3]]]

Table 2. Material properties of perforated plates.

[[

[3]]]

3.5 Vane Bank Model

The vane bank assemblies consist of many vertical angled plates that are computationally expensive to model explicitly, since a prohibitive number of elements would be required. These parts have significant weight which is transmitted through the surrounding structure, so it is important to capture their gross inertial properties. Here the vane banks are modeled as a collection of point masses located at the center of mass for each vane bank section (Figure 4). The following masses were used for the vane bank sections, based on data found on provided drawings:

inner banks, 1575 lbm, 4 sections per bank;

middle banks, 1450 lbm, total 4 sections per bank; and
outer banks, 1515 lbm, 3 sections per bank.

These masses were applied to the base plates and vane top covers using the standard ANSYS point mass modeling option, element MASS21. ANSYS automatically distributes the point mass inertial loads to the nodes of the selected structure. The distribution algorithm minimizes the sum of the squares of the nodal inertial forces, while ensuring that the net forces and moments are conserved. Vane banks are not exposed to main steam lines directly, but rather shielded by the hoods.

The collective stiffness of the vane banks is expected to be small compared to the surrounding support structure and is neglected in the model. In the static case it is reasonable to expect that this constitutes a conservative approach, since neglecting the stiffness of the vane banks implies that the entire weight is transmitted through the adjacent vane bank walls and supports. In the dynamic case the vane banks exhibit only a weak response since (i) they have large inertia so that the characteristic acoustically-induced forces divided by the vane masses and inertias yield small amplitude motions, velocities and accelerations; and (ii) they are shielded from acoustic loads by the hoods, which transfer dynamic loads to the rest of the structure. Thus, compared to the hoods, less motion is anticipated on the vane banks so that approximating their inertial properties with equivalent point masses is justified. Nevertheless, the bounding parts, such as perforated plates, side panels, and top covers, are retained in the model. Errors associated with the point mass representation of the vane banks are compensated for by frequency shifting of the applied loads.

3.6 Water Inertia Effect on Submerged Panels

Water inertia was modeled by an increase in density of the submerged structure to account for the added hydrodynamic mass. This added mass was found by a separate hydrodynamic analysis (included in DRF-TVA-250B supporting this report) to be 0.1928 lbm/in^2 on the submerged skirt area. This is modeled by effectively increasing the material density for the submerged portions of the skirt. Since the skirt is 0.25 inches thick, the added mass is equivalent to a density increase of 0.771 lbm/in^3. This added water mass was included in the ANSYS model by appropriately modifying the density of the submerged structural elements when computing harmonic response. For the static stresses, the unmodified density of steel is used throughout.

3.7 Structural Damping

Structural damping was defined as 1% of critical damping for all frequencies. This damping is consistent with guidance given on pg. 10 of NRC RG-1.20 [15].

3.8 Mesh Details and Element Types

Shell elements were employed to model the skirt, hoods, perforated plates, side and end plates, trough bottom plates, reinforcements, base plates and cover plates. Specifically, the four-node, Shell Element SHELL63, was selected to model these structural components. This element models bending and membrane stresses, but omits transverse shear. The use of shell elements is appropriate for most of the structure where the characteristic thickness is small compared to the other plate dimensions. For thicker structures, such as the upper and lower

support rings, solid brick elements were used to provide the full 3D stress. Tie bars at dryer vane bank mid-height were modeled with BEAM188 beam elements. The elements SURF154 are used to assure proper application of pressure loading to the structure. Mesh details and element types are shown in Table 3 and Table 4, respectively.

The mesh is generated automatically by ANSYS with refinement near edges. The maximum allowable mesh spacing is specified by the user. Here a 2.5 inch maximum allowable spacing is specified everywhere except in the following areas: drain pipes (2 inch maximum spacing); perforated plates (2 inches); and the curved portions of the drain channels (1.5 inches). Details of the finite element mesh are shown in Figure 6. Numerical experiments carried out using the ANSYS code applied to simple analytically tractable plate structures with dimensions and mesh spacings similar to the ones used for the steam dryer, confirm that the natural frequencies are accurately recovered (less than 1% errors for the first modes). These errors are compensated for by the use of frequency shifting.

3.9 Connections Between Structural Components

Most connections between parts are modeled as node-to-node connections. This is the correct manner (i.e., within the finite element framework) of joining elements away from discontinuities. At joints between shells, this approach omits the additional stiffness provided by the extra weld material. Also, locally 3D effects are more pronounced. The latter effect is accounted for using weld factors. The deviation in stiffness due to weld material is negligible, since weld dimensions are on the order of the shell thickness. The consequences upon modal frequencies and amplitude are, to first order, proportional to t/L where t is the thickness and L a characteristic shell length. The errors committed by ignoring additional weld stiffness are thus small and readily compensated for by performing frequency shifts.

When joining shell and solid elements, however, the problem arises of properly constraining the rotations, since shell element nodes contain both displacement and rotational degrees of freedom at every node whereas solid elements model only the translations. A node-to-node connection would effectively appear to the shell element as a simply supported, rather than (the correct) cantilevered restraint and significantly alter the dynamic response of the shell structure.

To address this problem, constraint equations are used to properly connect adjacent shell- and solid-element modeled structures. Basically, all such constraints express the deflection (and rotation for shell elements) of a node, $\mathbf{R}_1$, on one structural component in terms of the deflections/rotations of the corresponding point, $\mathbf{P}_2$, on the other connected component. Specifically, the element containing $\mathbf{P}_2$ is identified and the deformations at $\mathbf{P}_2$ determined by interpolation between the element nodes. The following types of shell-solid element connections are used in the steam dryer model including the following:

1. Connections of shell faces to solid faces (Figure 7a). While only displacement degrees of freedom are explicitly constrained, this approach also implicitly constrains the rotational degrees of freedom when multiple shell nodes on a sufficiently dense grid are connected to the same solid face.
2. Connections of shell edges to solids (e.g., connection of the bottom of closure plates with the upper ring). Since solid elements do not have rotational degrees of freedom, the

coupling approach consisted of having the shell penetrate into the solid by one shell thickness and then constraining both the embedded shell element nodes (inside the solid) and the ones located on the surface of the solid structure (see Figure 7b). Numerical tests involving simple structures showed that this approach and penetration depth reproduce both the deflections and stresses of the same structure modeled using only solid elements or ANSYS' bonded contact technology. Continuity of rotations and displacements is achieved.

The use of constraint conditions rather than the bonded contacts advocated by ANSYS for connecting independently meshed structural components confers better accuracy and useful numerical advantages to the structural analysis of the steam dryer including better conditioned and smaller matrices. The smaller size results from the fact that equations and degrees of freedom are eliminated rather than augmented (in Lagrange multiplier-based methods) by additional degrees of freedom. Also, the implementation of contact elements relies on the use of very high stiffness elements (in penalty function-based implementations) or results in indefinite matrices (Lagrange multiplier implementations) with poorer convergence behavior compared to positive definite matrices.

The upper support ring rests on four support blocks which resist vertical and lateral displacement. Because the contact region between the blocks and upper support ring is small, the ring is considered free to rotate about the radial axis. Specifically nodal constraints (zero relative displacement) are imposed over the contact area between the steam dryer upper support ring and the support blocks. Two nodes on each support block are fixed as indicated in Figure 8. One node is at the center of the support block surface facing the vessel and the other node is 0.5" offset inside the block towards the steam dryer, half way to the nearest upper support ring node. This arrangement approximates the nonlinear contact condition where the ring can tip about the block.

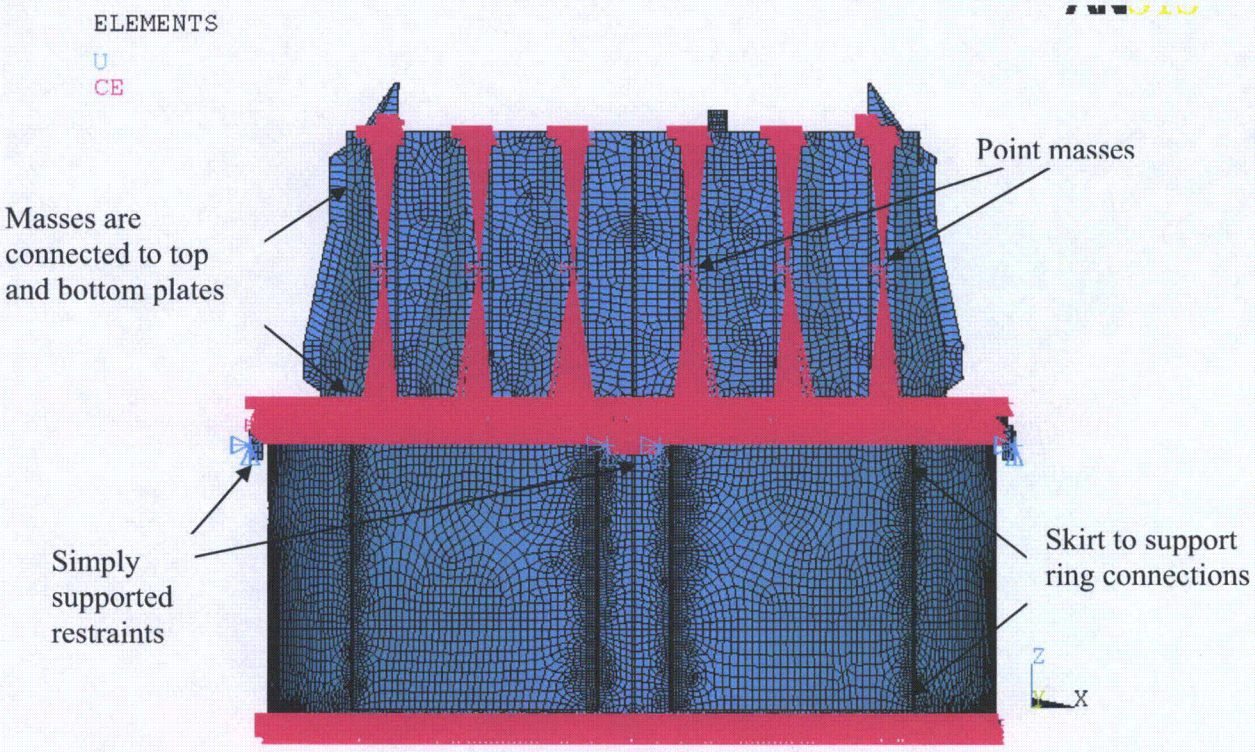

Figure 5. Point masses representing the vanes. The pink shading represents where constraint equations between nodes are applied.

Table 3. FE Model Summary.

Description	Quantity
Total Nodes[1]	153,520
Total Elements	191,597

1. Not including additional damper nodes and elements.

Table 4. Listing of Element Types.

Generic Element Type Name	Element Name	ANSYS Name
20-Node Quadratic Hexahedron	SOLID186	20-Node Hexahedral Structural Solid
10-Node Quadratic Tetrahedron	SOLID187	10-Node Tetrahedral Structural Solid
4-Node Elastic Shell	SHELL63	4-Node Elastic Shell
Mass Element	MASS21	Structural Mass
Pressure Surface Definition	SURF154	3D Structural Surface Effect
Beam element	BEAM188	3-D Finite Strain Beam
Damper element	COMBIN14	Spring-Damper

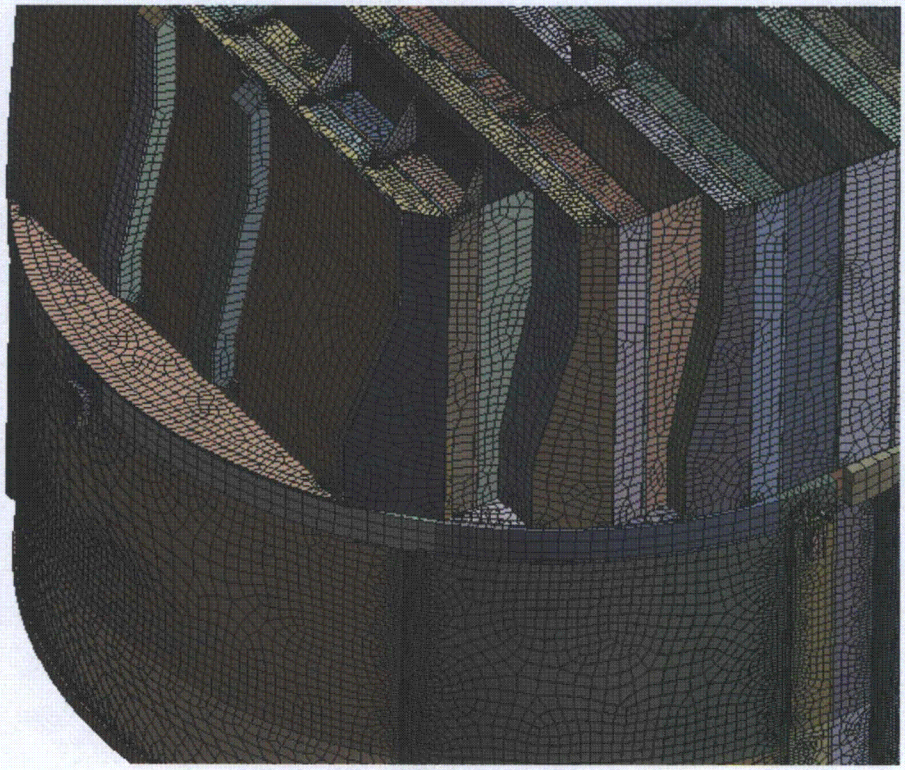

Figure 6a. Mesh overview.

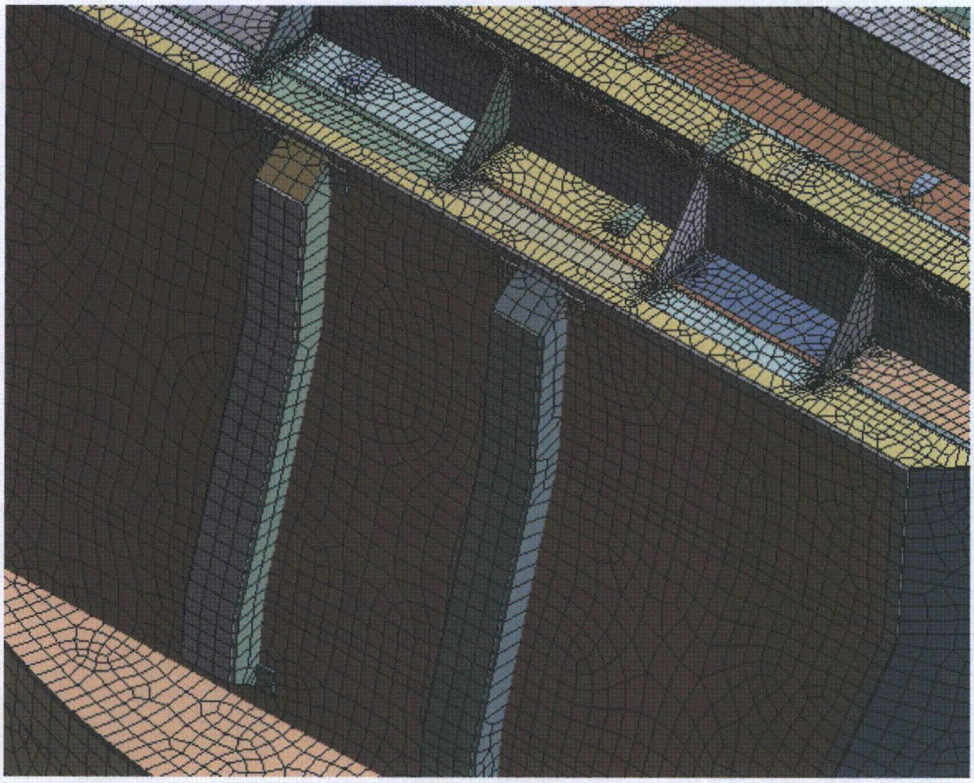

Figure 6b. Close-up of mesh showing hoods and hood assemblies.

Figure 6c. Close-up of mesh showing drain pipes and hood supports; supporting beams and base plates.

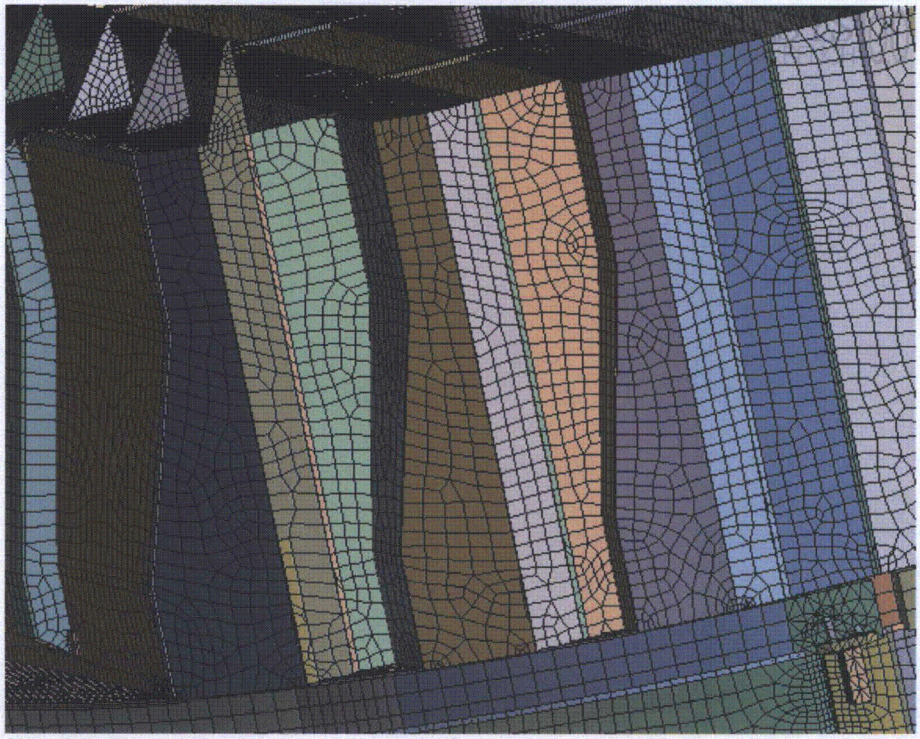

Figure 6d. Close-up of mesh showing node-to-node connections between various plates.

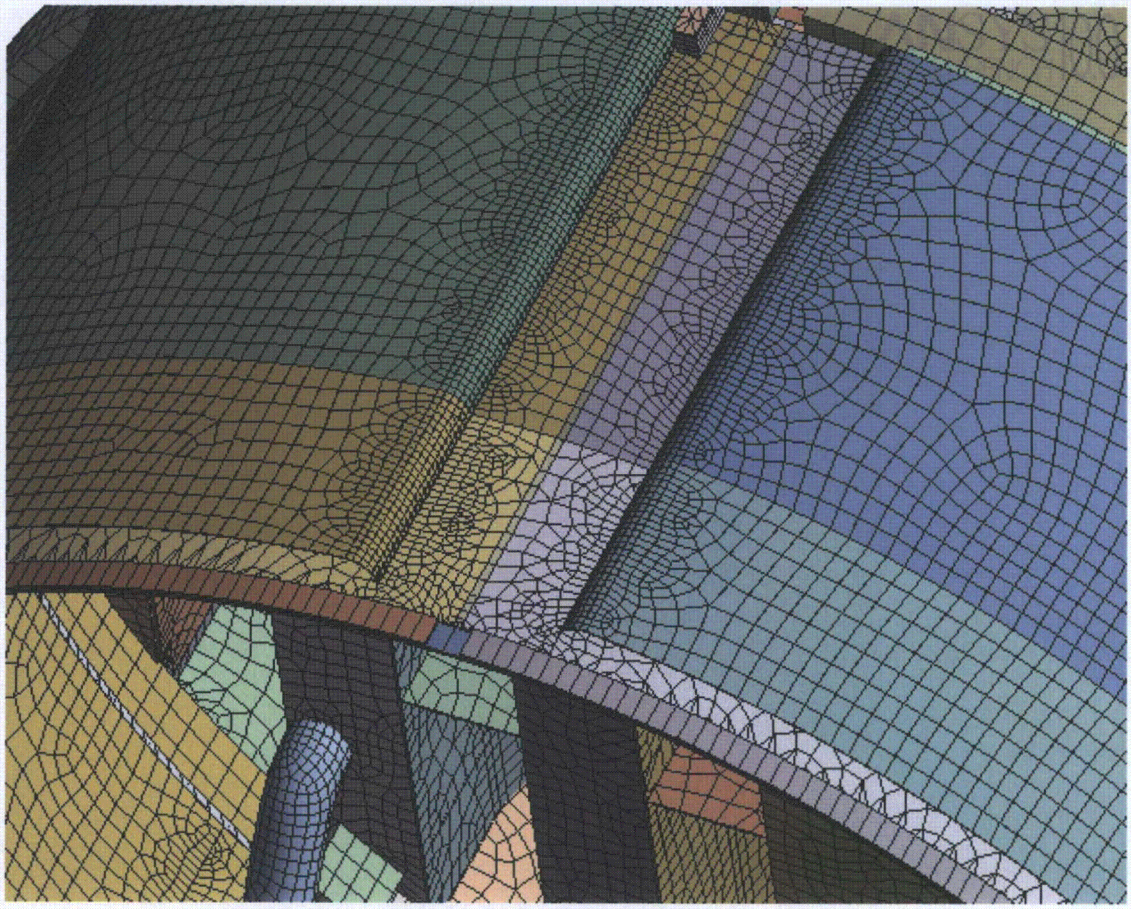

Figure 6e. Close-up of mesh showing node-to-node connections between the skirt and drain channels. Note – cut-out holes are not shown in this model.

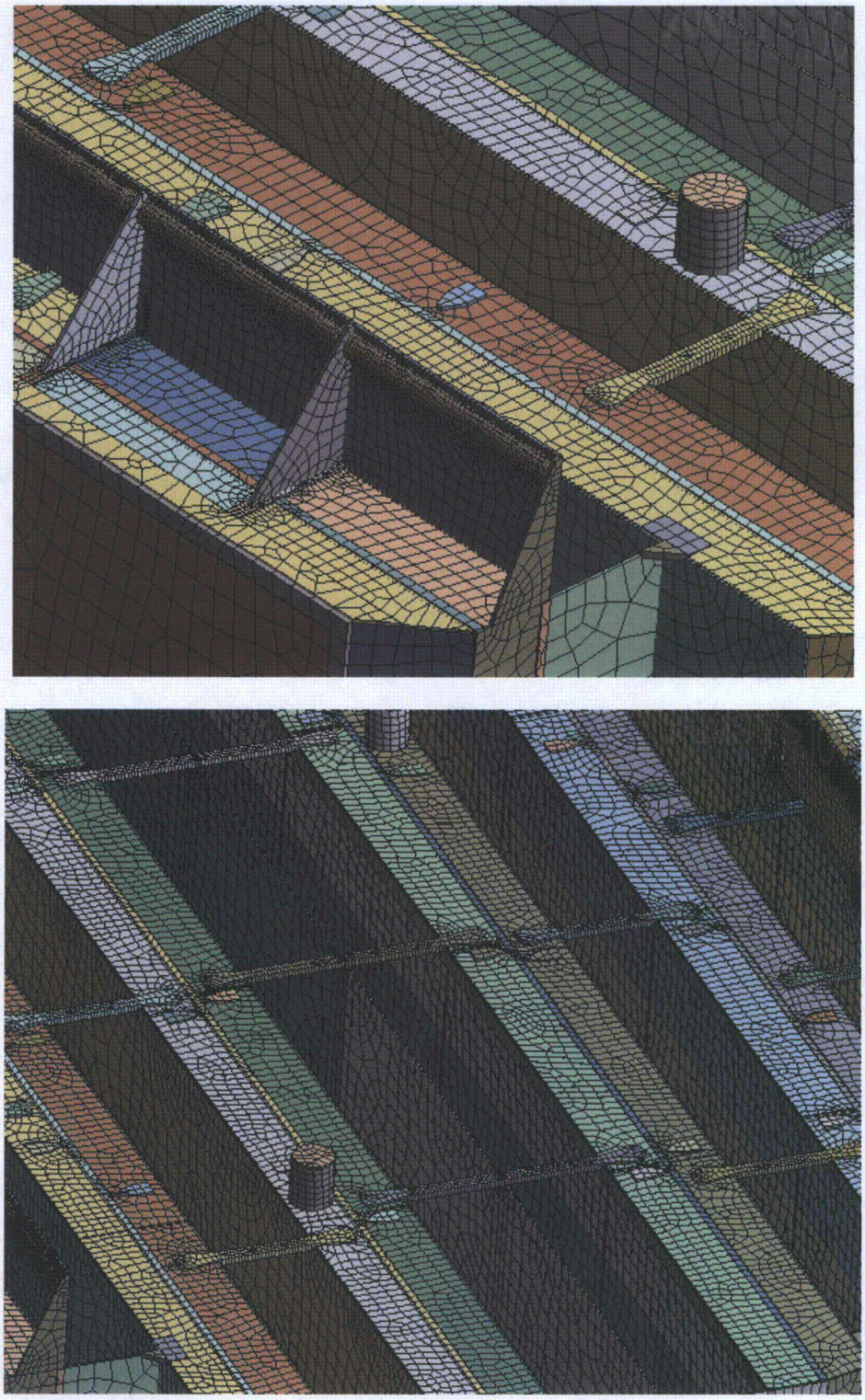

Figure 6f. Close-up view of tie bars connecting vane cover plates and adjacent to the steam dam.

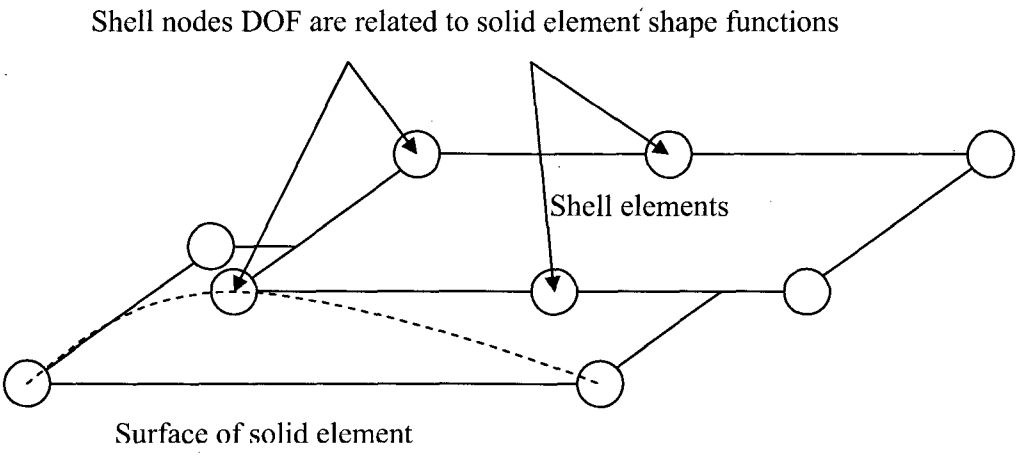

Figure 7a. Face-to-face shell to solid connection.

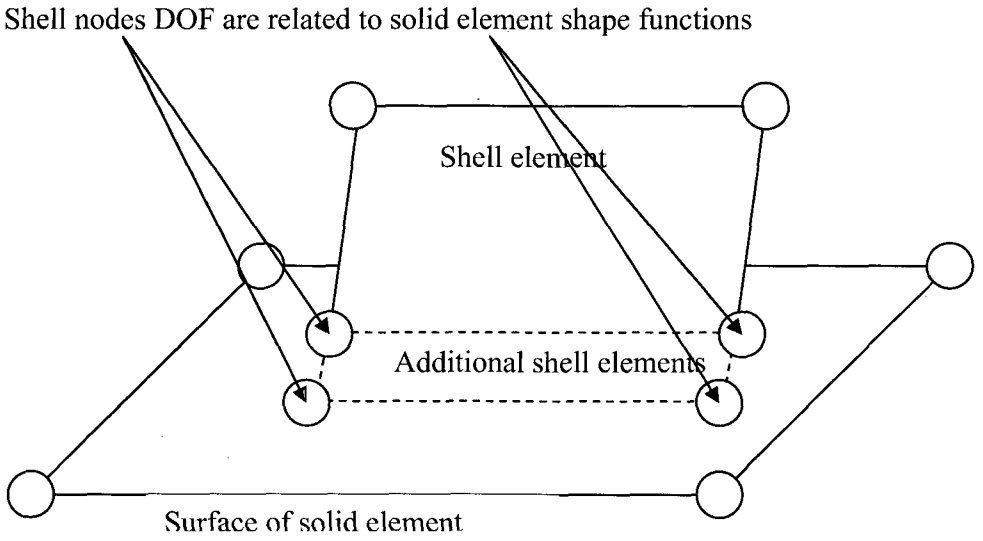

Figure 7b. Shell edge-to-solid face connection.

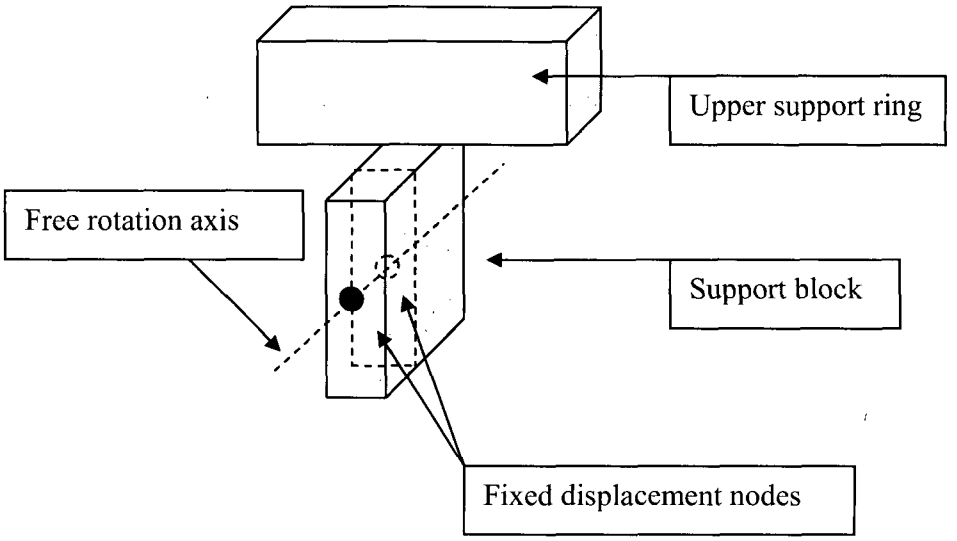

Figure 8. Boundary conditions. Inside node is half way between outer surface of support block and upper support ring.

3.10 Pressure Loading

The harmonic loads are produced by the pressures acting on the exposed surfaces of the steam dryer. At every frequency and for each MSL, the pressure distribution corresponding to a unit pressure at the MSL inlet is represented on a three-inch grid lattice grid (i.e., a mesh whose lines are aligned with the x-, y- and z-directions) that is superimposed over the steam dryer surface. This grid is compatible with the "TableLoads" format used by ANSYS to "paint" general pressure distributions upon structural surfaces. The pressures are obtained from the Helmholtz solver routine in the acoustic analysis [1].

In general, the lattice nodes do not lie on the surface, so that to obtain the pressure differences at the surface, it is necessary to interpolate the pressure differences stored at the lattice nodes. This is done using simple linear interpolation between the eight forming nodes of the lattice cell containing the surface point of interest. Inspection of the resulting pressures at selected nodes shows that these pressures vary in a well-behaved manner between the nodes with prescribed pressures. Graphical depictions of the resulting pressures and comparisons between the peak pressures in the original nodal histories and those in the final surface load distributions produced in ANSYS, all confirm that the load data are interpolated accurately and transferred correctly to ANSYS.

The harmonic pressure loads are only applied to surfaces above the water level, as indicated in Figure 9. In addition to the pressure load, the static loading induced by the weight of the steam dryer is analyzed separately. The resulting static and harmonic stresses are linearly combined to obtain total values which are then processed to calculate maximum and alternating stress intensities for assessment in Section 5.

[[

[3]]] This is useful since revisions in the loads model do not necessitate recalculation of the unit stresses.

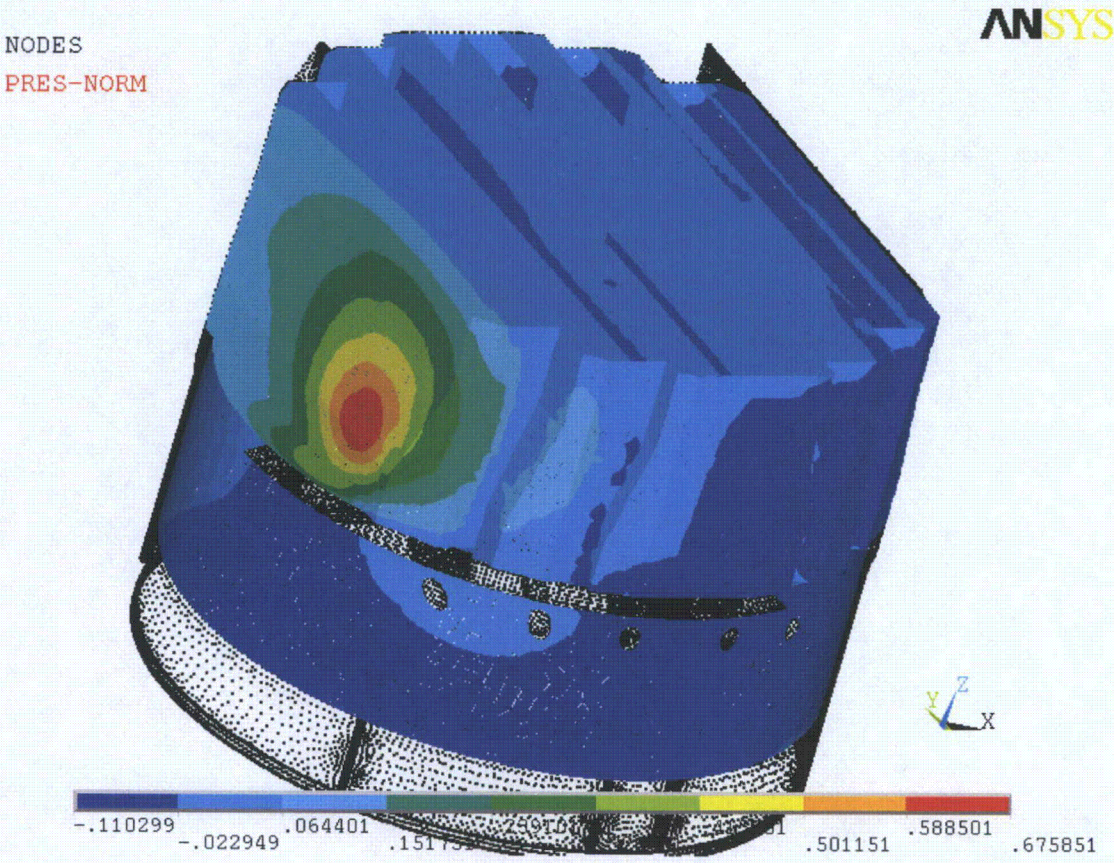

Figure 9a. Real part of unit pressure loading MSL C (in psid) on the steam dryer at 50.2 Hz. No loading is applied to the submerged surface.

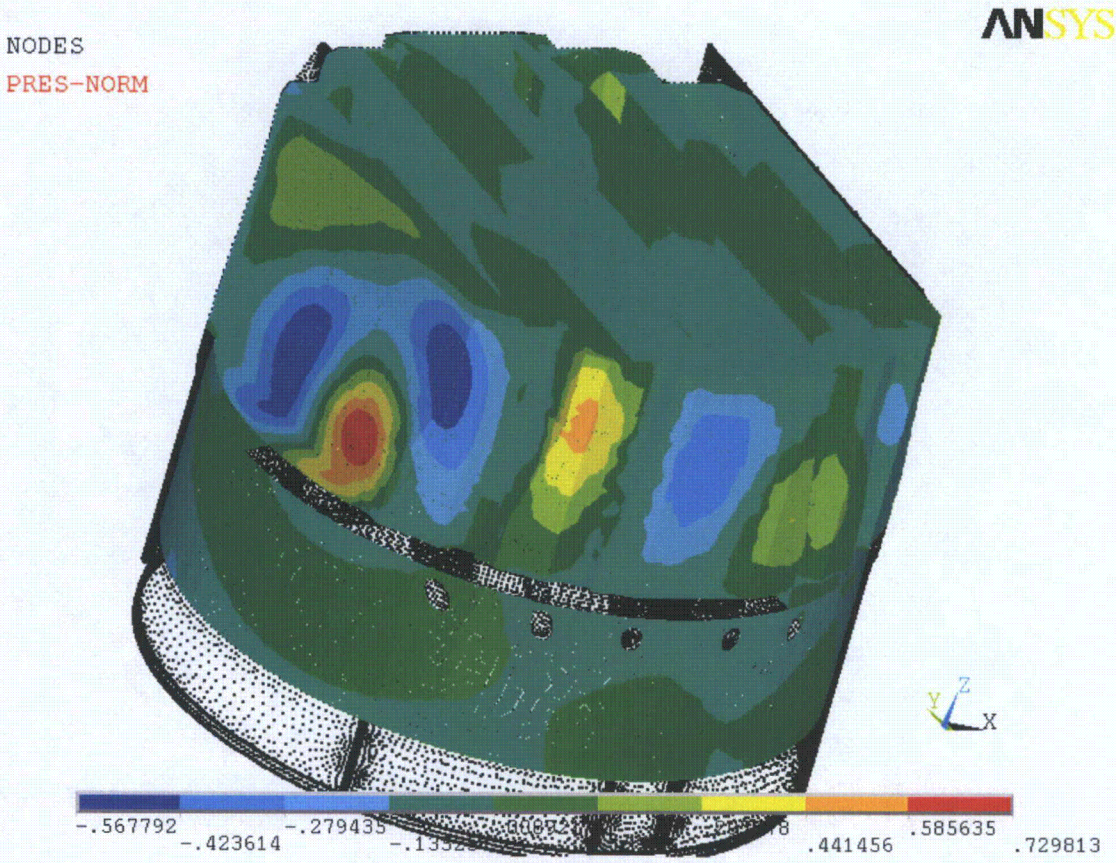

Figure 9b. Real part of unit pressure loading MSL C (in psid) on the steam dryer at 200.9 Hz. No loading is applied to the submerged surface.

4. Structural Analysis

The solution is decomposed into static and harmonic parts, where the static solution produces the stress field induced by the supported structure subjected to its own weight and the harmonic solution accounts for the harmonic stress field due to the unit pressure of given frequency in one of the main steam lines. All solutions are linearly combined, with amplitudes provided by signal measurements in each steam line, to obtain the final displacement and stress time histories. This decomposition facilitates the prescription of the added mass model accounting for hydrodynamic interaction and allows one to compare the stress contributions arising from static and harmonic loads separately. Proper evaluation of the maximum membrane and membrane+bending stresses requires that the static loads due to weight be accounted for. Hence both static and harmonic analyses are carried out.

4.1 Static Analysis

The results of the static analysis are shown in Figure 10. The locations with highest stress include the upper support ring areas near the support brackets with stress intensity 5,874 psi.

4.2 Harmonic Analysis

The harmonic pressure loads were applied to the structural model at all surface nodes described in Section 3.10. Typical stress intensity distributions over the structure are shown in Figure 11. Stresses were calculated for each frequency, and results from static and harmonic calculations were combined.

To evaluate maximum stresses, the stress harmonics including the static component are transformed into a time history using FFT, and the maximum and alternating stress intensities for the response, evaluated. According to ASME B&PV Code, Section III, Subsection NG-3216.2 the following procedure was established to calculate alternating stresses. For every node, the stress difference tensors, $\boldsymbol{\sigma}'_{nm} = \boldsymbol{\sigma}_n - \boldsymbol{\sigma}_m$, are considered for all possible pairs of the stresses $\boldsymbol{\sigma}_n$ and $\boldsymbol{\sigma}_m$ at different time levels, t_n and t_m. Note that all possible pairs require consideration, since there are no "obvious" extrema in the stress responses. However, in order to contain computational cost, extensive screening of the pairs takes place (see Section 2.3), so that pairs known to produce alternating stress intensities less than 1,500 psi are rejected. For each remaining stress difference tensor, the principal stresses S_1, S_2, S_3 are computed and the maximum absolute value among principal stress differences, $S_{nm} = \max\{|S_1 - S_2|, |S_1 - S_3|, |S_2 - S_3|\}$, obtained. The alternating stress at the node is then one-half the maximum value of S_{nm} taken over all combinations (n,m), i.e., $S_{alt} = \frac{1}{2}\max_{n,m}\{S_{nm}\}$. This alternating stress is compared against allowable values, depending on the node location with respect to welds.

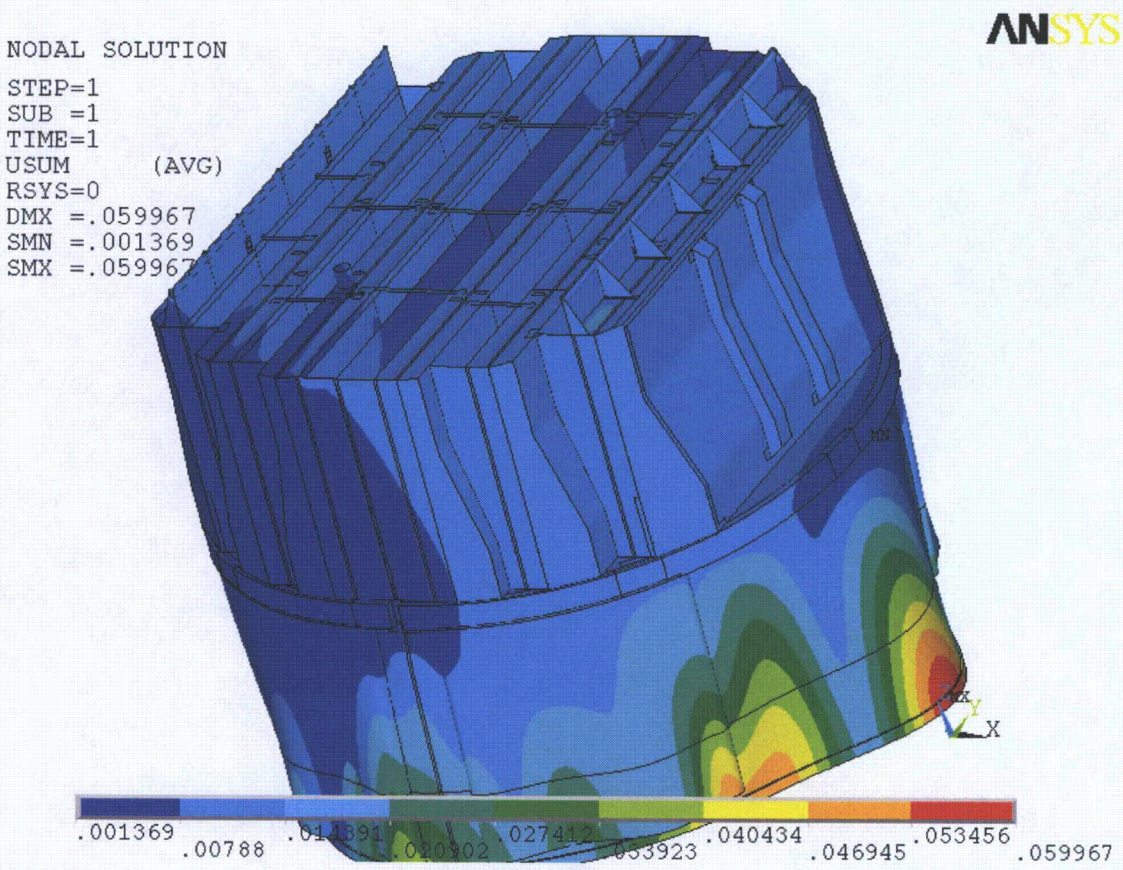

Figure 10a. Overview of static calculations showing displacements (in inches). Maximum displacement (DMX) is 0.06 inches. Note that displacements are amplified for visualization.

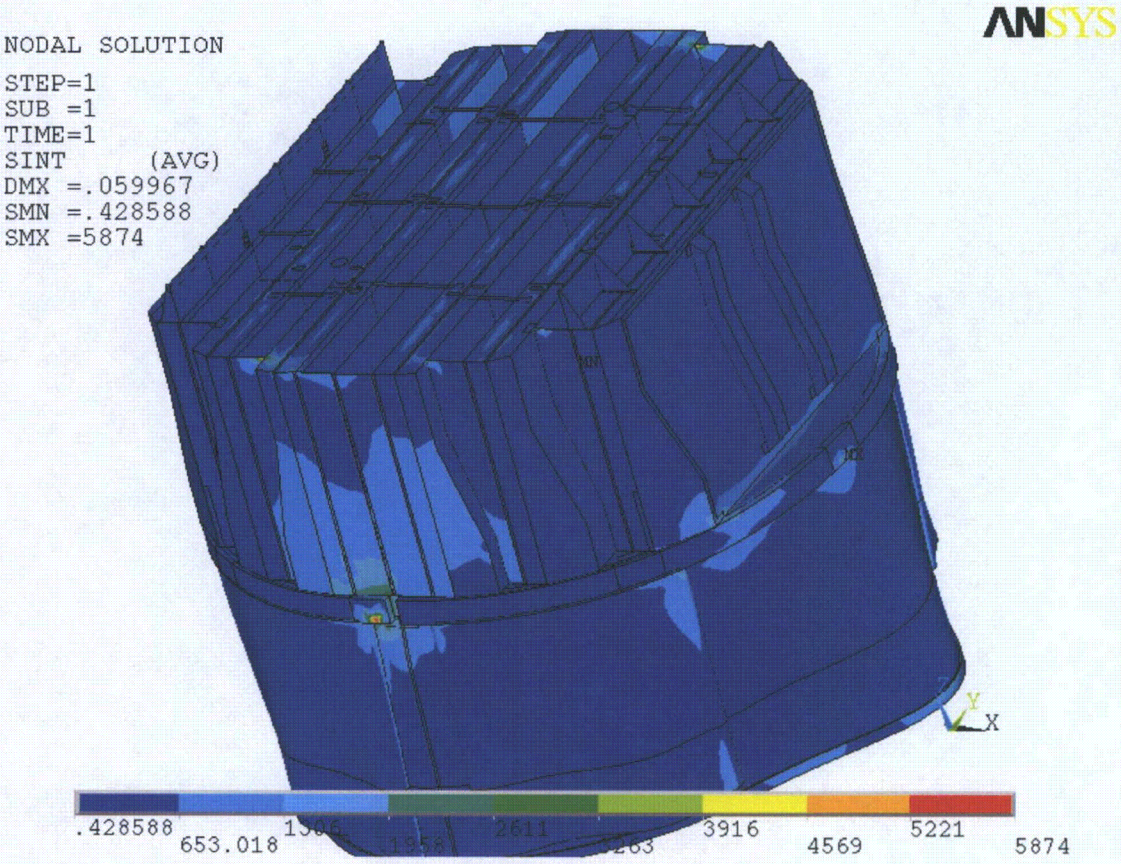

Figure 10b. Overview of static calculations showing stress intensities (in psi). Maximum stress intensity (SMX) is 5,874 psi. Note that displacements are amplified for visualization.

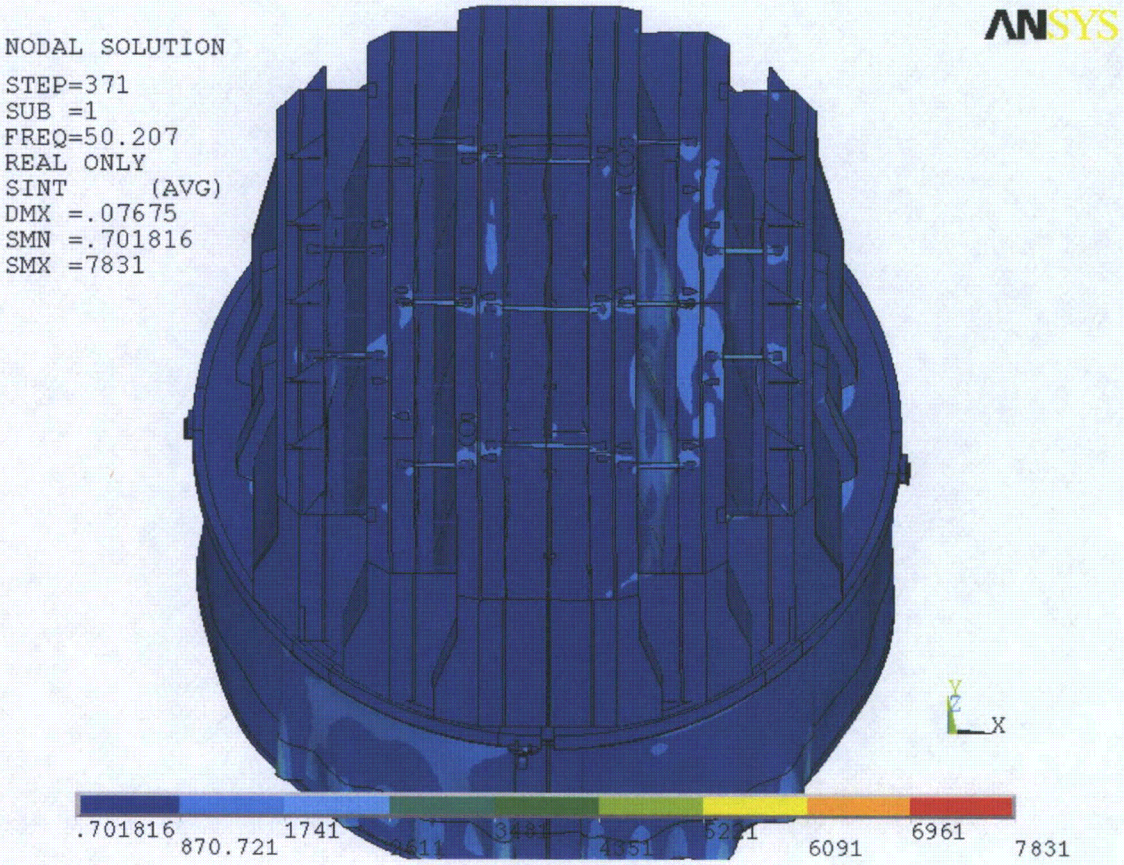

Figure 11a. Overview of harmonic calculations showing real part of stress intensities (in psi) along with displacements. Unit loading MSL C at 50.2 Hz.

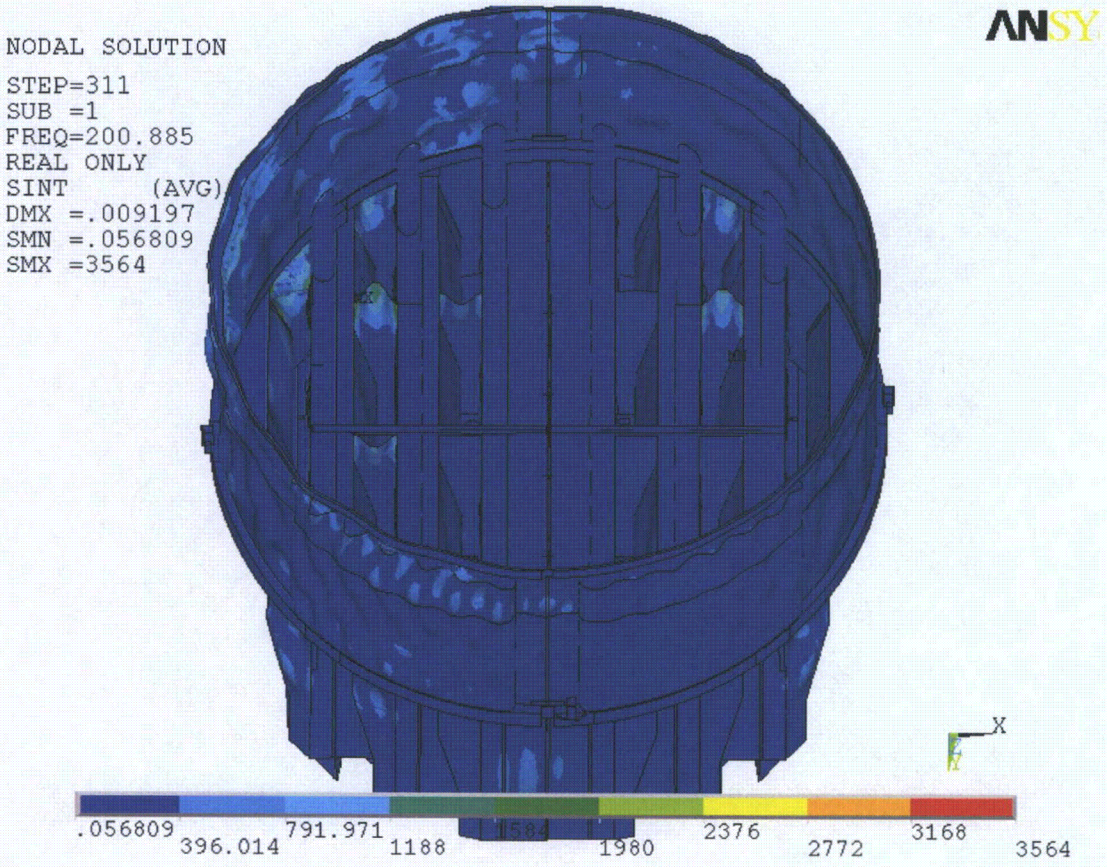

Figure 11b. Overview of harmonic calculations showing real part of stress intensities (in psi) along with displacements. Dryer is oriented to show high stress location at hood support. Unit loading MSL C at 200.9 Hz.

4.3 Post-Processing

The static and transient stresses computed at every node with ANSYS were exported into files for subsequent post-processing. These files were then read into separate customized software to compute the maximum and alternating stresses at every node. The maximum stress was defined for each node as the largest stress intensity occurring during the time history. Alternating stresses were calculated according to the ASME standard described above. For shell elements the maximum stresses were calculated separately at the mid-plane, where only membrane stress is present, and at top/bottom of the shell, where bending stresses are also present.

For nodes that are shared between several structural components or lie on junctions, the maximum and alternating stress intensities are calculated as follows. First, the nodal stress tensor is computed separately for each individual component by averaging over all finite elements meeting at the node and belonging to the same structural component. The time histories of these stress tensors are then processed to deduce the maximum and alternating stress intensities for each structural component. Finally, for nodes shared across multiple components, the highest of the component-wise maximum and alternating stresses is recorded as the "nodal" stress. This approach prevents averaging of stresses across components and thus yields conservative estimates for nodal stresses at the weld locations where several components are joined together.

The maximum stresses are compared against allowable values which depend upon the stress type (membrane, membrane+bending, alternating – Pm, Pm+Pb, S_{alt}) and location (at a weld or away from welds). These allowables are specified in the following section. For solid elements the most conservative allowable for membrane stress, Pm, is used, although bending stresses are nearly always present also. The structure is then assessed in terms of stress ratios formed by dividing allowables by the computed stresses at every node. Stress ratios less than unity imply that the associated maximum and/or alternating stress intensities exceed the allowable levels. Post-processing tools calculate the stress ratios, identifying the nodes with low stress ratios and generating files formatted for input to the 3D graphics program, TecPlot, which provides more general and sophisticated plotting options than currently available in ANSYS.

4.4 Computation of Stress Ratios for Structural Assessment

The ASME B&PV Code, Section III, subsection NG provides different allowable stresses for different load combinations and plant conditions. The stress levels of interest in this analysis are for the normal operating condition, which is the Level A service condition. The load combination for this condition is:

Normal Operating Load Combination = Weight + Pressure + Thermal

The weight and fluctuating pressure contributions have been calculated in this analysis and are included in the stress results. The static pressure differences and thermal expansion stresses are small, since the entire steam dryer is suspended inside the reactor vessel and all surfaces are exposed to the same conditions. Seismic loads only occur in Level B and C cases, and are not considered in this analysis.

Allowable Stress Intensities

The ASME B&PV Code, Section III, subsection NG shows the following (Table 5) for the maximum allowable stress intensity (Sm) and alternating stress intensity (Sa) for the Level A service condition. The allowable stress intensity values for type 304 stainless steel at operating temperature 550°F are taken from Table I-1.2 and Fig. I-9.2.2 of Appendix I of Section III, in the ASME B&PV Code. The calculation for different stress categories is performed in accordance with Fig. NG-3221-1 of Division I, Section III, subsection NG.

Table 5. Maximum Allowable Stress Intensity and Alternating Stress Intensity for all areas other than welds. The notation Pm represents membrane stress; Pb represents stress due to bending; Q represents secondary stresses (from thermal effects and gross structural discontinuities, for example); and F represents additional stress increments (due to local structural discontinuities, for example).

Type	Notation	Service Limit	Allowable Value (ksi)
Maximum Stress Allowables:			
General Membrane	Pm	Sm	16.9
Membrane + Bending	Pm + Pb	1.5 Sm	25.35
Primary + Secondary	Pm + Pb + Q	3.0 Sm	50.7
Alternating Stress Allowable:			
Peak = Primary + Secondary + F	S_{alt}	Sa	13.6

When evaluating welds, either the calculated or allowable stress was adjusted, to account for stress concentration factor and weld quality. Specifically:

- For maximum allowable stress intensity, the allowable value is decreased by multiplying its value in Table 5 by 0.55.

- For alternating stress intensity, the calculated weld stress intensity is multiplied by a weld stress intensity (fatigue) factor of 1.8, before comparison to the Sa value given above.

The weld factors of 0.55 and 1.8 were selected based on the observable quality of the shop welds and liquid penetrant NDE or VT testing of all welds during fabrication (tack and intermittent welds, inner stiffeners and lower tie bars were subject to VT). These factors are consistent with fatigue strength reduction factors recommended by the Welding Research Council, [16], and stress concentration factors at welds, provided in [17] and [18]. In addition, critical welds are subject to periodical visual inspections in accordance with the requirements of GE SIL 644 SIL and BWR VIP-139 [19]. Therefore, for weld stress intensities, the allowable values are shown in Table 6.

These factors (0.55 and 1.8) also conservatively presume that the structure is joined using fillet welds unless specified otherwise. Since fillet welds correspond to larger stress concentration factors than other types of welds, this assumption is a conservative one. When the weld is known to be a full penetration weld a weld factor of 1.4 may be used. In the current analysis this is used for the weld joining the middle closure plate and inner hood.

Table 6. Weld Stress Intensities.

Type	Notation	Service Limit	Allowable Value (ksi)
Maximum Stress Allowables:			
General Membrane	Pm	0.55 Sm	9.30
Membrane + Bending	Pm + Pb	0.825 Sm	13.94
Primary + Secondary	Pm + Pb + Q	1.65 Sm	27.89
Alternating Stress Allowables:			
Peak = Primary + Secondary + F	S_{alt}	Sa	13.6

Comparison of Calculated and Allowable Stress Intensities

The classification of stresses into general membrane or membrane + bending types was made according to the exact location, where the stress intensity was calculated; namely, general membrane, Pm, for middle surface of shell element, and membrane + bending, Pm + Pb, for other locations. For solid elements the most conservative, general membrane, Pm, allowable is used.

The structural assessment is carried out by computing stress ratios between the computed maximum and alternating stress intensities, and the allowable levels. Locations where any of the stresses exceed allowable levels will have stress ratios less than unity. Since computation of stress ratios and related quantities within ANSYS is time-consuming and awkward, a separate FORTRAN code was developed to compute the necessary maximum and alternating stress intensities, Pm, Pm+Pb, and S_{alt}, and then compare it to allowables. Specifically, the following quantities were computed at every node:

1. The maximum membrane stress intensity, Pm (evaluated at the mid-thickness location for shells),
2. The maximum membrane+bending stress intensity, Pm+Pb, (taken as the largest of the maximum stress intensity values at the bottom, top, and mid thickness locations, for shells),
3. The alternating stress, S_{alt}, (the maximum value over the three thickness locations is taken).
4. The stress ratio due to a maximum stress intensity assuming the node lies at a non-weld location (note that this is the minimum ratio obtained considering both membrane stresses and membrane+bending stresses):
   SR-P(nw) = min{ Sm/Pm, 1.5 * Sm/(Pm+Pb) }.
5. The alternating stress ratio assuming the node lies at a non-weld location,
   SR-a(nw) = Sa / (1.1 * S_{alt}),
6. The same as 4, but assuming the node lies on a weld,
   SR-P(w)=SR-P(nw) * 0.55
7. The same as 5, but assuming the node lies on a weld,
   SR-a(w)=SR-a(nw) / 1.8. (for the full penetration weld connecting the middle closure plate and inner hood a weld factor of 1.4 instead of 1.8 is used so that SR-a(w) = SR-a(nw) / 1.4)

Also for undersized welds undersize weld factors are applied to the stresses when computing stress ratios. In the present analysis undersize weld factor is used on the horizontal weld connecting the T-bar and base plates (the undersize weld factor, f_{usw}=2). The undersized vertical weld connecting the steam dam to the end gussets will be reinforced prior to EPU operation to restore an appropriately sized weld so that no undersize weld factor is needed. Note that in steps 4 and 6, the minimum of the stress ratios based on Pm and Pm+Pb, is taken. The allowables listed in Table 5, Sm=16,900 psi and Sa=13,600 psi. The factors, 0.55 and 1.8 (or 1.4 for the cited full penetration groove weld), are the weld factors discussed above. The factor of 1.1 accounts for the differences in Young's moduli for the steel used in the steam dryer and the values assumed in alternating stress allowable. According to NG-3222.4 in subsection NG of Section III of the ASME Code, the effect of elastic modulus upon alternating stresses is taken into account by multiplying alternating stress S_{alt} at all locations by the ratio, E/E_{model}=1.1, where:

$E = 28.3\ 10^6$ psi, as shown on Fig. I-9.2.2. ASME BP&V Code
$E_{model} = 25.55\ 10^6$ psi (Table 1)

The appropriate maximum and alternating stress ratios, SR-P and SR-a, are thus determined and a final listing of nodes having the smallest stress ratios is generated. The nodes with stress ratios lower than 4 are plotted in TecPlot (a 3D graphics plotting program widely used in engineering communities [20]). These nodes are tabulated and depicted in the following Results Section.

4.5 Finite Element Sub-modeling

In order to maintain computational costs at a feasible level, the steam dryer model is predominantly comprised of shell elements. These elements are well suited for structures such as the steam dryer consisting of shell-like components and tend to produce conservative estimates of the stresses. In some cases however, such as welded junctions involving multiple components, shell element models can overestimate the nominal stress intensities in the vicinity of the junctions. In such cases a more refined analysis using solid elements to capture the complete 3D stress distribution, is warranted. Therefore, to efficiently analyze complex structures such as steam dryers, a standard engineering practice is to first analyze the structure using a shell-based model. If any locations with high stresses are identified these regions are examined in greater detail using 3D solid elements to obtain a more definitive stress prediction.

In the BFN1 steam dryer, four locations shown in Figure 12 were identified as requiring a more refined stress analysis: (i) the bottom of the reinforced skirt/drain channel junction and adjacent stress relief cut-out; (ii) the intersection between the bottom of the hood, hood support (stiffener) and base plate and adjacent stress relief cut-out; (iii) the weld connecting the mid-height tie bars to the perforated plates and (iv) the inner hood/hood support weld. The first location is characterized by a previously thickened continuous weld that wraps around the bottom of the drain channel and up along the interior of the channel. The location is further modified by adding an additional 2" of weld inside the drain channel and introducing a cut-out hole at the bottom of the drain channel adjacent to the weld to relieve local stresses. The second location involves the junction between three elements and experiences high stresses Prior sub-model analysis at this location showed that actual stresses computed on the basis of a high

resolution solid element model are lower by a factor of 0.79 [21]. When simulating EPU operating conditions without filtering however, the stress reduction is insufficient and therefore a stress relief cut-out near the weld will be inserted at the bottom of each hood stiffener prior to power ascension to EPU. The third location and fourth locations experience stress ratios below the target level at EPU when the biases and uncertainties are revised over the new frequency intervals and low power noise is left in the signal.

These locations were examined using the 3D solid element sub-modeling procedures described in [21] and Appendix A of [22], and validated against both high resolution solid models of the full structure and sub-structuring results in [23] and [24]. Results for the first two locations without stress relief cut-outs were previously reported in [21]. The same locations have been re-analyzed with stress relief cut-outs (see [25] for the hood stiffener analysis) included using the same sub-modeling approaches. The third and fourth locations were similarly analyzed using the approach in Appendix A of [22]. In each of the last two cases a 6"×6"×6" sub-model is extracted from the global model. The sub-model is first represented using shell elements and a combination of perimeter forces on the intersection edges and a distributed body force applied to match the component stresses in the vicinity of the high stress location. The stress intensity at the high stress location is calculated and a highly detailed solid element representation of the sub-model including the welds is generated. The same forces and body force distribution are applied to this solid element sub-model and the stresses calculated. Linearized stresses are extracted from several paths in the weld [21, 22, 24, 26] and the highest such stress identified. The stress reduction factors (SRFs) are obtained as the ratio between the shell- and solid-element sub-model stresses.

Based on these models, the nominal stress intensities computed by the 3D solid element model are lower than those obtained with the shell-based FEA used to analyze the complete steam dryer by factors of (see Table 7): (i) 0.49 for the bottom 2 inches of the skirt/drain channel weld (a total of sixteen nodes) and (ii) 0.53 for the inner hood/hood support/base plate junction when the stress relief cut-out is added; (iii) 0.5 for the tie bar/perforated plate connections and (iv) 0.77 for the inner hood/hood support weld. The variation of stress reduction factor among these locations is strictly dependent on the individual geometry and general loading characteristics. The discontinuity stresses computed in a shell model at a weld joint between two orthogonal members are often quite conservative because the shell element depiction does not provide any credit for the stress distribution associated with the specific weld geometry. The stress intensities predicted by the shell element-based analysis at these locations are therefore first multiplied by these factors to obtain more accurate estimates of the nominal stresses. These are then multiplied by the 1.8 weld factor before comparing against allowable values to obtain the alternating stress ratios.

Table 7. Summary of stress reduction factors obtained using sub-model analysis.

	Location	Stress Reduction Factor
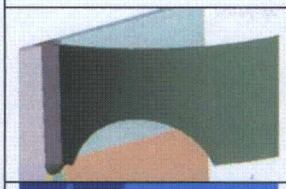	1. Last 2" at bottom of drain channel/skirt weld with cut-out stress relief hole included.	0.49 [21] and [22]
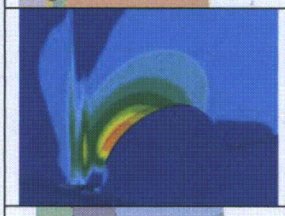	2. Inner hood/hood support/middle base plate with cut-out stress relief hole included.	0.53 [25]
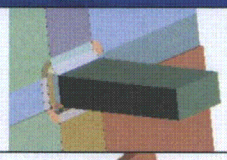	3. Mid-height tie-bar/perforated plate.	0.50 [22]
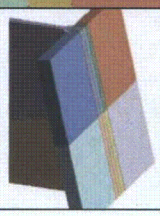	4. Inner hood/hood support.	0.77 [22]

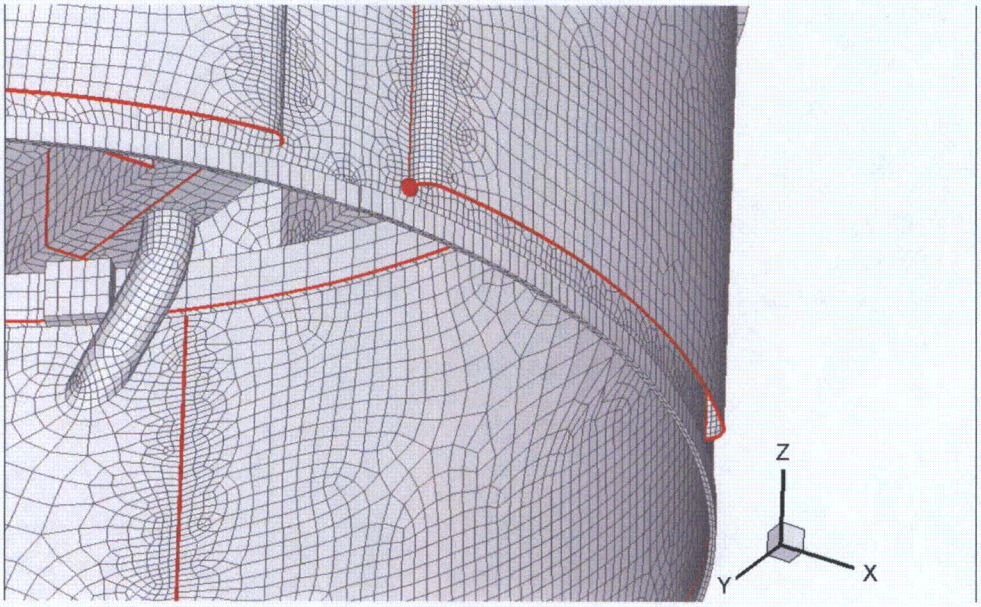

Figure 12a. Location of node on drain channel/skirt weld analyzed with sub-model using the same methodology summarized in [21] and [22].

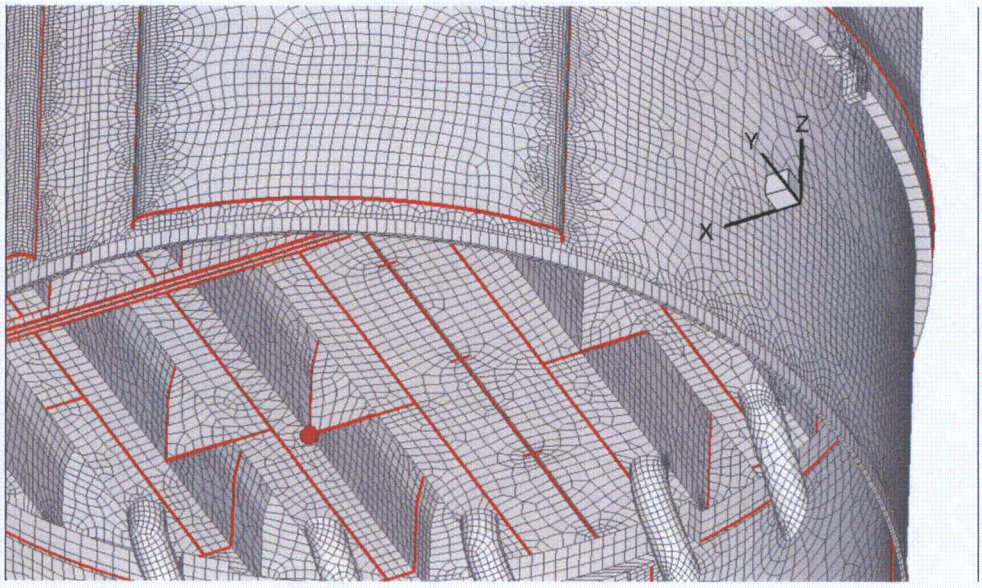

Figure 12b. Location of node on inner hood/hood support/middle base plate weld analyzed with sub-model in [25].

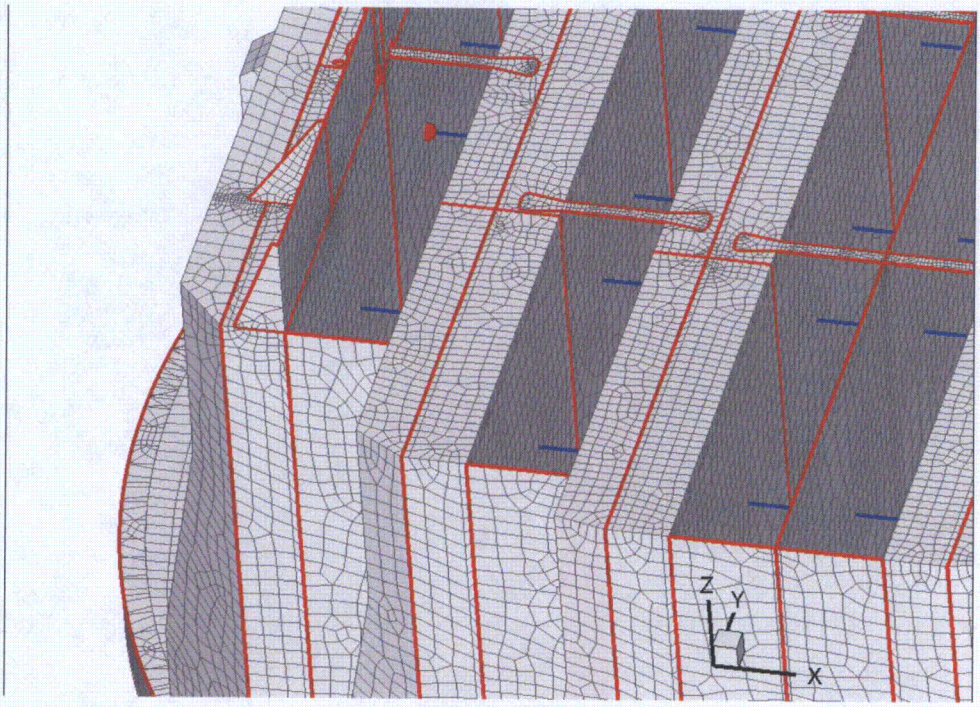

Figure 12c. Location of node on tie bar/perforated plate weld analyzed with sub-model analysis procedure in Appendix A of [22].

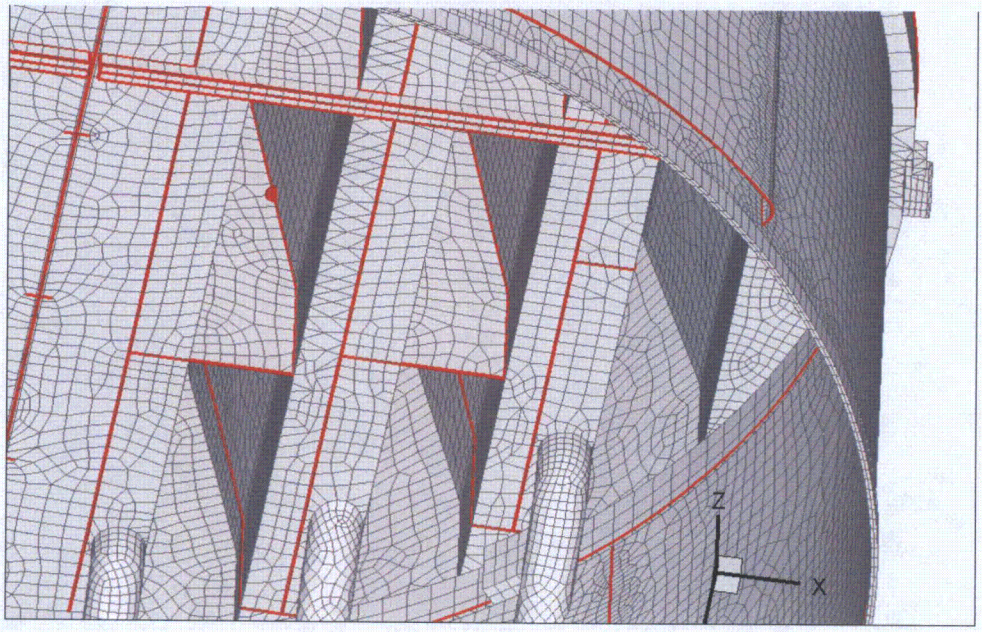

Figure 12d. Location of node on inner hood/hood support weld analyzed with sub-model analysis procedure in Appendix A of [22].

5. Results at EPU Conditions

The stress intensities and associated stress ratios resulting from the Rev. 4 acoustic/hydrodynamic loads [2] with associated biases and uncertainties factored in, are presented below. The bias due to finite frequency discretization and uncertainty associated with the finite element model itself, are also factored in. In the following sections the highest maximum and alternating stress intensities are presented to indicate which points on the dryer experience significant stress concentration and/or modal response (Section 5.2). The lowest stress ratios obtained by comparing the stresses against allowable values, accounting for stress type (maximum and alternating) and location (on or away from a weld), are also reported (Section 5.3). Finally the frequency dependence of the stresses at nodes experiencing the lowest stress ratios is depicted in the form of accumulative PSDs (Section 5.4).

In each section results are presented both at nominal conditions (no frequency shift) and with frequency shift included. Unless specified otherwise, frequency shifts are generally performed at 2.5% increments. The tabulated stresses and stress ratios are obtained using a 'blanking' procedure that is designed to prevent reporting a large number of high stress nodes from essentially the same location on the structure. In the case of stress intensities this procedure is as follows. The relevant stress intensities are first computed at every node and then nodes sorted according to stress level. The highest stress node is noted and all neighboring nodes within 10 inches of the highest stress node and its symmetric images (i.e., reflections across the x=0 and y=0 planes) are "blanked" (i.e., excluded from the search for subsequent high stress locations). Of the remaining nodes, the next highest stress node is identified and its neighbors (closer than 10 inches) blanked. The third highest stress node is similarly located and the search continued in this fashion until all nodes are either blanked or have stresses less than half the highest value on the structure. For stress ratios, an analogous blanking procedure is applied. Thus the lowest stress ratio of a particular type in a 10" neighborhood and its symmetric images is identified and all other nodes in these regions excluded from listing in the table. Of the remaining nodes, the one with the lowest stress ratio is reported and its neighboring points similarly excluded, and so on until all nodes are either blanked or have a stress ratio higher than 4.

The measured CLTP strain gage signals contain significant contributions from non-acoustic sources such as sensor noise, MSL turbulence and pipe bending vibration that contribute to the hoop strain measurements. The ACM analysis does not distinguish between the acoustic and non-acoustic fluctuations in the MSL signals that can lead to sizeable, but fictitious acoustic loads and resulting stresses on the dryer. One way to filter these fictitious loads is to collect data with the system maintained at operating pressure (1000 psi) and temperature, but low (less than 20% of CLTP) flow. By operating the recirculation pumps at this condition, the background plant noise and vibrations remain present. At these conditions the acoustic loads are known to be negligible so that collected data, referred to as the 1000# data, originate entirely from non-acoustic sources such as sensor noise and mechanical vibrations. This information is valuable since it allows one to now distinguish between the acoustic and non-acoustic content in the CLTP signal and therefore modify the CLTP loads so that only the acoustic component is retained. In previous analyses of the BFN1 dryer, these low power signals were subtracted. In the present implementation however, no filtering using low power data is performed.

The applied load includes all biases and uncertainties for both the ACM (summarized in [2]) and the FEM. For the latter there are three main contributors to the bias and uncertainty. The first is an uncertainty (25.26%) that accounts for modeling idealizations (e.g., vane bank mass model), geometrical approximations and other discrepancies between the modeled and actual dryer such as neglecting of weld mass and stiffness in the FEA. The second contributor is a bias (9.53% - note that this has been increased from the 5.72% value previously used in [9]) accounting for discretization errors associated with using a finite size mesh, upon computed stresses. The third contributor is also a bias and compensates for the use of a finite discretization schedule in the construction of the unit solutions. The frequencies are spaced such that at 1% damping the maximum (worst case) error in a resonance peak is 5%. The average error for this frequency schedule is 1.72%.

It is significant to note that the applied loads reflect revised bias and uncertainty values over new frequency intervals: 60-70 Hz and 70-100 Hz. The higher bias and uncertainty values in the 60-70 Hz range strongly influence the limiting stresses values, but are also overly conservative. This is because when specifying new frequency intervals the ACM should be recalibrated over these intervals before calculating the bias and uncertainty values. Because it is resource-intensive and would constitute further revisions to the ACM model (to Rev. 5) this model re-calibration was not performed. Consequently the revised biases and uncertainties are higher than they would be if the ACM had been matched to data over the new intervals.

5.1. Results at Predicted EPU Using Bump Up Factors

[[

[3]]]

The predictions below are obtained under this third option. The resulting alternating stress ratio at EPU is SR-a=2.03 when all frequency shifts are considered.

5.2 General Stress Distribution and High Stress Locations

The maximum stress intensities obtained by post-processing the ANSYS stress histories for EPU at nominal frequency and with frequency shift operating conditions are listed in Table 8. Contour plots of the stress intensities over the steam dryer structure are shown on Figure 13 (nominal frequency) and Figure 14 (maximum stress over all nine frequency shifts including nominal). The figures are oriented to emphasize the high stress regions. Note that these stress intensities *do not* account for weld factors but include end-to-end bias and uncertainty and incorporate results from sub-modeling (see Section 4.5). Further, it should be noted that since the allowable stresses vary with location, stress intensities do not necessarily correspond to regions of primary structural concern. Instead, structural evaluation is more accurately made in terms of the stress ratios which compare the computed stresses to allowable levels with due account made for stress type and weld factors and also account for stress corrections obtained using high-detail solid element sub-models. Comparisons on the basis of stress ratios are made in Section 5.2.

For the membrane stresses (Pm) the high stress regions tend to occur at: (i) the restraint locations for the upper support ring and (ii) the upper edges of the closure plates, particularly where they connect to the inner hood. The first location is a very localized stress location and is believed to be significantly overestimated as a 'hot-spot' in the FEA. It experiences high stresses since the entire weight of the structure is transmitted through relatively small pads to the external structure. This stress is dominated by the static component. The closure plates experience high stresses since they restrain any motion of the adjacent vane banks. Note that the inner hood/closure plate weld also experiences high alternating stresses, but these occur several feet below the top of this weld. Other locations with relatively high Pm include the bottoms of the hood/hood support/base plate junctions and the connections between the bottom support beam spanning the dryer, and the vane banks (see Figure 13b). Frequency shifting does not significantly alter the high Pm stress locations and comparison of Table 8a and b shows that the leading Pm stress nodes are identical with and without frequency shifting. Again, this is due to the dominance of the static (deadweight) load.

The membrane + bending stress (Pm+Pb) distributions evidence a stronger modal response. Modal excitations are most pronounced on the skirt and the inner hood. Stress concentrations are observed at several locations coinciding with welds. The highest stress location is the same as for the highest membrane stress and lies near the dryer supports. Note that this stress occurs in a solid element where no distinction is made between the membrane and bending stresses (this distinction is only appropriate for thin members such as shell and beam elements). The next three entries for Pm+Pb are also the same as the leading locations for membrane stresses Pm and involve either the USR support, the closure plate connections to the hoods or vane bank end plates, or the large mid-plate near its connection to the central tie bars. These stresses also appear to be dominated by the static component since alternating stresses are comparatively low. Moreover, frequency shifting does not change the order of the leading Pm+Pb stress locations. Other locations where Pm+Pb stresses are significant include the bottom corners of the outer hood, the drain channel welds, the outer panels of the inner hoods, the top tie bars and the gussets used to support the steam dams.

The highest alternating stress intensities at any frequency shift occur on the large middle plate spanning the dryer at its center section. The alternating stress distributions in Figure 13 and Figure 14 indicate significant modal response on the inner hood , outer panels of the inner hood, the end plate of the outer hood, approximately mid-way on the inner hood/closure plate weld, , the skirt and drain channels. The submerged components (skirt and drain channels), though not exposed to direct acoustic forcing, evidence a pronounced modal response due to coupling with the upper steam dryer structure subjected to acoustic loads. The inner hood vibrations induced high stresses in the associated attachment structures, particularly the closure plate connecting the inner hood and middle vane bank, and motivated the thinning of the section of the slanted inner hood outboard of the closure plate.

Finally, for reference the highest stress intensities at any frequency shift for the locations in Table 8b are recomputed using the CLTP loads (again, without noise removal) and reported in Table 8c. The alternating stresses are generally approximately lower at CLTP by slightly over 35% thus reflecting the velocity square scaling. This is not surprising since most of the leading

alternating stress locations are dominated by contributions in the 60-65 Hz range where the velocity scaling applies.

Table 8a. Locations with highest predicted stress intensities at EPU conditions at zero frequency shift.

Stress Category	Location	Weld	Location (in)(a)			node(b)	Stress Intensities (psi)		
			x	y	z		Pm	Pm+Pb	S_{alt}
Pm	Upper Support Ring (USR)/Seismic Block/Support Part	No	122.1	-10	-9.5	142984	9001	9001	3055
"	USR part/Support/Support Part	No	7	122.3	-9.5	143092	7648	7648	2379
"	Top Cover Inner Hood/Middle Closure Plate/Inner Hood	Yes	-31.5	-108.4	88.9	111296	6622	7713	2164
"	Middle Closure Plate	No	-33.9	-108.4	88.9	6934	6092	6347	1842
"	Hood Support	No	-37.5	59.8	0	9309	5291	5339	3464
Pm+Pb	USR/Seismic Block/Support Part	No	122.1	-10	-9.5	142984	9001	9001	3055
"	Top Cover Inner Hood/Middle Closure Plate/Inner Hood	Yes	-31.5	-108.4	88.9	111296	6622	7713	2164
"	USR part/Support/Support Part	No	7	122.3	-9.5	143092	7648	7648	2379
"	Middle Closure Plate	No	-33.9	-108.4	88.9	6934	6092	6347	1842
"	Mid Plate	No	0	-3	88.9	116595	229	5428	5110
S_{alt}	Mid Plate	No	0	-3	88.9	116595	229	5428	5110
	Mid Plate	No	0	56.8	88.9	107485	62	4749	4428
"	Top Cover Middle Hood	No	-55.4	-31.4	88.9	4517	664	3939	3701
"	Hood Support	No	-37.5	59.8	0	9309	5291	5339	3464
"	Middle Closure Plate/Inner Hood/Top Cover/Tbar	Yes	-39.8	0	0	129266	4775	4822	3349

Notes for Table 8 and Table 9.

(a) Spatial coordinates are in a reference frame with origin at the intersection of the steam dryer centerline and the plane containing the base plates (this plane also contains the top of the USR and the bottom edges of the hoods). The y-axis is parallel to the hoods, the x-axis is normal to the hoods pointing from MSL C/D to MSL A/B, and the z-axis is vertical, positive up.

(b) Node numbers are retained for further reference.

(c) For the stitch weld connecting the T-bar to the base plates an undersize weld factor of 2.0 has been applied. Also parts retention analysis has been carried out separately [28] to verify that the T-bar, which is a secondary structural member, remains attached.

(1-4) Appropriate stress reduction factor for the welds and modifications listed in Table 7 have been applied. The number refers to the particular location and corresponding stress reduction factor in Table 7.

Table 8b. Locations with highest predicted stress intensities taken over all frequency shifts at EPU conditions.

Stress Category	Location	Weld	Location (in)(a)			node(b)	Stress Intensities (psi)			% Freq. Shift
			x	y	z		Pm	Pm+Pb	S_{alt}	
Pm	USR/Seismic Block/Support Part	No	122.1	-10	-9.5	142984	10056	10056	3863	5
"	USR part/Support/Support Part	No	7	122.3	-9.5	143092	7809	7809	2664	2.5
"	Top Cover Inner Hood/Middle Closure Plate/Inner Hood	Yes	31.5	108.4	88.9	113527	7344	8085	2671	7.5
"	Middle Closure Plate	No	33.9	108.4	88.9	6246	6473	6824	2240	7.5
"	Hood Support	No	-37.5	59.8	0	9309	5977	6001	3943	5
Pm+Pb	USR/Seismic Block/Support Part	No	122.1	-10	-9.5	142984	10056	10056	3863	5
"	Top Cover Inner Hood/Middle Closure Plate/Inner Hood	Yes	31.5	108.4	88.9	113527	7344	8085	2671	7.5
"	USR part/Support/Support Part	No	7	122.3	-9.5	143092	7809	7809	2664	2.5
"	Middle Closure Plate	No	33.9	108.4	88.9	6246	6473	6824	2240	7.5
"	Mid Plate	No	0	-3	88.9	116595	290	6281	5523	2.5
S_{alt}	Mid Plate	No	0	-3	88.9	116595	290	6281	5523	5
"	Mid Plate	No	0	56.8	88.9	107485	91	5307	5276	5
"	Inner Hood	No	35.8	85.1	38.2	46289	323	4470	4367	-2.5
"	Middle Closure Plate/Inner Hood	Yes	35.8	108.4	38	113478	921	4461	4361	-2.5
"	Top Cover Middle Hood	No	-55.4	-31.4	88.9	4517	664	4560	3967	-5

See Table 8a for notes (a)-(c) and (1)-(4).

Table 8c. Highest stress intensities at any frequency shift for the nodes listed in Table 8b at CLTP conditions.

Stress Category	Location	Weld	Location (in)(a)			node(b)	Stress Intensities (psi)			% Freq. Shift
			x	y	z		Pm	Pm+Pb	S_{alt}	
Pm	USR/Seismic Block/Support Part	No	122.1	-10	-9.5	142984	8847	8847	2761	5
"	USR part/Support/Support Part	No	7	122.3	-9.5	143092	7174	7174	1977	2.5
"	Top Cover Inner Hood/Middle Closure Plate/Inner Hood	Yes	31.5	108.4	88.9	113527	6657	7340	1907	7.5
"	Middle Closure Plate	No	33.9	108.4	88.9	6246	5949	6297	1692	7.5
"	Hood Support	No	-37.5	59.8	0	9309	4778	4795	2920	5
Pm+Pb	USR/Seismic Block/Support Part	No	122.1	-10	-9.5	142984	8847	8847	2761	5
"	Top Cover Inner Hood/Middle Closure Plate/Inner Hood	Yes	31.5	108.4	88.9	113527	6657	7340	1907	7.5
"	USR part/Support/Support Part	No	7	122.3	-9.5	143092	7174	7174	1977	2.5
"	Middle Closure Plate	No	33.9	108.4	88.9	6246	5949	6297	1692	7.5
"	Mid Plate	No	0	-3	88.9	116595	250	4514	4100	2.5
S_{alt}	Mid Plate	No	0	-3	88.9	116595	250	4514	4100	2.5
"	Mid Plate	No	0	56.8	88.9	107485	67	3899	3883	5
"	Inner Hood	No	35.8	85.1	38.2	46289	269	3218	3151	-2.5
"	Middle Closure Plate/Inner Hood	Yes	35.8	108.4	38	113478	836	3271	3151	-2.5
"	Top Cover Middle Hood	No	-55.4	-31.4	88.9	4517	504	3307	2808	-5

See Table 8a for notes (a)-(c) and (1)-(4).

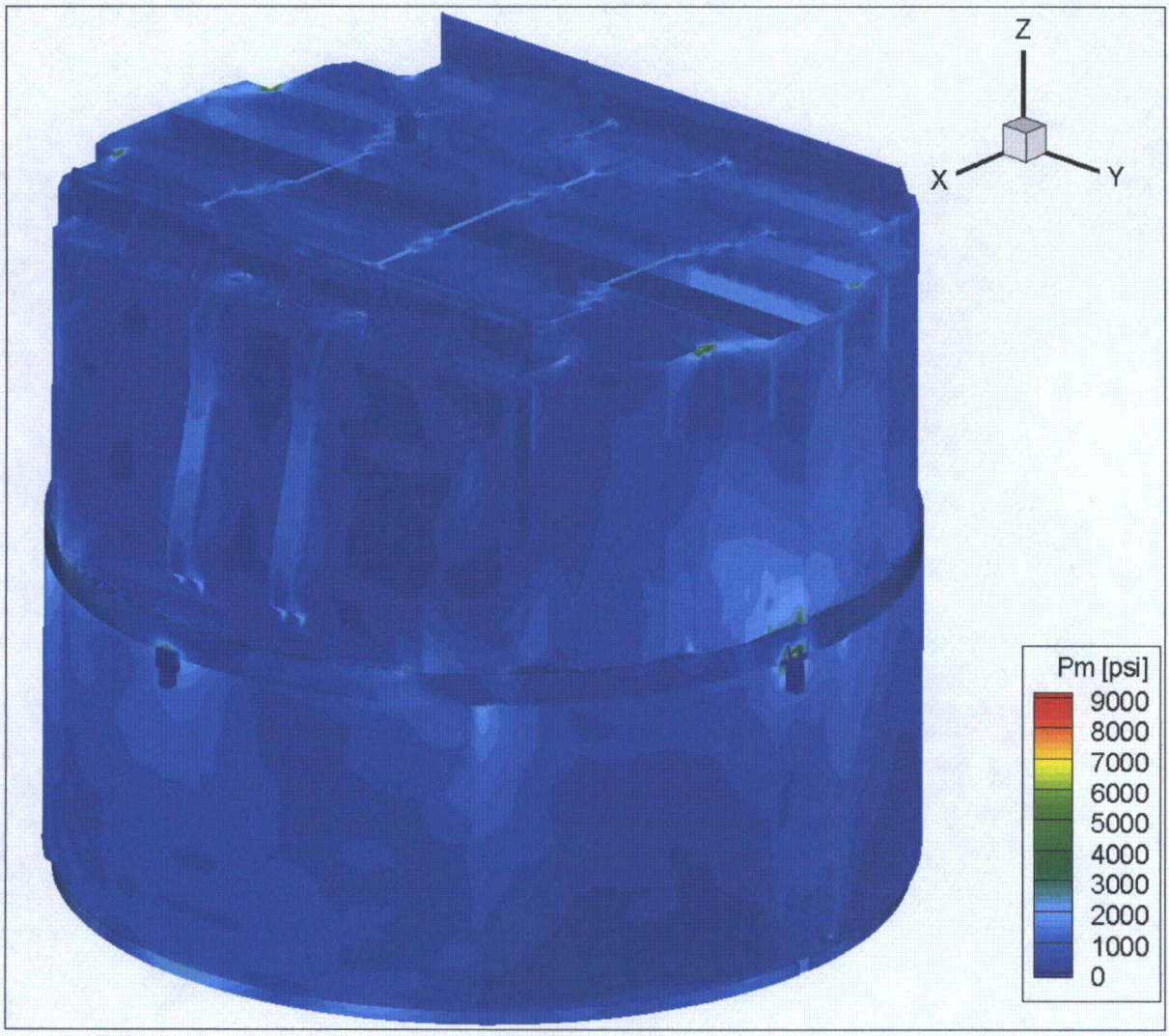

Figure 13a. Contour plot of maximum membrane stress intensity, Pm, for EPU load. The maximum stress intensity is 9001 psi. First view.

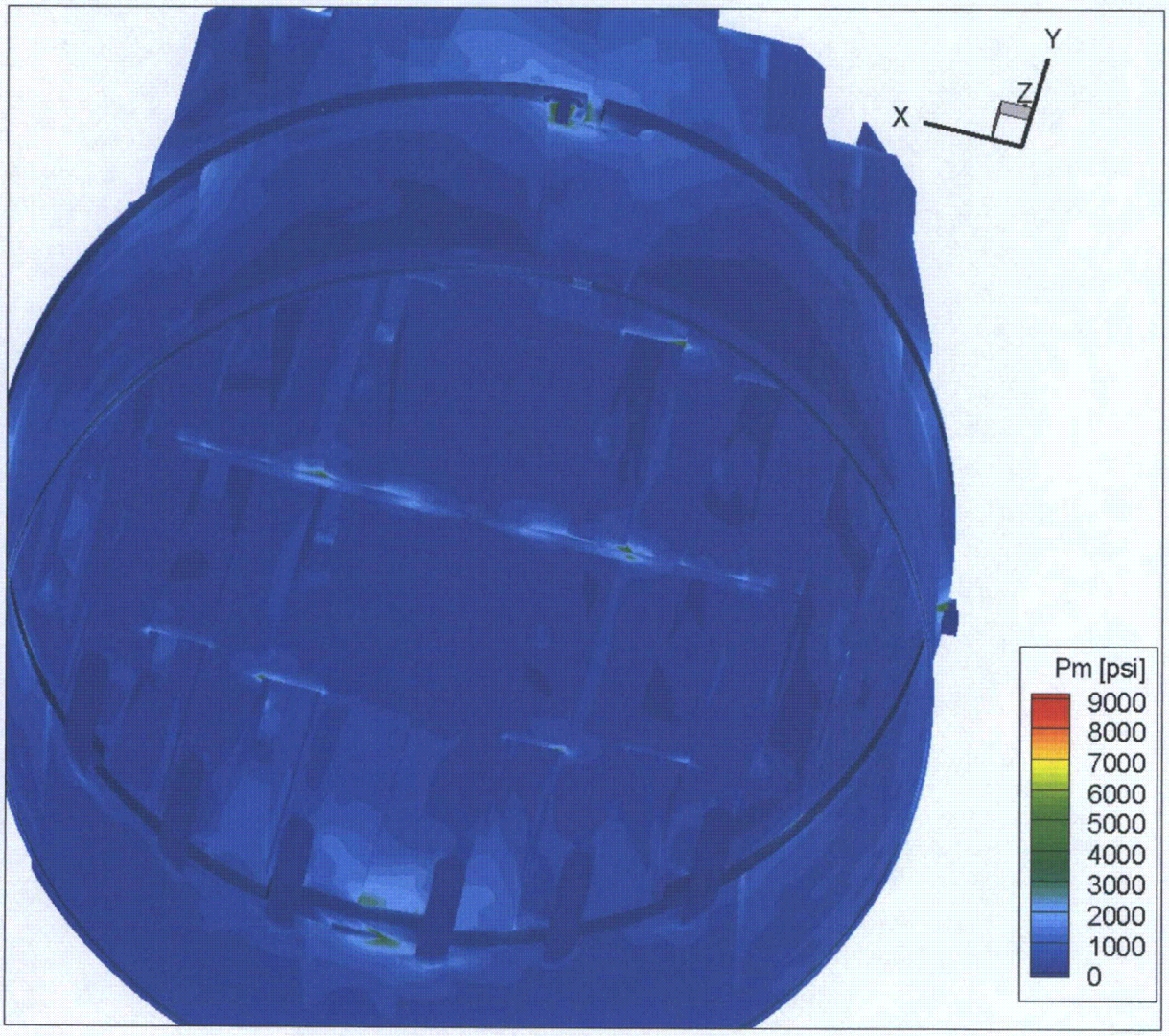

Figure 13b. Contour plot of maximum membrane stress intensity, Pm, for EPU load. Second view from below.

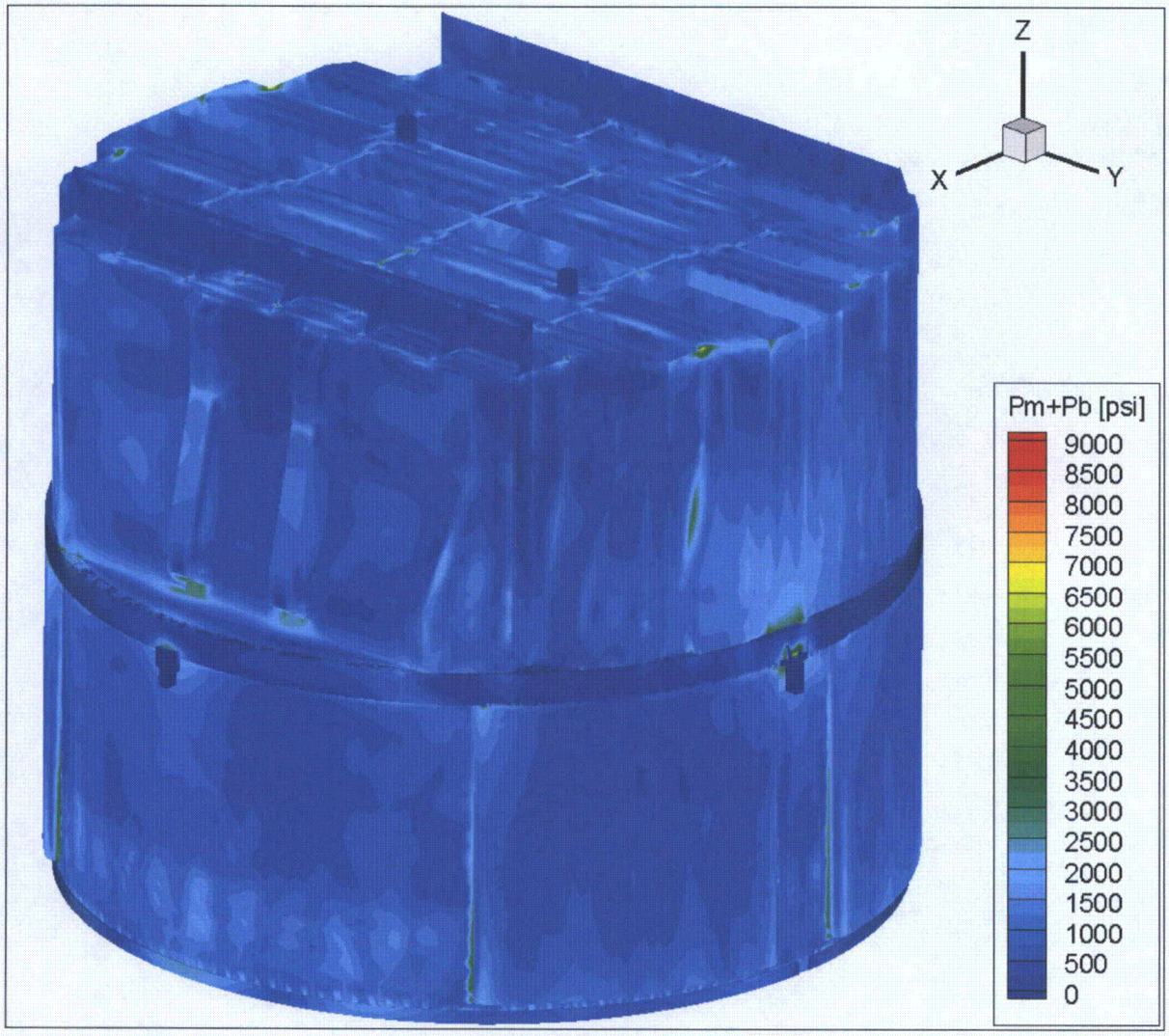

Figure 13c. Contour plot of maximum membrane+bending stress intensity, Pm+Pb, for EPU load. The maximum stress intensity is 9001 psi. First view.

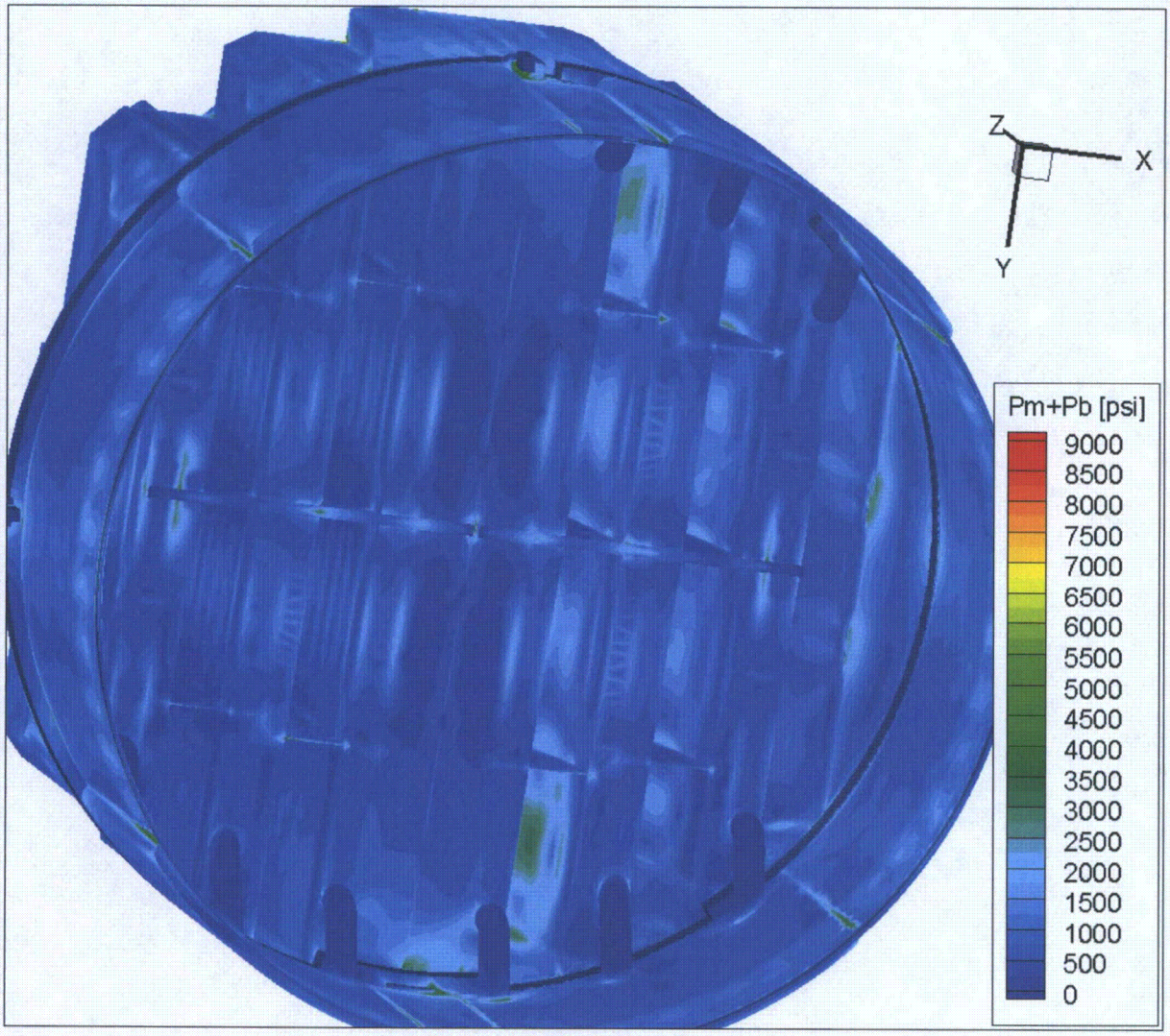

Figure 13d. Contour plot of maximum membrane+bending stress intensity, Pm+Pb, for EPU load. Second view from below.

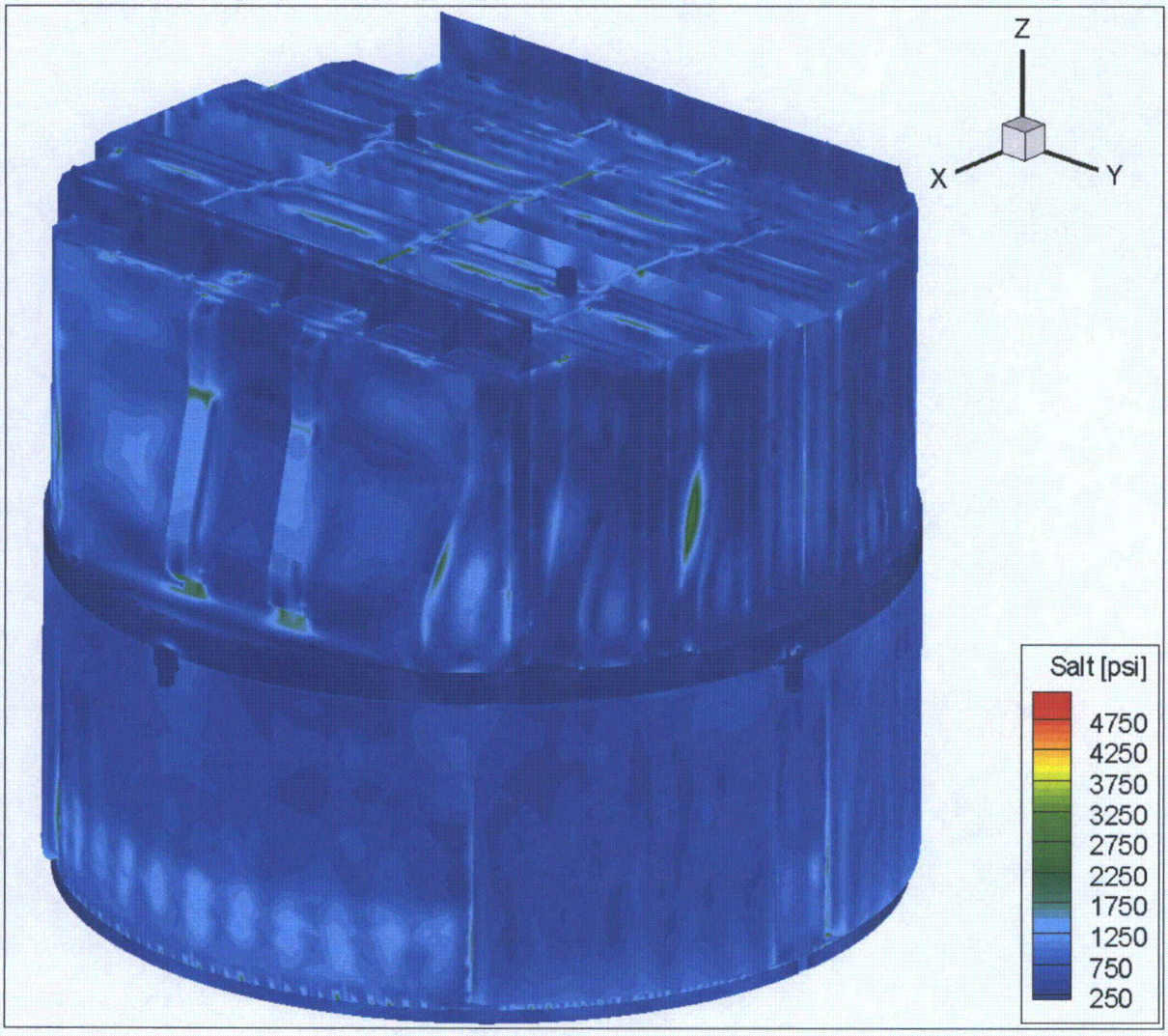

Figure 13e. Contour plot of alternating stress intensity, S_{alt}, for EPU load. The maximum alternating stress intensity is 5110 psi.

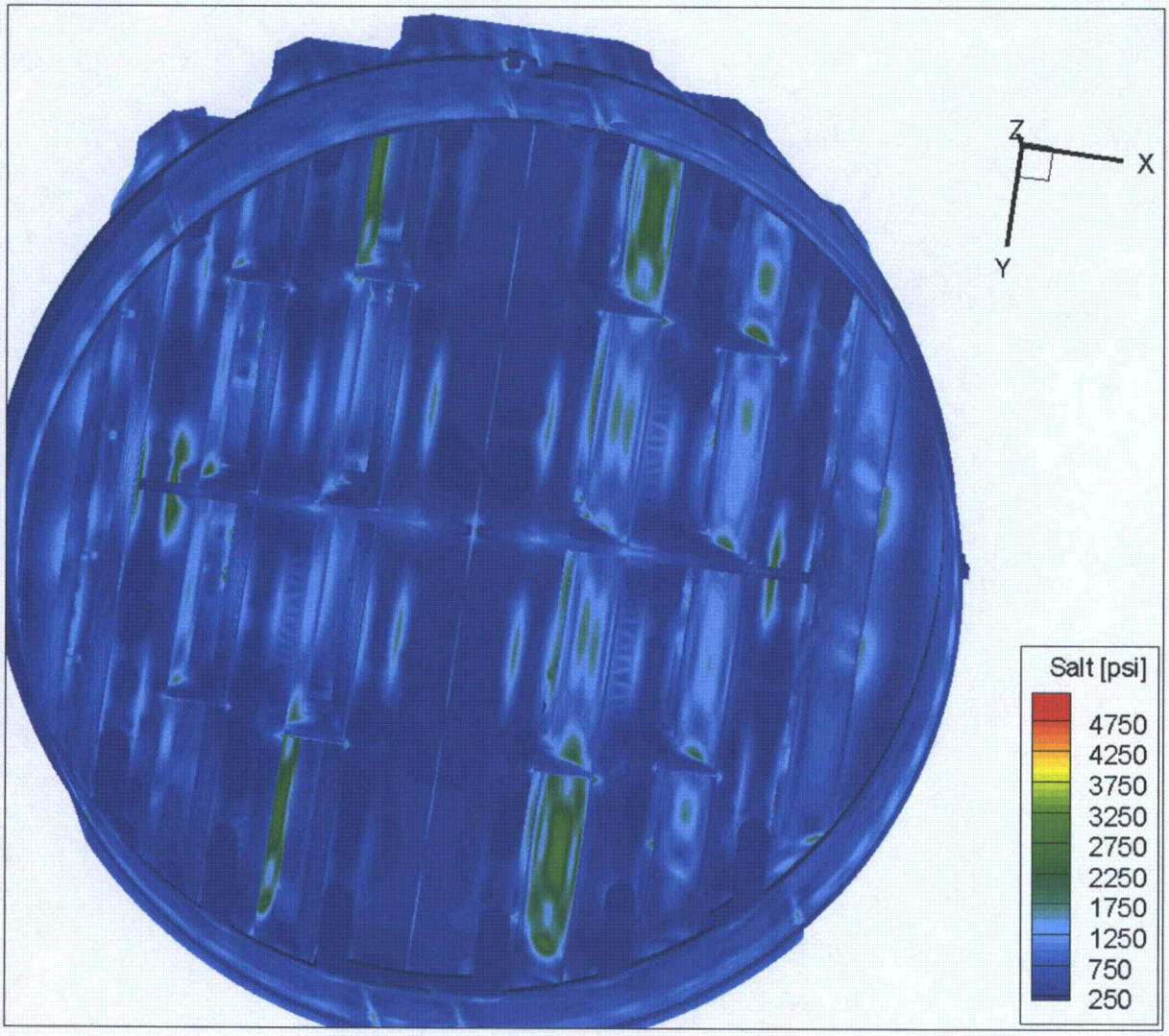

Figure 13f. Contour plot of alternating stress intensity, S_{alt}, for EPU load. Second view from below.

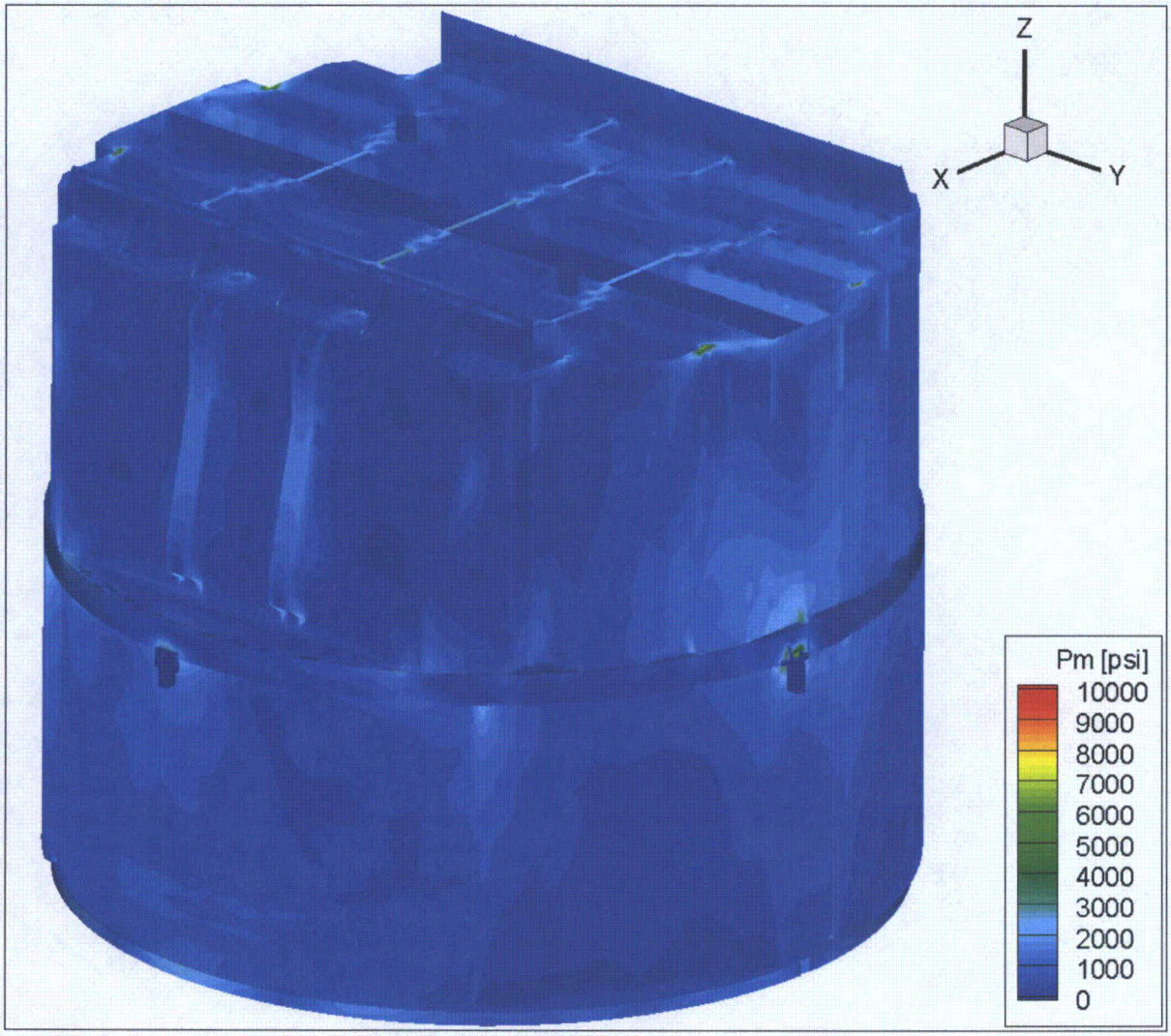

Figure 14a. Contour plot of maximum membrane stress intensity, Pm, for EPU operation with frequency shifts. The recorded stress at a node is the maximum value taken over all frequency shifts. The maximum stress intensity is 10056 psi.

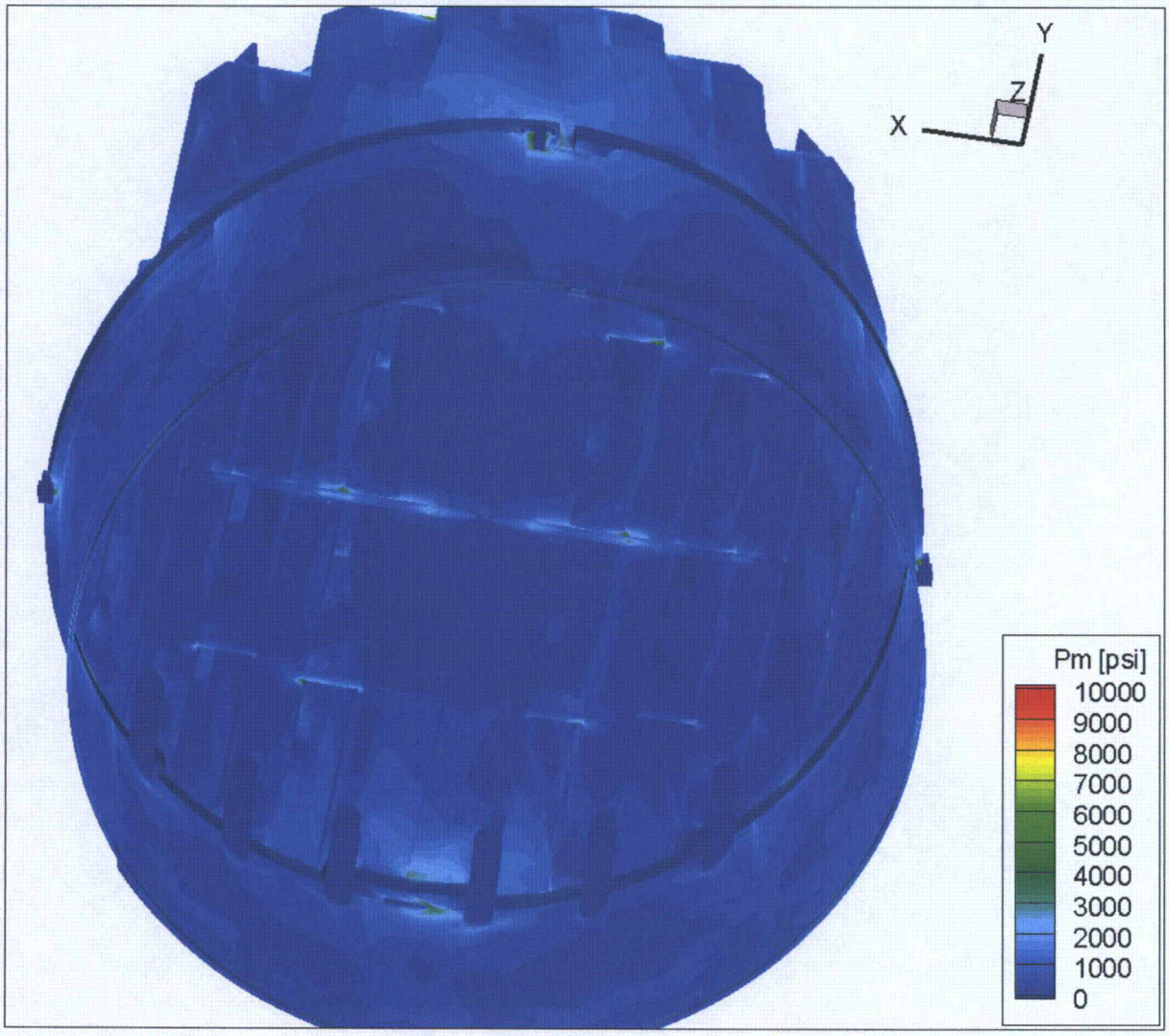

Figure 14b. Contour plot of maximum membrane stress intensity, Pm, for EPU operation with frequency shifts. The recorded stress at a node is the maximum value taken over all frequency shifts. Second view from below.

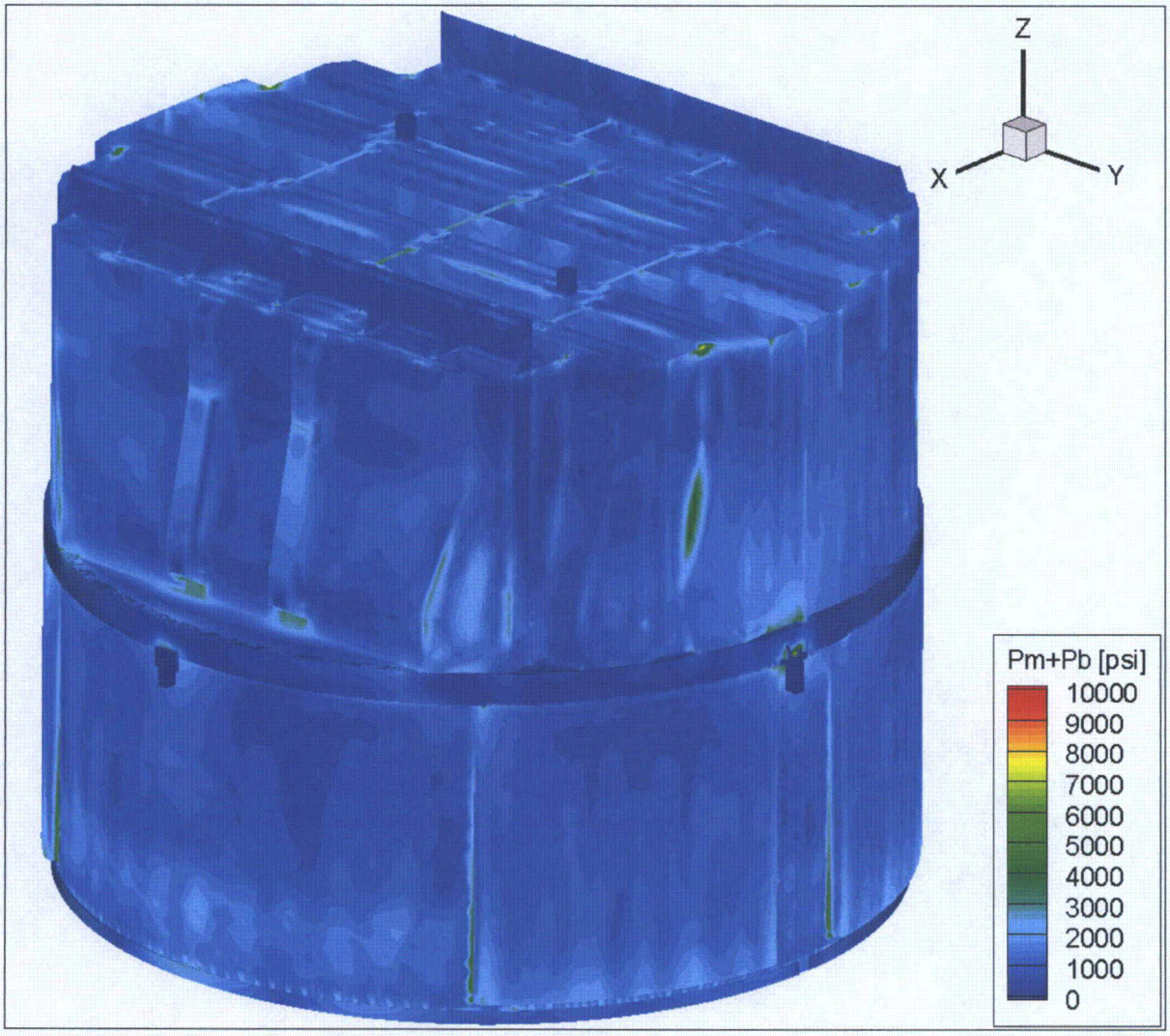

Figure 14c. Contour plot of maximum membrane+bending stress intensity, Pm+Pb, for EPU operation with frequency shifts. The recorded stress at a node is the maximum value taken over all frequency shifts. The maximum stress intensity is 10056 psi. First view.

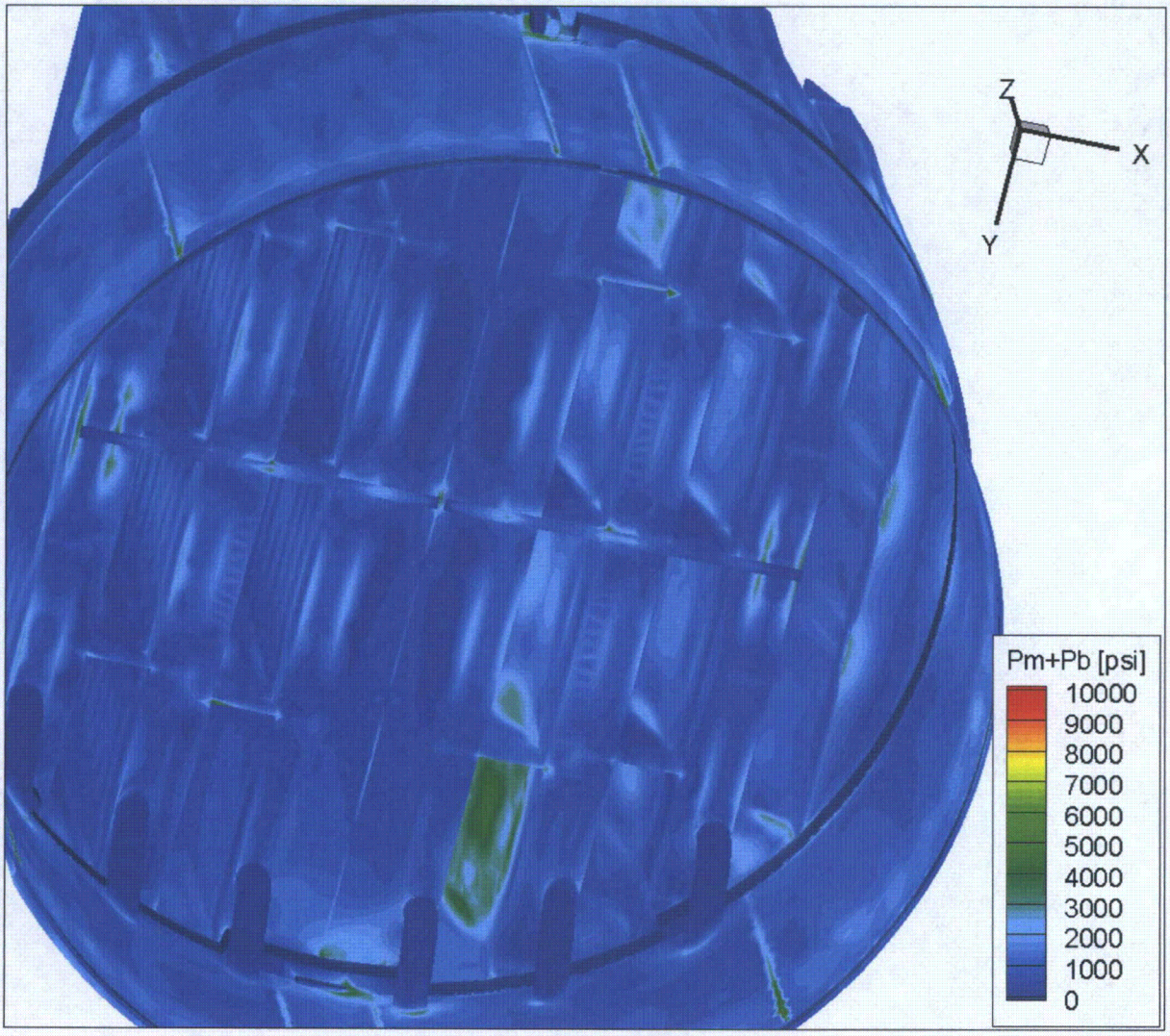

Figure 14d. Contour plot of maximum membrane+bending stress intensity, Pm+Pb, for EPU operation with frequency shifts. This second view from beneath reveals high stress and modal response of interior hood supports.

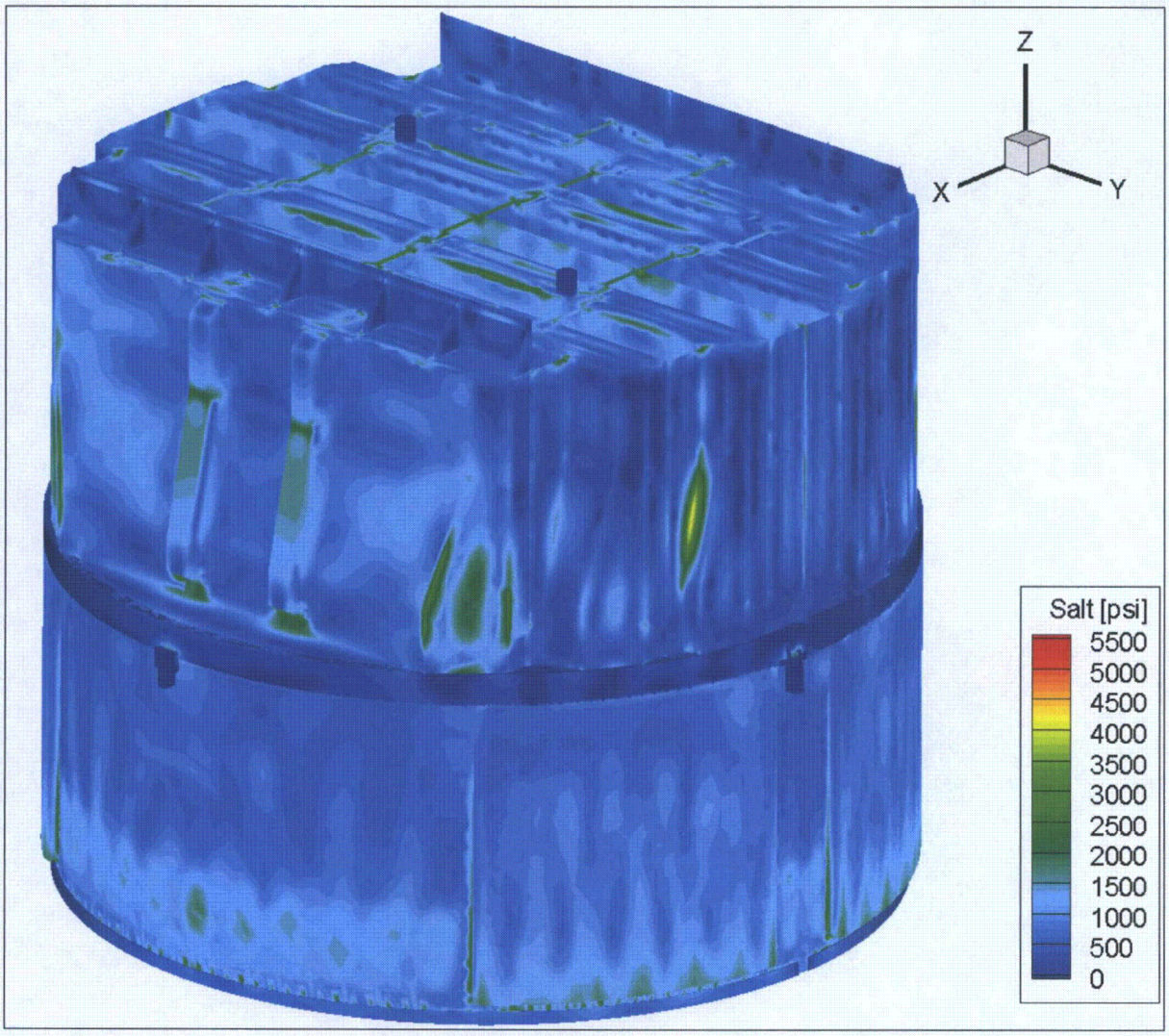

Figure 14e. Contour plot of alternating stress intensity, S_{alt}, for EPU operation with frequency shifts. The recorded stress at a node is the maximum value taken over all frequency shifts. The maximum alternating stress intensity is 5523 psi.

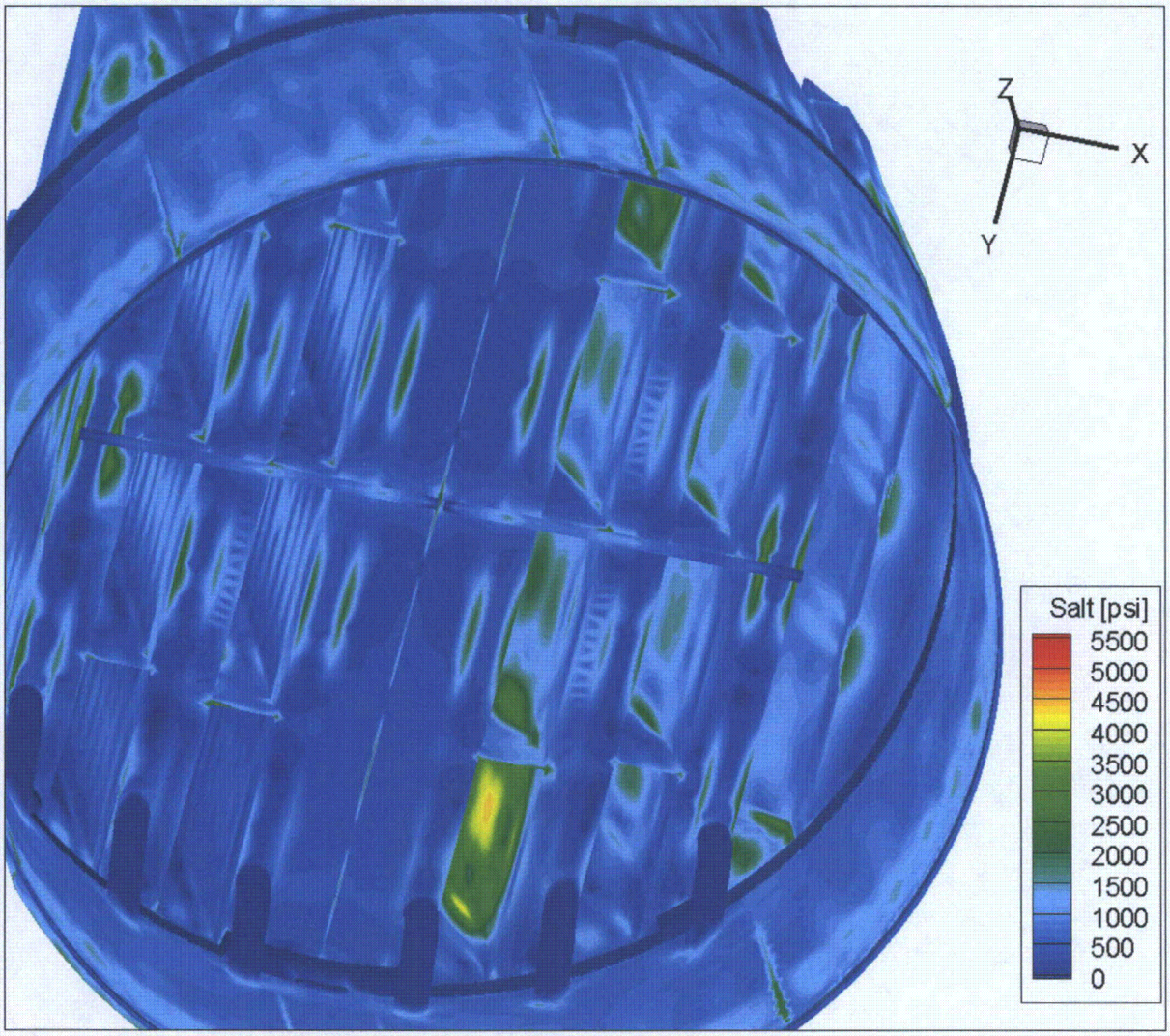

Figure 14f. Contour plot of alternating stress intensity, S_{alt}, for EPU operation with frequency shifts. The recorded stress at a node is the maximum value taken over all frequency shifts. Second view from below.

5.3 Load Combinations and Allowable Stress Intensities

The stress ratios computed for CLTP at nominal frequency and with frequency shifting are listed in Table 9. The stress ratios are grouped according to type (SR-P for maximum membrane and membrane+bending stress, SR-a for alternating stress) and location (away from welds or on a weld). The tabulated nodes are also depicted in Figure 15 (no frequency shift) and Figure 16 (all frequency shifts included). The plots corresponding to maximum stress intensities depict all nodes with stress ratios SR-P≤4, whereas the plots of alternating stress ratios display all nodes with SR-a≤4 or SR-a≤5 as indicated. For convenience the tables now also list the (unshifted) signal frequency where the highest stress contribution occurs. This is estimated from stress Fourier harmonic having the largest amplitude which in most cases corresponds to the PSD peak.

The limiting alternating stress location on the steam dryer occurs at the inmost end of the stitch weld connecting the inner base plate to the T-bar (alternatively referred to as the middle support beam or rib). This weld is undersized and thus is subject to an undersize weld factor of 2.0 in addition to the 1.8 weld factor. However, the T-bar is a secondary structural member in that it is not required to maintain structural integrity (it is believed that the T-bar component was required for transportation and assembly of the two steam dryer halves). While secondary structural members are not required to meet stress fatigue endurance levels it must nevertheless be shown that these members do not produce or become loose parts. This analysis is conducted separately [28]. Briefly, it is shown that a failure in the stitch weld is ultimately self-arresting and that the stresses in the remaining weld fall below allowable levels and the T-bar remains connected to the steam dryer. In the present analysis, the two limiting points (one for the innermost end of each of the two T-bars) are excluded from the list of high stress locations.

If one excludes the T-bar ends from the list of high stress locations on account of its classification as a secondary member, then the limiting alternating stress ratio is SR-a=2.03 and occurs on weld joining the middle closure plate to the inner hood. This limiting alternating stress ratio occurs at the -2.5% frequency shift; at zero shift its values is SR-a=3.00 indicating that the stress changes by 48% as a result of frequency shifting. The leading alternating stress locations in Table 9b generally occur on: (i) components involving the inner hood (the closure plate, lower tie bars and stiffeners); (ii) the intersection between the hood, hood support and base plate; (iii) the bottom of the weld joining the drain channel to the skirt; (iv) the skirt/lower support ring connection; (v) the inner hood/hood support welds; (vi) front ends of the steam dam gusset pads; (vii) the ends of the new tie bars; and (viii) the ends of the vane bank end walls. In addition, the undersized stitch weld joining the T-bar to the base plates appears multiple times. All of these locations lie on welds. Of the 23 locations listed, 15 exhibit the strongest stress response over the 61-65 Hz frequency range. This lies within the range where higher bias and uncertainty have been applied due to range subdivision into new intervals. This adds conservatism since the ACM model has not been recalibrated for the most recent frequency intervals.

The minimum stress ratio due to maximum stress intensity at no frequency shift is SR-P=1.44 and occurs at the top of the middle closure plate connecting to the inner hood; it reduces to 1.39 when all frequency shifts are included.

Finally, the highest stress intensities (and lowest stress ratios) at any frequency shift for the locations in Table 9b are recomputed using the CLTP loads without noise removal and reported in Table 9c. The limiting alternating stress ratio at any frequency shift in this table is SR-a=2.77 and occurs on the bottom of the drain channel/skirt weld. To confirm that this is the limiting node on the dryer, a real time calculation is carried out where the CLTP stresses are computed at: (i) all non-weld nodes having an alternating stress ratio, SR-a<4 at EPU; (ii) all weld nodes with SR-a<3 at EPU and (iii) all weld nodes with SR-a<4 at EPU and dominant frequency in the range 85-138 Hz (only this range is significantly affected by the bump-up factors taking into account frequency shifting). There are 838 such nodes and the limiting alternating stress ratio for these nodes is indeed at node 108329 with the stresses and stress ratios listed in Table 9c. Hence the limiting alternating stress ratio at any frequency shift on the dryer at CLTP with noise retained is SR-a=2.77. This is value used to generating the limit curves. Since acoustic loads scale roughly with the square of the steam flow, another estimate of the EPU limiting stress can be obtained from SR-a=2.77/1.35=2.05. This is slightly higher than the estimate obtained using the bump-up factors. Close agreement is expected since the dominant frequencies lie outside the range where bump-up factors are applied. The conservative estimate of the EPU alternating stress ratio remains SR-a=2.03 as already established above.

In summary, when excluding the T-bar ends as discussed above, the lowest alternating stress ratio at EPU occurs on the weld connecting the inner hood and closure plate at the -2.5% frequency shift. The lowest value at any frequency shift is SR-a=2.03 indicating that stresses are below target levels. The lowest stress ratio associated with a maximum stress is SR-P=1.27. This value is dominated by the static component and is only weakly altered by acoustic loads. Since all the applied loads already account for all end-to-end biases and uncertainties, these values imply that the target stress levels for EPU operation are met.

Table 9a. Locations with minimum stress ratios for EPU conditions with no frequency shift. Stress ratios are grouped according to stress type (maximum – SR-P; or alternating – SR-a) and location (away from a weld or at a weld). Bold text indicates minimum stress ratio of any type on the structure. Locations are depicted in Figure 15.

Stress Ratios at Non-Welds

Stress Ratio	Location	Location (in.) (a)			node(b)	Stress Intensity (psi)			Stress Ratio		Dom. Freq. [Hz.]
		x	y	z		Pm	Pm+Pb	S_{alt}	SR-P	SR-a	
SR-P	1. USR/Seismic Block/Support Part	122.1	-10	-9.5	142984	9001	9001	3055	1.88	4.05	62.3
"	2. USR part/Support/Support Part	7	122.3	-9.5	143092	7648	7648	2379	2.21	5.20	19.3
"	3. Middle Closure Plate	-33.9	-108.4	88.9	6934	6092	6347	1842	2.77	6.71	21.5
"	4. Hood Support	-37.5	59.8	0	9309	5291	5339	3464	3.19	3.57	63.5
SR-a	1. Middle Plate	0	-3	88.9	116595	229	5428	5110	4.67	2.42	63.5
"	2. Middle Plate	0	56.8	88.9	107485	62	4749	4428	5.34	2.79	64.0

See Table 8a for notes (a)-(c) and (1)-(4).

Table 9a (cont.). Locations with minimum stress ratios for EPU conditions with no frequency shift. Stress ratios are grouped according to stress type (maximum – SR-P; or alternating – SR-a) and location (away from a weld or at a weld). Bold text indicates minimum stress ratio of any type on the structure. Locations are depicted in Figure 15.

Stress Ratios Due to Maximum Stress at Welds (SR-P)

Location	Location (in.) (a)			node(b)	Stress Intensity (psi)			Stress Ratio		Dom. Freq. [Hz.]
	x	y	z		Pm	Pm+Pb	S_{alt}	SR-P	SR-a	
1. Top Cover Inner Hood/Middle Closure Plate/Inner Hood	**-31.5**	**-108.4**	**88.9**	**111296**	**6622**	**7713**	**2164**	**1.40**	**4.08**	**21.5**
2. Middle Base Plate/Tbar(c)	41.8	0	0	129303	2793	2836	1519	1.66	2.26	47.5
3. Hood Support/Thin Vane Bank Thin/Inner Base Plate/Vane Bank Section/Tbar(c)	-24	0	0	129259	2378	2392	1254	1.95	2.74	62.6
4. Splice Bar/USR Part	-2.2	-119	0	142959	4098	4098	650	2.27	10.56	59.4
5. Splice Bar/Straddle	6.1	118.8	-12.5	141630	3968	3968	616	2.34	11.15	36.7
6. Middle Base Plate/Hood Support/Inner Hood(2)	39.8	-59.8	0	113046	3849	3910	2583	2.41	2.66	64.1
7. Top Cover Inner Hood/Inner Hood	-31.5	-110.1	88.9	111297	3775	4035	1204	2.46	5.70	21.5
8. New Gusset/Thin Gusset Pad	88.4	0	88.9	111491	3528	3635	2272	2.63	3.02	64.1
9. Middle Base Plate/Hood Support/Middle Hood/Tbar(c)	70.8	0	0	129315	2020	2122	1802	2.73	2.33	110.8
10. Submerged Drain Channel/Skirt	91	-76.7	-97.6	108511	405	4978	1765	2.80	3.89	63.0
11. New Gusset/Thin Gusset Pad	-88.4	-31.4	88.9	123922	3281	3296	2174	2.83	3.16	63.5
12. Hood Support/Inner Hood	-39.8	59.8	2.5	112028	3261	3470	2304	2.85	2.98	63.5
13. Outer Closure Plate/Middle Hood/Middle Top Plate Mod	62.5	-85	88.9	132162	2685	4653	2803	3.00	3.15	64.1

Table 9a (cont.). Locations with minimum stress ratios for EPU conditions with no frequency shift. Stress ratios are grouped according to stress type (maximum – SR-P; or alternating – SR-a) and location (away from a weld or at a weld). Bold text indicates minimum stress ratio of any type on the structure. Locations are depicted in Figure 15.

Alternating Stress Ratios at Welds (SR-a)

Location	Location (in.) (a)			node(b)	Stress Intensity (psi)			Stress Ratio		Dom. Freq. [Hz.]
	x	y	z		Pm	Pm+Pb	S_{alt}	SR-P	SR-a	
1. Middle Base Plate/Vane Bank Thin/Tbar(c)	-77	0	0	129283	1328	3620	3155	3.85	2.18	64.1
2. Middle Base Plate/Tbar(c)	41.8	0	0	129303	2793	2836	1519	1.66	2.26	47.5
3. Submerged Drain Channel/Skirt(1)	-11.5	118.4	-100.5	108329	1447	4289	2946	3.25	2.33	64.1
4. Top Cover Middle Hood/Top Cover Overlap/Top Thick Plate	55	-32.4	88.9	120701	693	3026	2888	4.61	2.38	63.5
5. Hood Support/Middle Hood	66.6	-54.6	38.9	114171	254	2831	2689	4.92	2.55	109.0
6. Middle Base Plate/Hood Support/Inner Hood(2)	39.8	-59.8	0	113046	3849	3910	2583	2.41	2.66	64.1
7. Outer Hood/Hood Assembly/Hood Assembly Base	102	-22.6	4	110736	2739	3530	2569	3.39	2.67	63.5
8. Outer Closure Plate/Middle Hood	62.5	85	88.9	112763	2300	3705	3236	3.76	2.73	61.0
9. Hood Support/Thin Vane Bank/Inner Base Plate/Tbar(c)	-24	0	0	129259	2378	2392	1254	1.95	2.74	62.6
10. Top Cover Inner Hood/Top Cover Overlap/Top Thick Plate	24	46.9	88.9	131616	554	2563	2503	5.44	2.74	63.0
11. Hood Support/Inner Hood	31.6	0	59.2	112591	965	2550	2485	5.47	2.76	58.4
12. Top Cover Inner Hood/Inner Hood/Shell Tie Bar	31.5	65.9	88.9	123496	1855	2699	2484	5.01	2.76	62.3
13. Top Cover Middle Bank/Thick Tie Bar Base	52.8	45.2	88.9	112787	577	2591	2368	5.38	2.90	63.0

See Table 8a for notes (a)-(c) and (1)-(4).

Table 9b. Locations with minimum stress ratios at EPU conditions with frequency shifts. Stress ratios at every node are recorded as the lowest stress ratio identified during the frequency shifts. Stress ratios are grouped according to stress type (maximum – SR-P; or alternating – SR-a) and location (away from a weld or at a weld). Bold text indicates minimum stress ratio of any type on the structure. Locations are depicted in Figure 16.

Stress Ratios at Non-Welds

Stress Ratio	Location	Location (in.) (a)			node(b)	Stress Intensity (psi)			Stress Ratio		% Freq. Shift	Dom. Freq. [Hz.]
		x	y	z		Pm	Pm+Pb	S_{alt}	SR-P	SR-a		
SR-P	1. USR/Seismic Block/Support Part	122.1	-10	-9.5	142984	10056	10056	3863	1.68	3.20	5	14.8
"	2. USR part/Support/Support Part	7	122.3	-9.5	143092	7809	7809	2664	2.16	4.64	2.5	17.9
"	3. Middle Closure Plate	33.9	108.4	88.9	6246	6473	6824	2240	2.61	5.52	7.5	62.6
"	4. Hood Support	-37.5	59.8	0	9309	5977	6001	3943	2.83	3.14	5	62.6
SR-a	1. Mid Plate	0	-3	88.9	116595	290	6281	5523	4.04	2.24	5	61.4
"	2. Mid Plate	0	56.8	88.9	107485	91	5307	5276	4.78	2.34	5	61.4
"	3. Inner hood	35.8	85.1	38.2	46289	323	4470	4367	5.67	2.83	-2.5	61.0

See Table 8a for notes (a)-(c) and (1)-(4).

Table 9b (cont.). Locations with minimum stress ratios at EPU conditions with frequency shifts. Stress ratios at every node are recorded as the lowest stress ratio identified during the frequency shifts. Stress ratios are grouped according to stress type (maximum – SR-P; or alternating – SR-a) and location (away from a weld or at a weld). Bold text indicates minimum stress ratio of any type on the structure. Locations are depicted in Figure 16.

Stress Ratios Due to Maximum Stress at Welds (SR-P)

Location	Location (in.) (a)			node(b)	Stress Intensity (psi)			Stress Ratio		% Freq. Shift	Dom. Freq. [Hz.]
	x	y	z		Pm	Pm+Pb	S_{alt}	SR-P	SR-a		
1. Top Cover Inner Hood/Middle Closure Plate/Inner Hood	**31.5**	**108.4**	**88.9**	**113527**	**7344**	**8085**	**2671**	**1.27**	**3.31**	**7.5**	62.6
2. Middle Base Plate/Tbar(c)	41.8	0	0	129303	2914	2980	1519	1.60	2.26	-10	46.3
3. Hood Support/Vane Bank Thin/Inner Base Plate/Vane Bank Section/Tbar(c)	-24	0	0	129259	2378	2392	1423	1.95	2.41	0	62.6
4. Middle Base Plate/Hood Support/Inner Hood(2)	39.8	-59.8	0	113046	4638	4996	3347	2.00	2.05	7.5	62.6
5. Splice Bar/USR Part	-2.2	-119	0	142959	4270	4270	756	2.18	9.08	7.5	33.7
6. Splice Bar/Straddle	6.1	118.8	-12.5	141630	4137	4137	760	2.25	9.04	-2.5	61.6
7. New Gusset/Thin Gusset Pad	88.4	0	88.9	111491	4121	4150	2781	2.26	2.47	10	45.8
8. Top Cover Inner Hood/Inner Hood	-31.5	-110.1	88.9	111297	4001	4260	1502	2.32	4.57	5	56.0
9. Submerged Drain Channel/Skirt	91	-76.7	-97.6	108511	488	5848	2617	2.38	2.62	7.5	62.6
10. Outer Closure Plate/Middle Hood	-62.5	85	88.9	125852	3399	5741	3531	2.43	2.50	10	62.6
11. Hood Support/Inner Hood	-39.8	59.8	2.5	112028	3638	3783	2619	2.56	2.62	5	62.6
12. Submerged Drain Channel /Skirt	-11.5	118.4	-97.6	108332	417	5418	3204	2.57	2.14	10	62.6
13. New Gusset/Thin Gusset Pad	88.4	-31.4	88.9	132301	3575	3598	2292	2.60	3.00	10	45.8
14. Middle Base Plate/Hood Support/Middle Hood/Tbar(c)	70.8	0	0	129315	2341	2462	1945	2.68	2.15	2.5	61.5
15. Submerged Drain Channel /Skirt	91	-76.7	-86.8	108522	539	4896	2555	2.85	2.69	7.5	64.5
16. Outer Closure Plate/Closure Plate Mod	65.5	-85	88.9	110531	2639	4851	2503	2.87	2.74	10	62.6
17. Submerged Drain Channel /Skirt(1)	11.5	-118.4	-100.5	108481	1445	4715	3306	2.96	2.08	10	63.8
18. Submerged Drain Channel /Skirt(1)	91	76.7	-100.5	108562	758	4606	2448	3.03	2.81	10	62.6

See Table 8a for notes (a)-(c) and (1)-(4).

Table 9b (cont.). Locations with minimum stress ratios at EPU conditions with frequency shifts. Stress ratios at every node are recorded as the lowest stress ratio identified during the frequency shifts. Stress ratios are grouped according to stress type (maximum – SR-P; or alternating – SR-a) and location (away from a weld or at a weld). Bold text indicates minimum stress ratio of any type on the structure. Locations are depicted in Figure 16.

Alternating Stress Ratios at Welds (SR-a)

Location	Location (in.) (a)			node(b)	Stress Intensity (psi)			Stress Ratio		% Freq. Shift	Dom. Freq. [Hz.]
	x	y	z		Pm	Pm+Pb	S_{alt}	SR-P	SR-a		
1. Middle Closure Plate/Inner Hood	35.8	108.4	38	113478	921	4461	4361	3.13	2.03	-2.5	53.5
2. Middle Base Plate/Vane Bank Thin/Tbar(c)	-77	0	0	129283	1328	3873	3352	3.6	2.05	2.5	56.9
3. Middle Base Plate/Hood Support/Inner Hood(2)	39.8	-59.8	0	113046	4638	4996	3347	2.00	2.05	7.5	62.6
4. Submerged Drain Channel/Skirt(1)	-11.5	118.4	-100.5	108329	1504	4612	3331	3.02	2.06	10	63.5
5. Bottom Perf. Entry/Outer End Wall/Outer Side Panel/Vane Bank Mod	-86	85	24	109919	531	3401	3271	4.10	2.1	10	136.5
6. Submerged Drain Channel/Skirt	11.5	-118.4	-97.6	108484	465	5192	3240	2.69	2.12	7.5	110.8
7. Hood Support/Inner Hood	-31.6	0	59.2	111325	1204	3363	3068	4.15	2.24	7.5	62.6
8. Middle Base Plate/Tbar(c)	41.8	0	0	129303	2914	2980	1519	1.60	2.26	0	46.3
9. Inner Hood/Middle Closure Plate/ Top Cover	-31.5	108.4	88.9	112248	6902	6942	3898	1.35	2.27	7.5	62.6
10. Mid Bottom Perf Exit/Mid Top Perf. Exit/Tie Bar(3)	-77	-9.6	62.9	118086	327	3032	3023	4.60	2.27	2.5	63.0
11. Top Cover Middle Hood/Top Cover Overlap/Top Thick Plate	55	-32.4	88.9	120701	780	3188	3022	4.37	2.27	-5	111.0
12. Middle Base Plate/Vane Bank Thin	-86	-7.2	0	126035	540	3286	3009	4.24	2.28	5	61.3
13. Outer End Wall Ext/Outer End Wall	-94	76.4	0	108815	926	3186	2998	4.38	2.29	10	136.5
14. Hood Support/Inner Hood(4)	35.2	59.8	41.3	113288	458	2993	2975	4.66	2.31	-2.5	53.5
15. Lower Support Ring (LSR)/Submerged Skirt	-119	-0.6	-103.5	130246	892	3124	2973	4.46	2.31	-5	61.4
16. Vane Bank/Thick Vane Bank	-86	-28.7	12.1	115685	339	3082	2965	4.52	2.32	7.5	61.3

See Table 8a for notes (a)-(c) and (1)-(4).

Table 9b (cont.). Locations with minimum stress ratios at EPU conditions with frequency shifts. Stress ratios at every node are recorded as the lowest stress ratio identified during the frequency shifts. Stress ratios are grouped according to stress type (maximum – SR-P; or alternating – SR-a) and location (away from a weld or at a weld). Bold text indicates minimum stress ratio of any type on the structure. Locations are depicted in Figure 16.

Alternating Stress Ratios at Welds (SR-a)

Location	Location (in.) (a)			node(b)	Stress Intensity (psi)			Stress Ratio		% Freq. Shift	Dom. Freq. [Hz.]
	x	y	z		Pm	Pm+Pb	S_{alt}	SR-P	SR-a		
17. Top Cover Inner Bank/Top Thick Plate/Shell Tie Bar	-15	-3.2	88.9	128889	2777	3926	2946	3.35	2.33	7.5	62.6
18. Outer Closure Plate/Middle Hood/Middle Top Plate Mod/Closure	62.5	85	88.9	112763	2681	4185	3740	3.33	2.36	7.5	62.6
19. Outer Hood/Hood Assembly/Hood Assembly Base	-102	22.6	4	111790	2864	3912	2907	3.25	2.36	5	63.5
20. LSR/Submerged Skirt	91.2	-76.4	-103.5	130724	322	4422	2903	3.15	2.37	10	63.2
21. Top Cover Inner Hood/Inner Hood	-31.5	28	88.9	111874	872	2968	2852	4.7	2.41	10	62.6
22. Hood Support/Vane Bank Thin/Inner Cover Plate/Vane Bank Section/Tbar(c)	-24	0	0	129259	2378	2392	1423	1.95	2.41	7.5	62.6
23. LSR/Submerged Skirt	83	85.3	-103.5	130633	412	3256	2816	4.28	2.44	-5	61.4

See Table 8a for notes (a)-(c) and (1)-(4).

Table 9c. Minimum stress ratios at any frequency shift for the nodes listed in Table 9b computed at CLTP conditions. Locations are depicted in Figure 16.

Stress Ratios at Non-Welds

Stress Ratio	Location	Location (in.) (a)			node(b)	Stress Intensity (psi)			Stress Ratio		% Freq. Shift	Dom. Freq. [Hz.]
		x	y	z		Pm	Pm+Pb	S_{alt}	SR-P	SR-a		
SR-P	1. USR/Seismic Block/Support Part	122.1	-10	-9.5	142984	8847	8847	2761	1.91	4.48	5	14.8
"	2. USR part/Support/Support Part	7	122.3	-9.5	143092	7174	7174	1977	2.36	6.26	2.5	19.3
"	3. Middle Closure Plate	33.9	108.4	88.9	6246	5949	6297	1692	2.84	7.31	7.5	62.6
"	4. Hood Support	-37.5	59.8	0	9309	4778	4795	2920	3.54	4.23	5	62.6
SR-a	1. Mid Plate	0	-3	88.9	116595	250	4514	4100	5.62	3.02	2.5	63.0
"	2. Mid Plate	0	56.8	88.9	107485	67	3899	3883	6.50	3.18	5	61.4
"	3. Inner hood	35.8	85.1	38.2	46289	269	3218	3151	7.88	3.92	-2.5	60.7

See Table 8a for notes (a)-(c) and (1)-(4).

Table 9c (cont.). Minimum stress ratios at any frequency shift for the nodes listed in Table 9b computed at CLTP conditions. Locations are depicted in Figure 16.

Stress Ratios Due to Maximum Stress at Welds (SR-P)

Location	Location (in.) (a)			node(b)	Stress Intensity (psi)			Stress Ratio		% Freq. Shift	Dom. Freq. [Hz.]
	x	y	z		Pm	Pm+Pb	S_{alt}	SR-P	SR-a		
1. Top Cover Inner Hood/Middle Closure Plate/Inner Hood	**31.5**	**108.4**	**88.9**	**113527**	**6657**	**7340**	**1907**	**1.40**	**4.62**	**7.5**	**62.6**
2. Middle Base Plate/Tbar(c)	41.8	0	0	129303	2530	2581	1096	1.84	3.13	-5	48.0
3. Hood Support/Vane Bank Thin/Inner Base Plate/Vane Bank Section/Tbar(c)	-24	0	0	129259	1992	2005	1042	2.33	3.30	0	62.6
4. Middle Base Plate/Hood Support/Inner Hood(2)	39.8	-59.8	0	113046	3681	3944	2430	2.52	2.83	7.5	62.6
5. Splice Bar/USR Part	-2.2	-119	0	142959	4065	4065	557	2.29	12.33	7.5	33.7
6. Splice Bar/Straddle	6.1	118.8	-12.5	141630	3909	3909	558	2.38	12.30	-2.5	61.6
7. New Gusset/Thin Gusset Pad	88.4	0	88.9	111491	3295	3306	1946	2.82	3.53	10	62.6
8. Top Cover Inner Hood/Inner Hood	-31.5	-110.1	88.9	111297	3667	3936	1126	2.53	6.10	5	62.6
9. Submerged Drain Channel/Skirt	91	-76.7	-97.6	108511	398	5046	1868	2.76	3.68	7.5	45.1
10. Outer Closure Plate/Middle Hood	-62.5	85	88.9	125852	2675	4546	2483	3.07	3.55	10	62.6
11. Hood Support/Inner Hood	-39.8	59.8	2.5	112028	2901	3007	1938	3.20	3.54	5	62.6
12. Submerged Drain Channel /Skirt	-11.5	118.4	-97.6	108332	310	4543	2359	3.07	2.91	10	45.0
13. New Gusset/Thin Gusset Pad	88.4	-31.4	88.9	132301	2800	2803	1603	3.32	4.29	10	45.8
14. Middle Base Plate/Hood Support/Middle Hood/Tbar(c)	70.8	0	0	129315	1802	1906	1368	3.31	3.04	-5	62.6
15. Submerged Drain Channel /Skirt	91	-76.7	-86.8	108522	380	4234	1925	3.29	3.57	7.5	46.3
16. Outer Closure Plate/Closure Plate Mod	65.5	-85	88.9	110531	2129	3946	1767	3.53	3.89	10	62.6
17. Submerged Drain Channel /Skirt(1)	11.5	-118.4	-100.5	108481	1063	3815	2435	3.65	2.82	10	63.8
18. Submerged Drain Channel /Skirt(1)	91	76.7	-100.5	108562	581	3824	1778	3.65	3.86	10	62.2

See Table 8a for notes (a)-(c) and (1)-(4).

Table 9c (cont.). Minimum stress ratios at any frequency shift for the nodes listed in Table 9b computed at CLTP conditions. Locations are depicted in Figure 16.

Alternating Stress Ratios at Welds (SR-a)

Location	Location (in.) (a)			node(b)	Stress Intensity (psi)			Stress Ratio		% Freq. Shift	Dom. Freq. [Hz.]
	x	y	z		Pm	Pm+Pb	S_{alt}	SR-P	SR-a		
1. Middle Closure Plate/Inner Hood	35.8	108.4	38	113478	836	3271	3151	4.26	2.79	-2.5	60.7
2. Middle Base Plate/Vane Bank Thin/Tbar(c)	-77	0	0	129283	1105	2913	2319	4.79	2.96	2.5	61.4
3. Middle Base Plate/Hood Support/Inner Hood(2)	39.8	-59.8	0	113046	3681	3944	2430	2.52	2.83	7.5	62.6
4. Submerged Drain Channel/Skirt(1)	-11.5	118.4	-100.5	108329	1141	3780	2476	3.69	2.77	10	63.5
5. Bottom Perf. Entry/Outer End Wall/Outer Side Panel/Vane Bank Mod	-86	85	24	109919	461	2546	2388	5.48	2.88	10	136.5
6. Submerged Drain Channel/Skirt	11.5	-118.4	-97.6	108484	314	4265	2318	3.27	2.96	7.5	46.3
7. Hood Support/Inner Hood	-31.6	0	59.2	111325	902	2462	2252	5.66	3.05	7.5	63.5
8. Middle Base Plate/Tbar(c)	41.8	0	0	129303	2530	2581	1096	1.84	3.13	-2.5	52.2
9. Inner Hood/Middle Closure Plate/ Top Cover	-31.5	108.4	88.9	112248	5747	5813	2777	1.62	3.17	7.5	62.6
10. Mid Bottom Perf Exit/Mid Top Perf. Exit/Tie Bar(3)	-77	-9.6	62.9	118086	249	2226	2219	6.26	3.10	2.5	63.0
11. Top Cover Middle Hood/Top Cover Overlap/Top Thick Plate	55	-32.4	88.9	120701	589	2144	2032	6.50	3.38	-7.5	130.0
12. Middle Base Plate/Vane Bank Thin	-86	-7.2	0	126035	440	2463	2233	5.66	3.08	5	64.1
13. Outer End Wall Ext/Outer End Wall	-94	76.4	0	108815	867	2340	2169	5.96	3.17	10	136.5
14. Hood Support/Inner Hood(4)	35.2	59.8	41.3	113288	355	2201	2146	6.34	3.20	-2.5	60.7
15. Lower Support Ring (LSR)/Submerged Skirt	-119	-0.6	-103.5	130246	776	2427	2165	5.74	3.17	-5	61.4
16. Vane Bank/Thick Vane Bank	-86	-28.7	12.1	115685	279	2312	2191	6.03	3.13	7.5	62.6

See Table 8a for notes (a)-(c) and (1)-(4).

Table 9c (cont.). Minimum stress ratios at any frequency shift for the nodes listed in Table 9b computed at CLTP conditions. Locations are depicted in Figure 16.

Alternating Stress Ratios at Welds (SR-a)

Location	Location (in.) (a)			node(b)	Stress Intensity (psi)			Stress Ratio		% Freq. Shift	Dom. Freq. [Hz.]
	x	y	z		Pm	Pm+Pb	S_{alt}	SR-P	SR-a		
17. Top Cover Inner Bank/Top Thick Plate/Shell Tie Bar	-15	-3.2	88.9	128889	2193	3157	2155	4.24	3.19	7.5	62.6
18. Submerged Drain Channel/Skirt	62.5	85	88.9	112763	1877	2914	2614	4.78	3.37	7.5	62.6
19. Outer Hood/Hood Assembly/Hood Assembly Base	-102	22.6	4	111790	2249	3162	2089	4.13	3.29	5	63.5
20. LSR/Submerged Skirt	91.2	-76.4	-103.5	130724	232	3660	2159	3.81	3.18	10	63.2
21. Top Cover Inner Hood/Inner Hood	-31.5	28	88.9	111874	719	2157	2086	6.46	3.29	10	62.6
22. Hood Support/Vane Bank Thin/Inner Cover Plate/Vane Bank Section/Tbar(c)	-24	0	0	129259	1992	2005	1042	2.33	3.30	7.5	62.6
23. LSR/Submerged Skirt	83	85.3	-103.5	130633	303	2316	1973	6.02	3.48	-5	61.4

See Table 8a for notes (a)-(c) and (1)-(4).

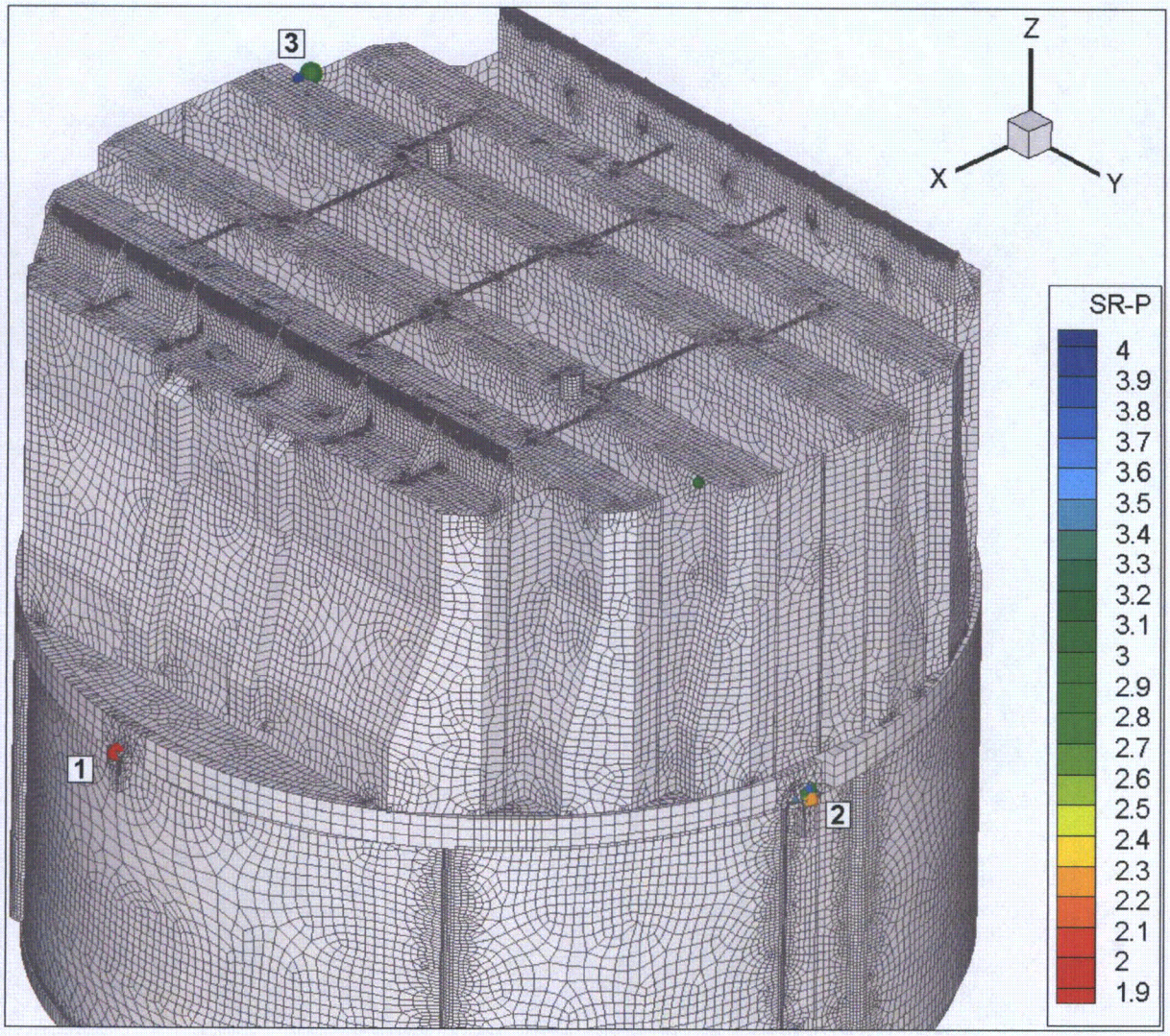

Figure 15a. Locations of smallest maximum stress ratios, SR-P≤4, at non-welds for nominal EPU operation. Numbers refers to the enumerated locations for SR-P values at non-welds in Table 9a. First view showing locations 1-3.

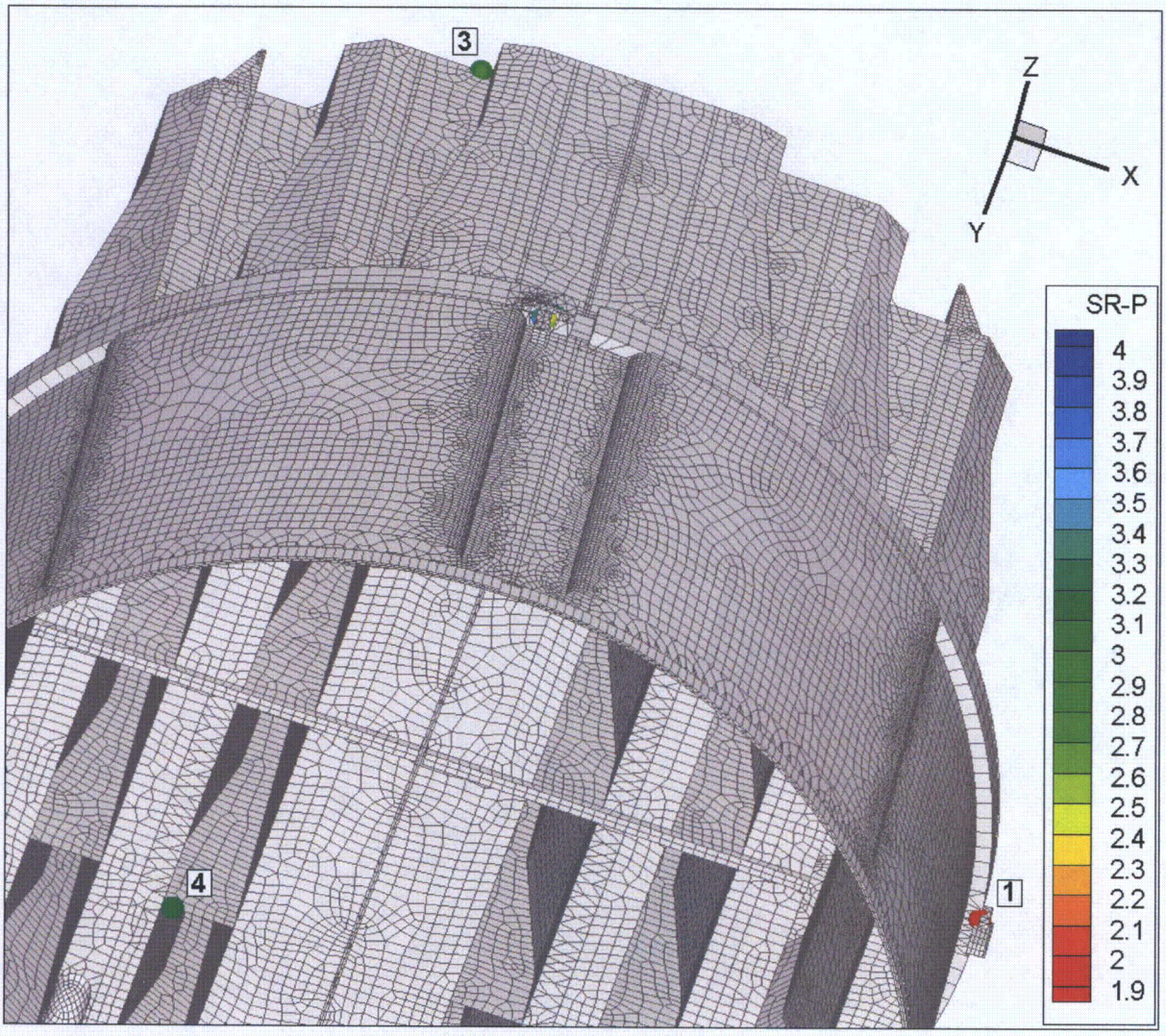

Figure 15b. Locations of smallest maximum stress ratios, SR-P≤4, at non-welds for nominal EPU operation. Numbers refers to the enumerated locations for SR-P values at non-welds in Table 9a. Second view showing locations 1, 3 and 4.

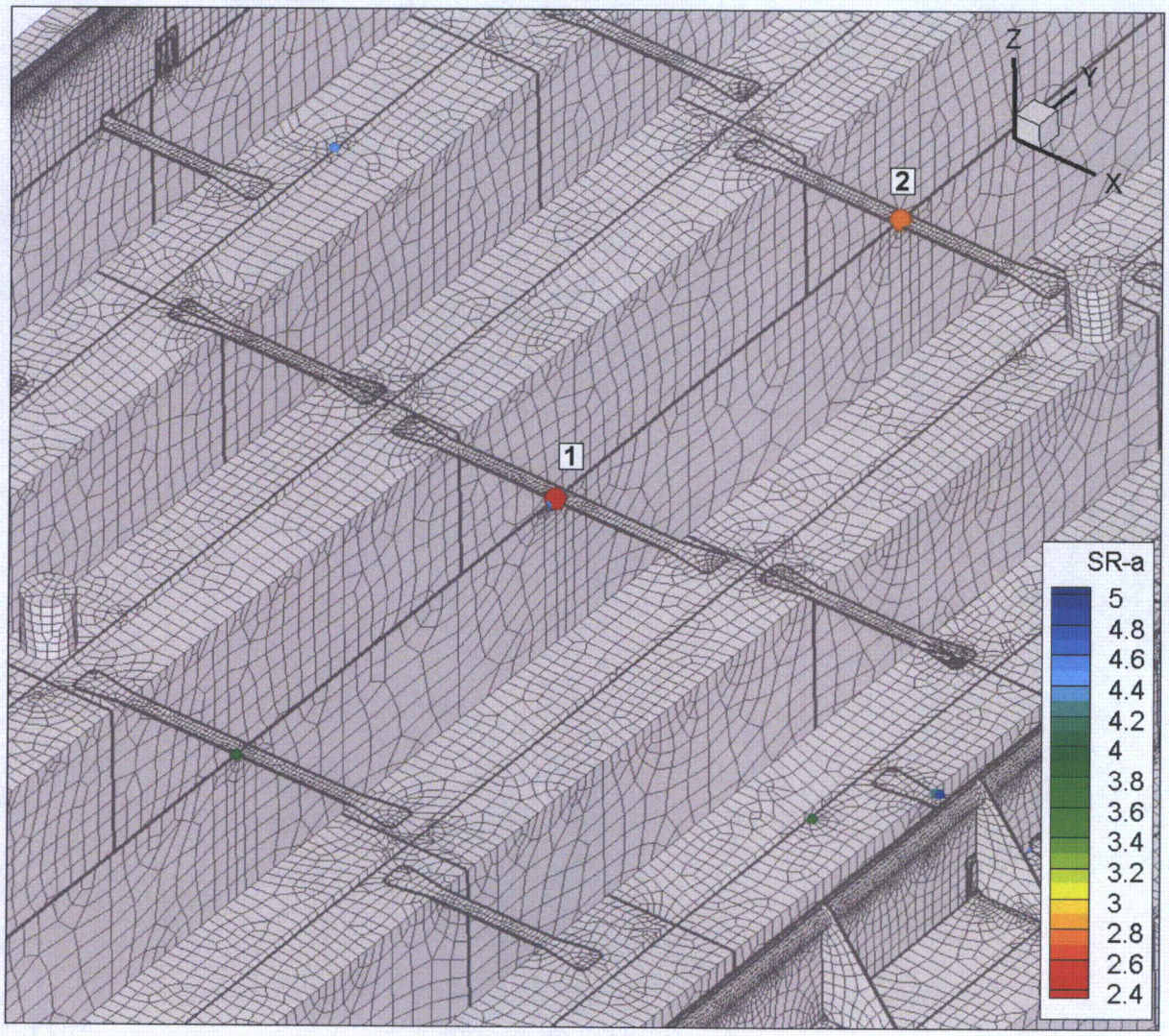

Figure 15c. Locations of smallest alternating stress ratios, SR-a≤5, at non-welds for nominal EPU operation. Numbers refers to the enumerated locations for SR-a values at non-welds in Table 9a.

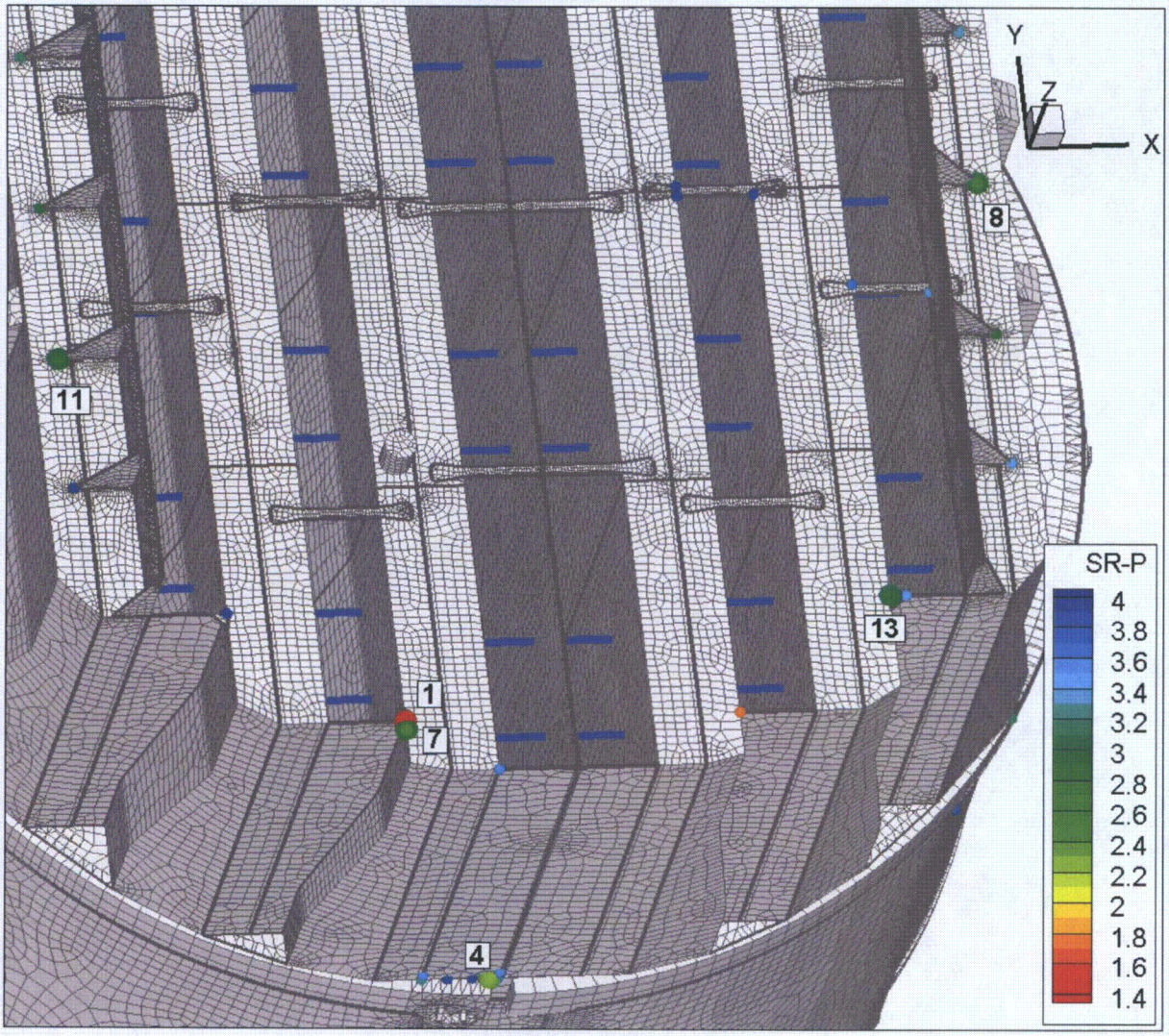

Figure 15d. Locations of smallest maximum stress ratios, SR-P≤4, at welds for nominal EPU operation. Numbers refer to the enumerated locations for SR-P values at welds in Table 9a. First view showing locations 1, 4, 7, 8, 11 and 13.

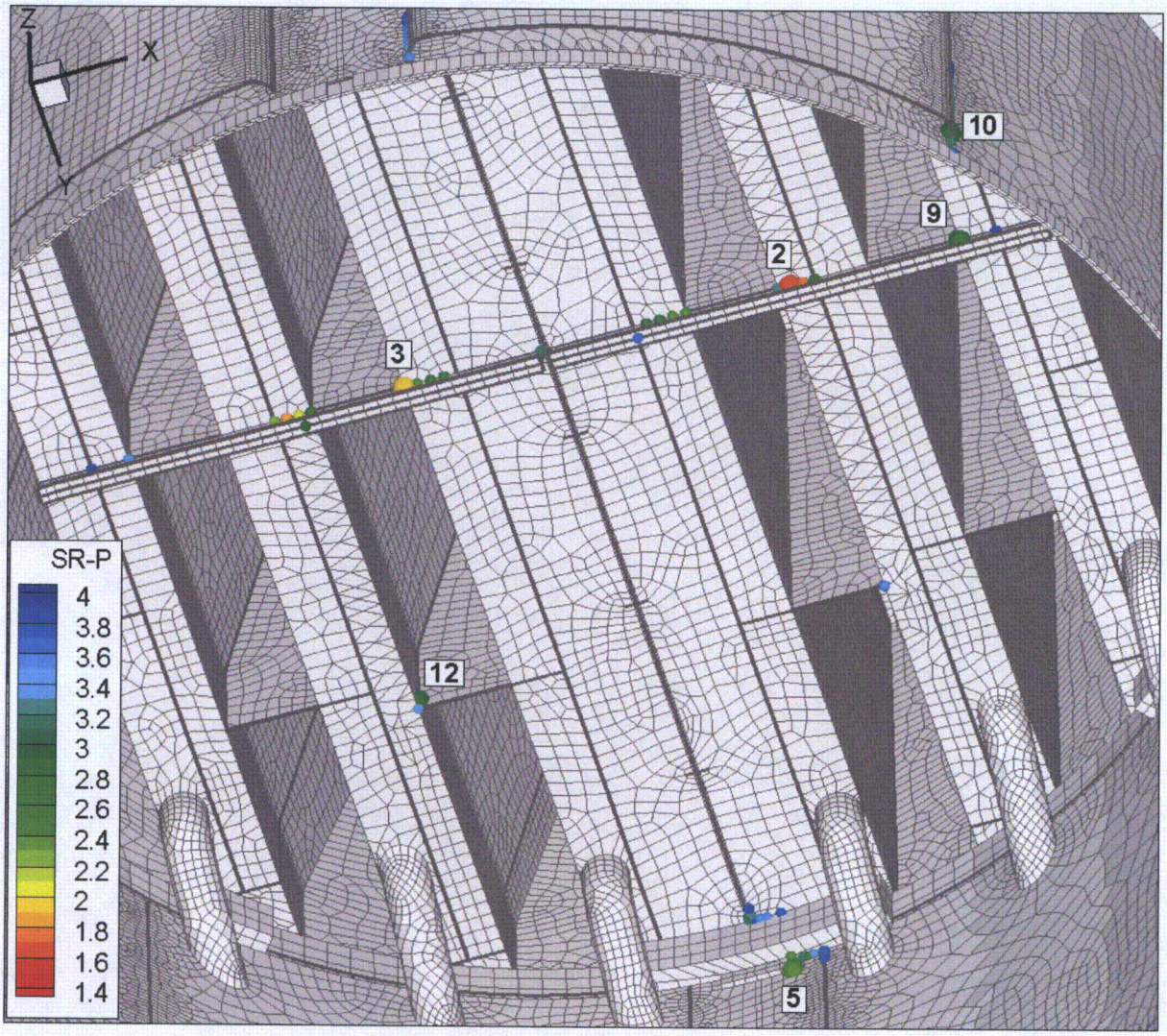

Figure 15e. Locations of smallest maximum stress ratios, SR-P≤4, at welds for nominal EPU operation. Numbers refer to the enumerated locations for SR-P values at welds in Table 9a. Third view showing locations 2, 3, 5, 9, 10 and 12.

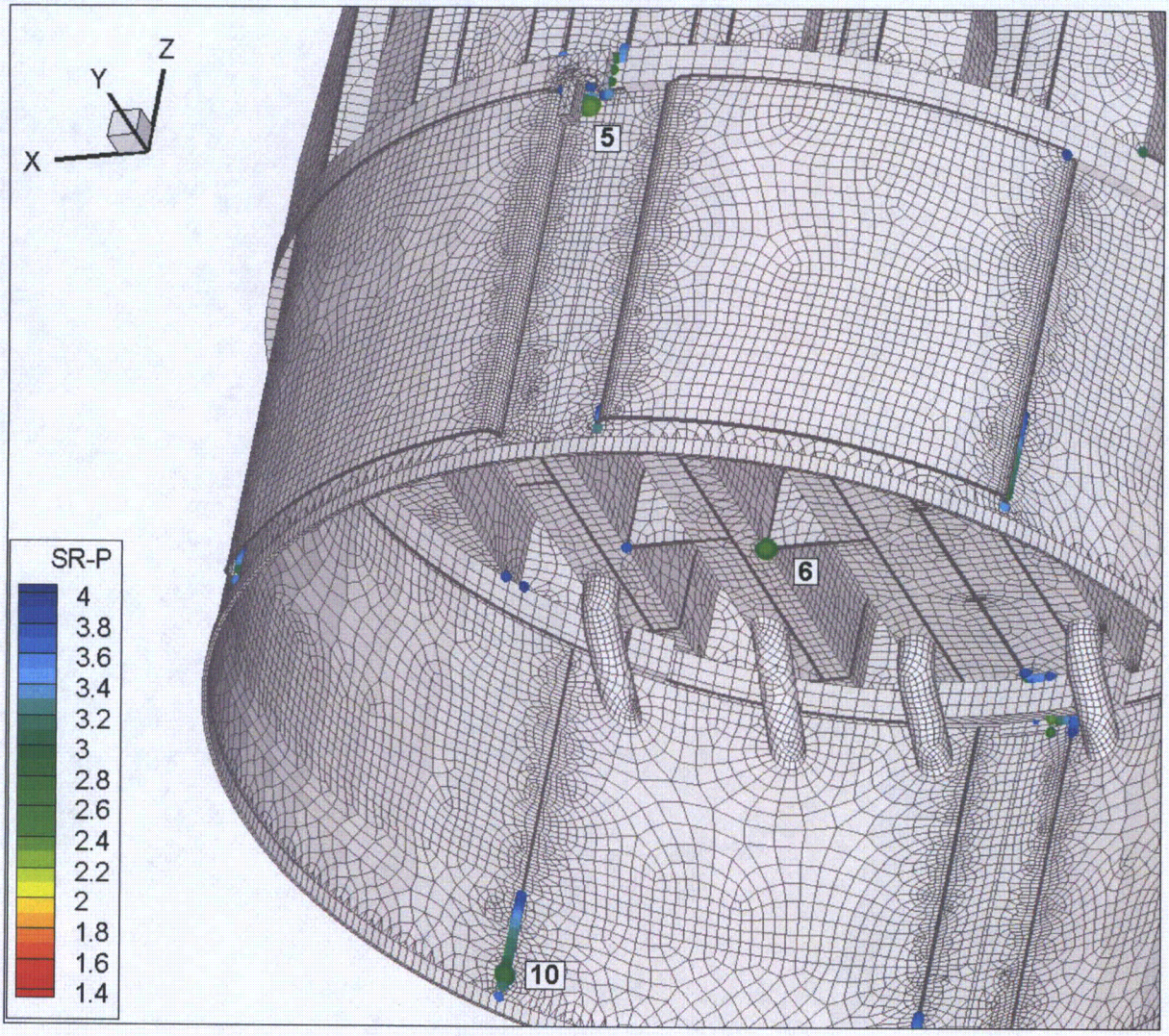

Figure 15f. Locations of smallest maximum stress ratios, SR-P≤4, at welds for nominal EPU operation. Numbers refer to the enumerated locations for SR-P values at welds in Table 9a. Second view showing locations 5, 6 and 10.

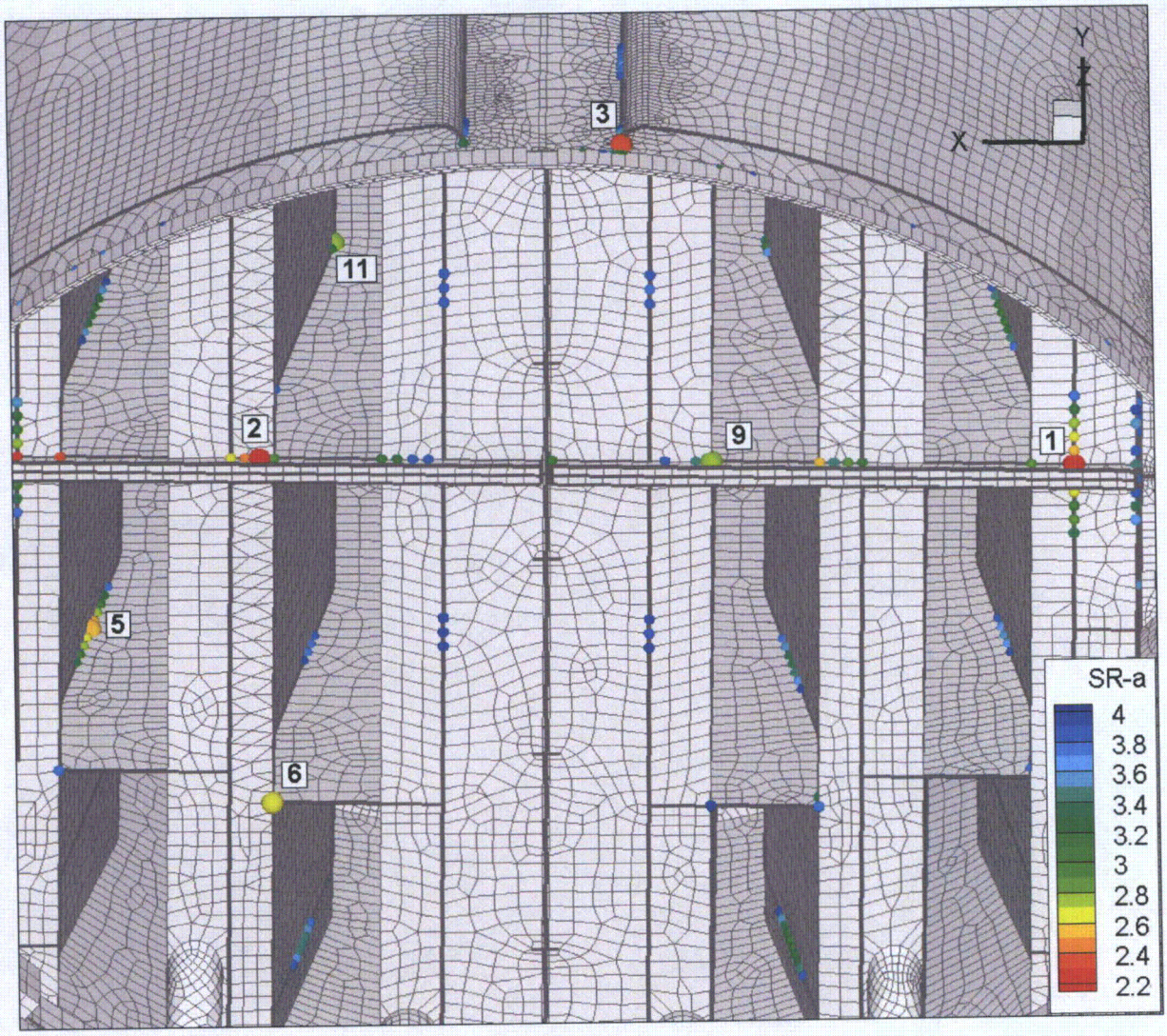

Figure 15g. Locations of minimum alternating stress ratios, SR-a≤4, at welds for nominal EPU operation. Numbers refer to the enumerated locations for SR-a values at welds in Table 9a. First view showing locations 1-3, 5, 6, 9 and 11.

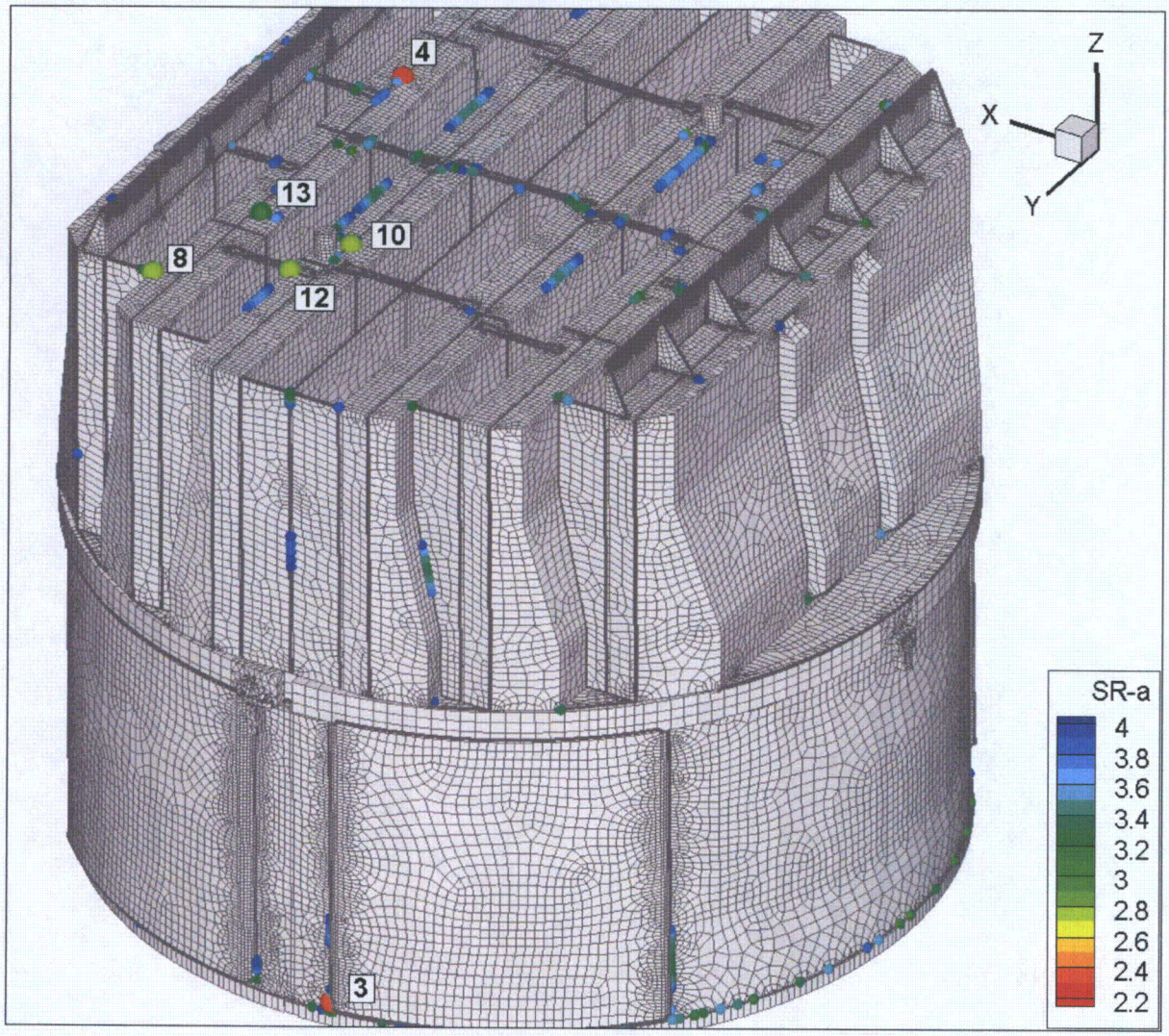

Figure 15h. Locations of minimum alternating stress ratios, SR-a≤4, at welds for nominal EPU operation. Numbers refer to the enumerated locations for SR-a values at welds in Table 9a. Second view showing locations 3, 4, 8, 10, 12 and 13.

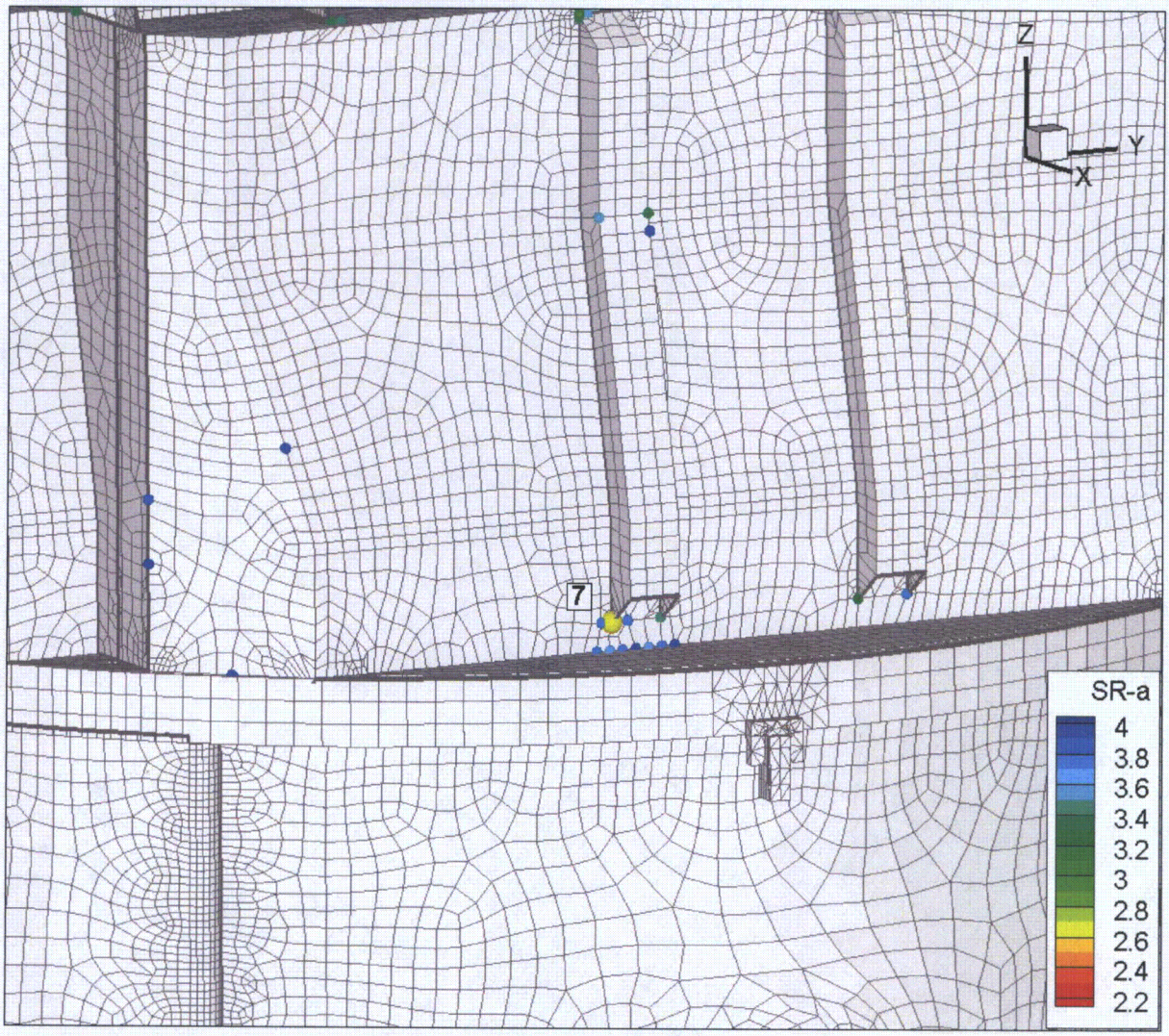

Figure 15i. Locations of minimum alternating stress ratios, SR-a≤4, at welds for nominal EPU operation. Numbers refer to the enumerated locations for SR-a values at welds in Table 9a. Second view showing location 7.

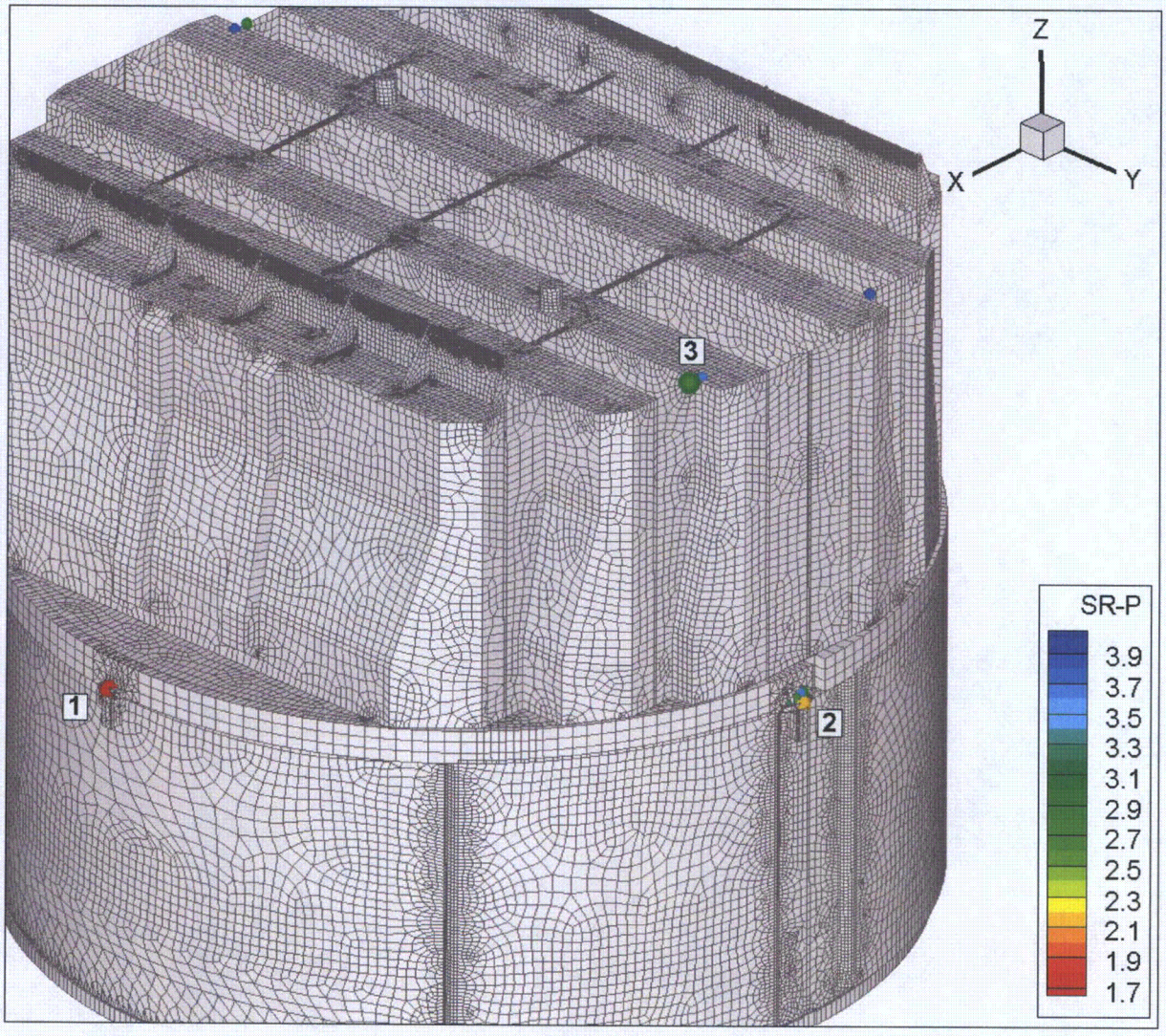

Figure 16a. Locations of minimum stress ratios, SR-P≤4, associated with maximum stress intensities at non-welds for EPU operation with frequency shifts. The recorded stress ratio is the minimum value taken over all frequency shifts. The numbers refers to the enumerated location for SR-P values at non-welds in Table 9b. This view shows locations 1-3.

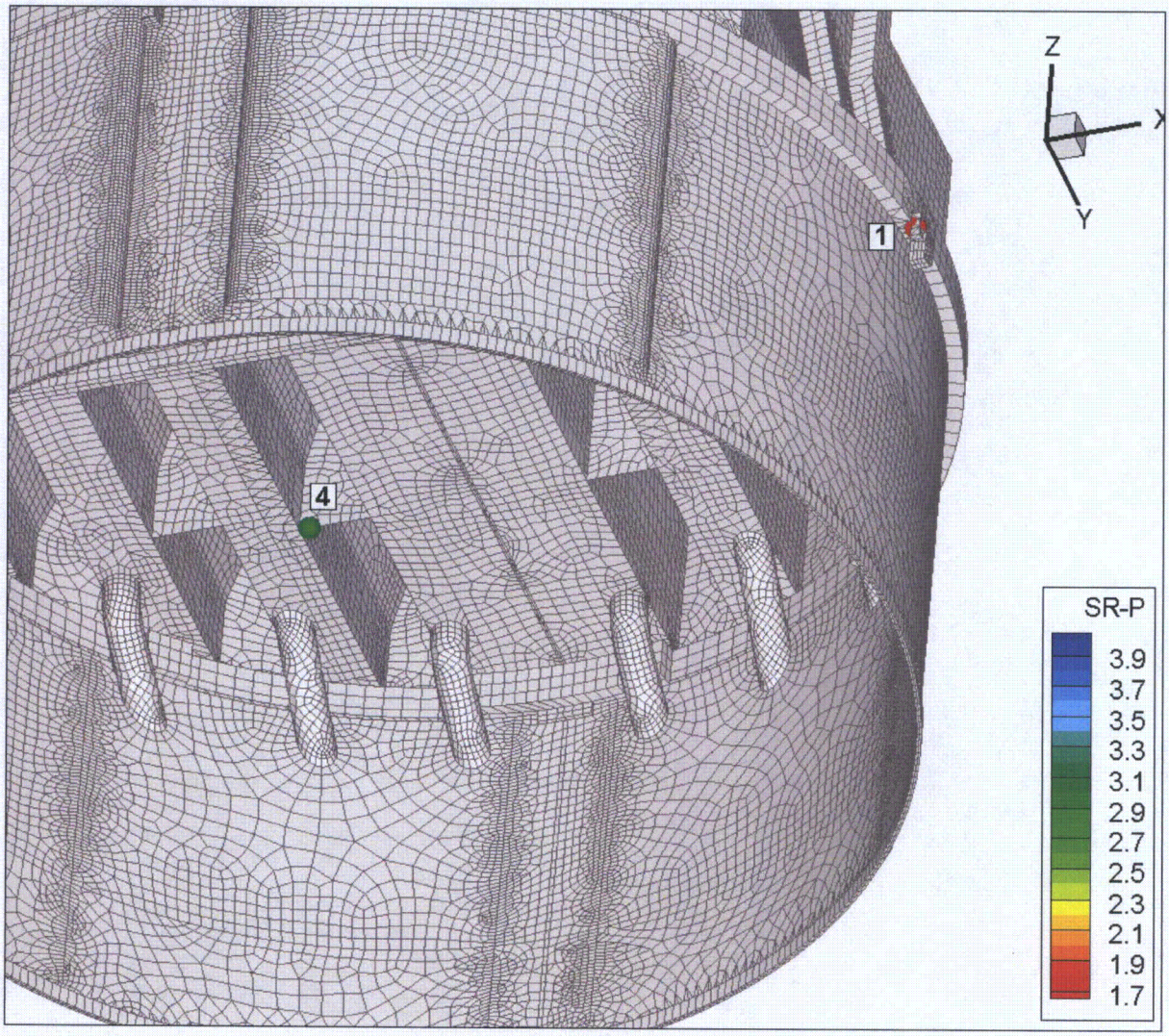

Figure 16b. Locations of minimum stress ratios, SR-P≤4, associated with maximum stress intensities at non-welds for EPU operation with frequency shifts. The recorded stress ratio is the minimum value taken over all frequency shifts. The numbers refers to the enumerated location for SR-P values at non-welds in Table 9b. This view shows locations 1 and 4.

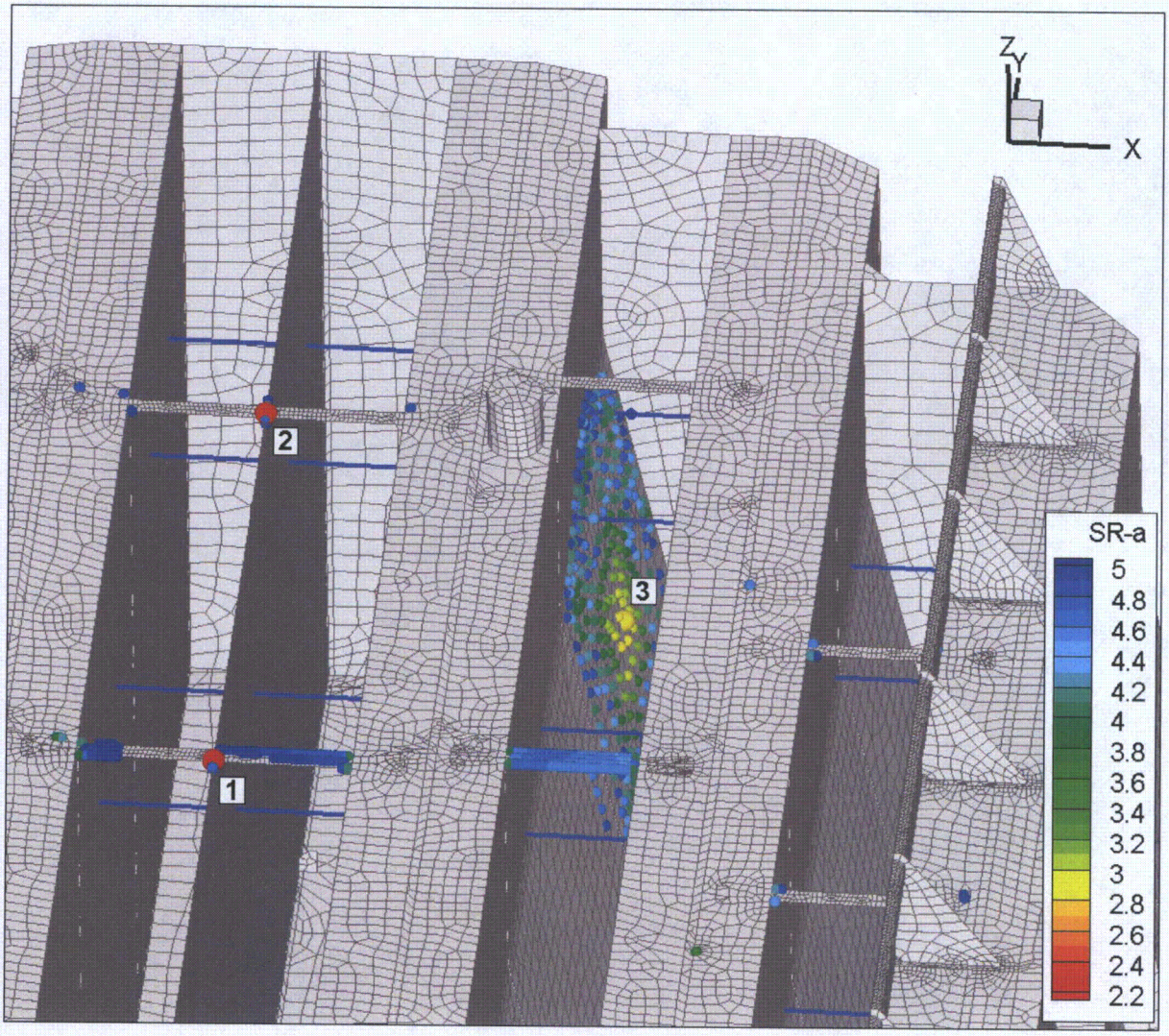

Figure 16c. Locations of minimum alternating stress ratios, SR-a≤5, associated with alternating stress intensities at non-welds for EPU operation with frequency shifts. The recorded stress ratio is the minimum value taken over all frequency shifts. The numbers refers to the enumerated location for SR-a values at non-welds in Table 9b.

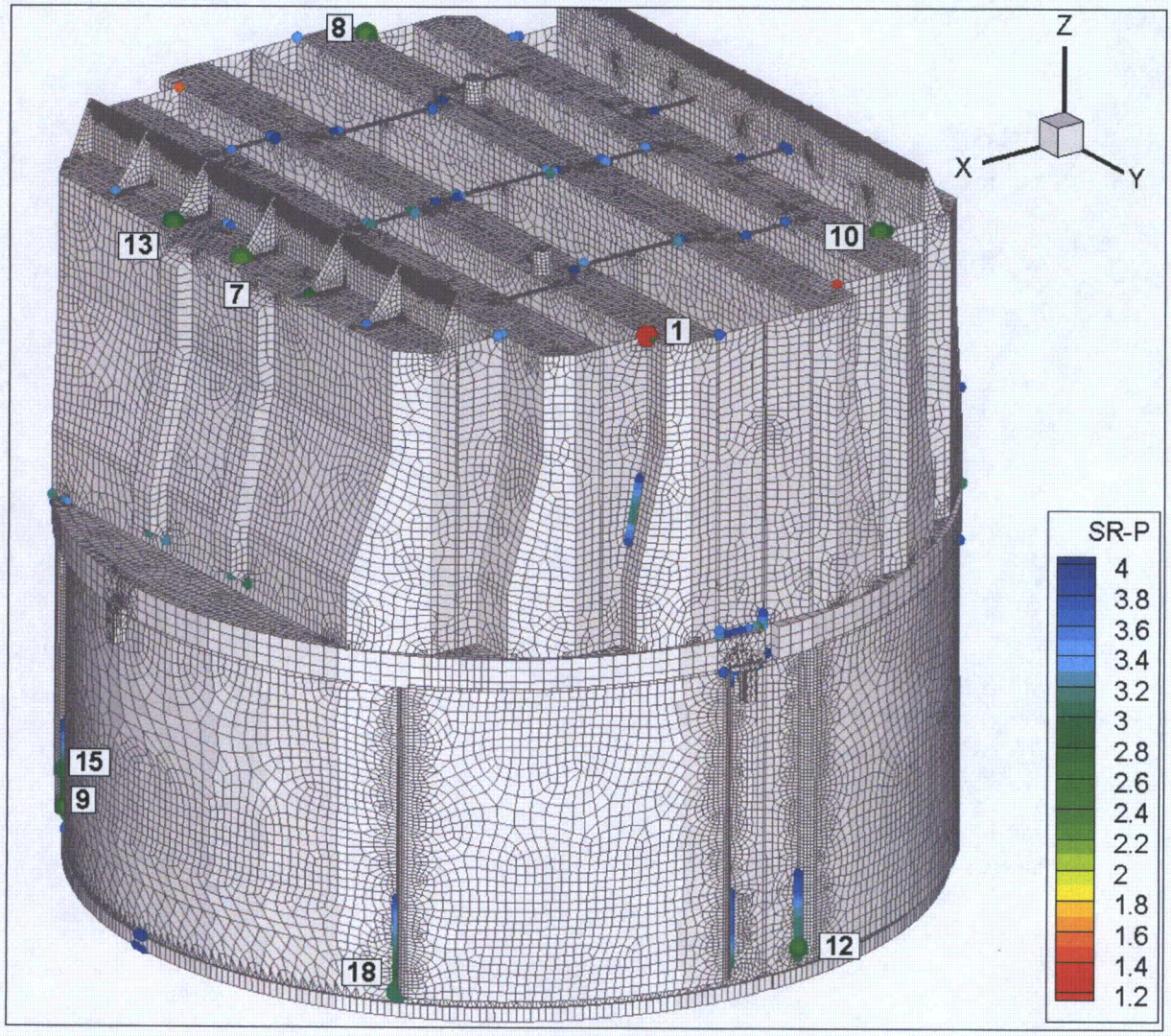

Figure 16d. Locations of minimum stress ratios, SR-P≤4, associated with maximum stress intensities at welds for EPU operation with frequency shifts. The recorded stress ratio at a node is the minimum value taken over all frequency shifts. Numbers refer to the enumerated locations for SR-P values at welds in Table 9b. This view shows locations 1, 7-10, 12, 13, 15 and 18.

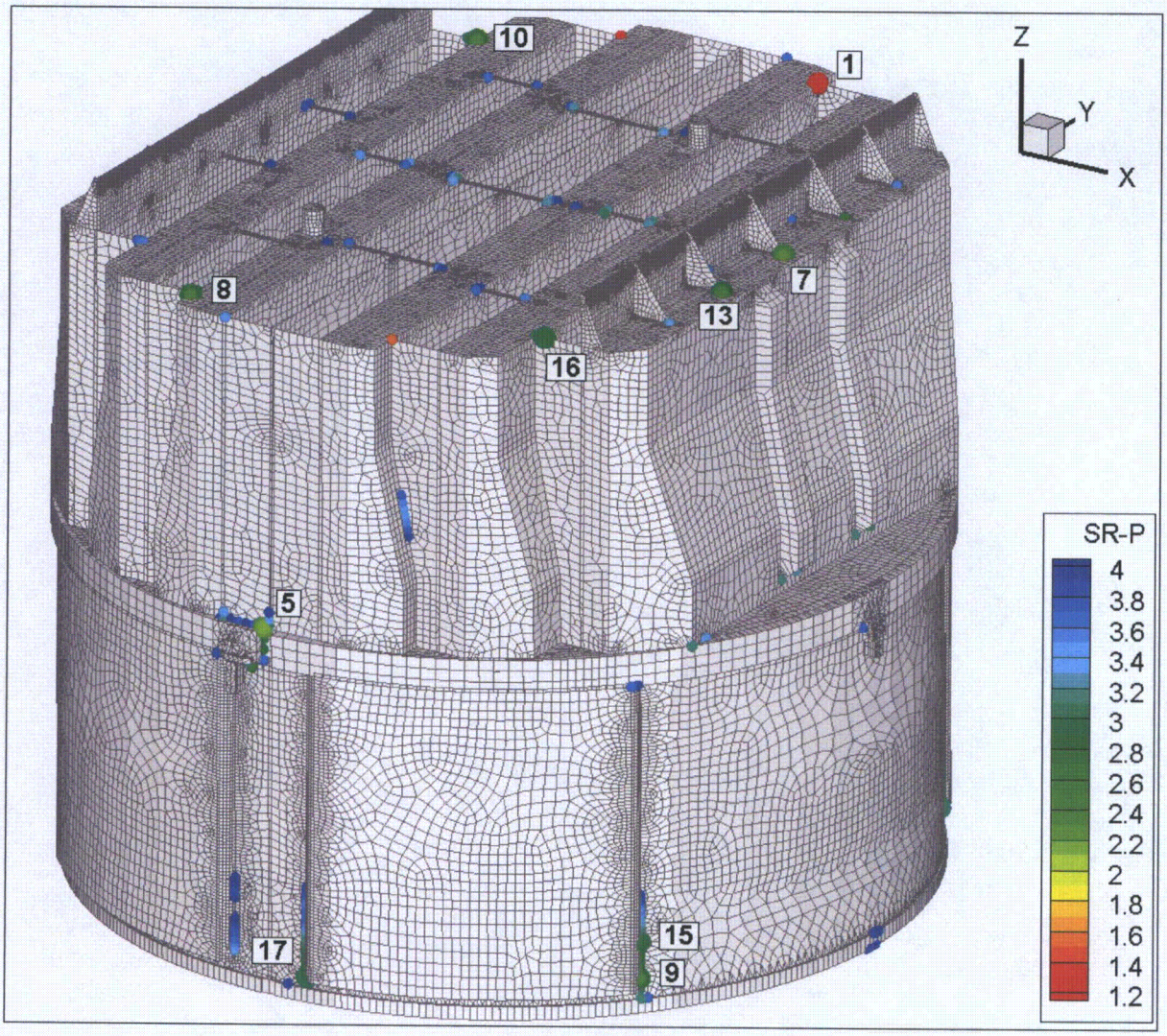

Figure 16e. Locations of minimum stress ratios, SR-P≤4, associated with maximum stress intensities at welds for EPU operation with frequency shifts. The recorded stress ratio at a node is the minimum value taken over all frequency shifts. Numbers refer to the enumerated locations for SR-P values at welds in Table 9b. This view shows locations 1, 5, 7-10, 13 and 15-17.

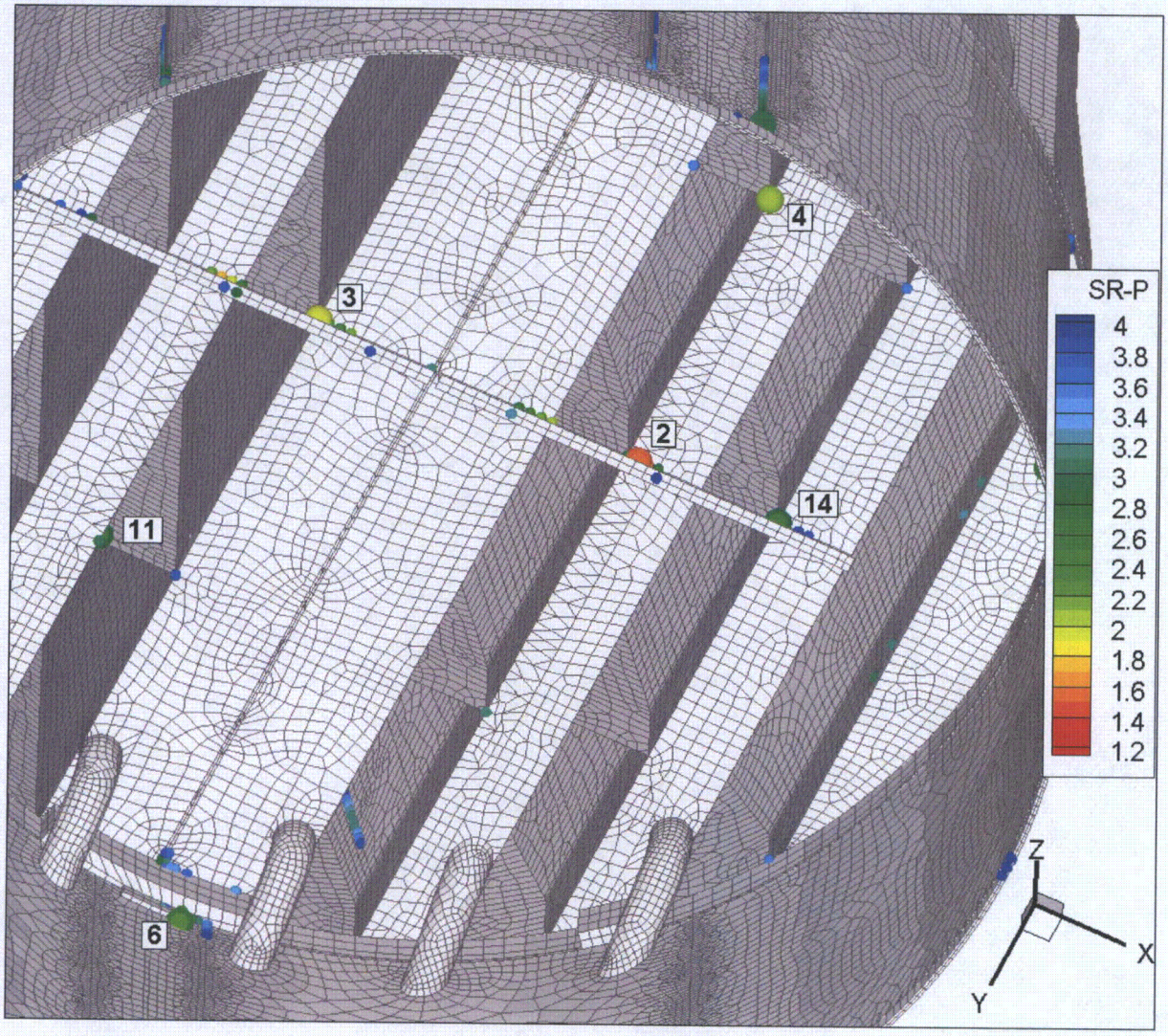

Figure 16f. Locations of minimum stress ratios, SR-P≤4, associated with maximum stress intensities at welds for EPU operation with frequency shifts. The recorded stress ratio at a node is the minimum value taken over all frequency shifts. Numbers refer to the enumerated locations for SR-P values at welds in Table 9b. This view shows locations 2-4, 6, 11 and 14.

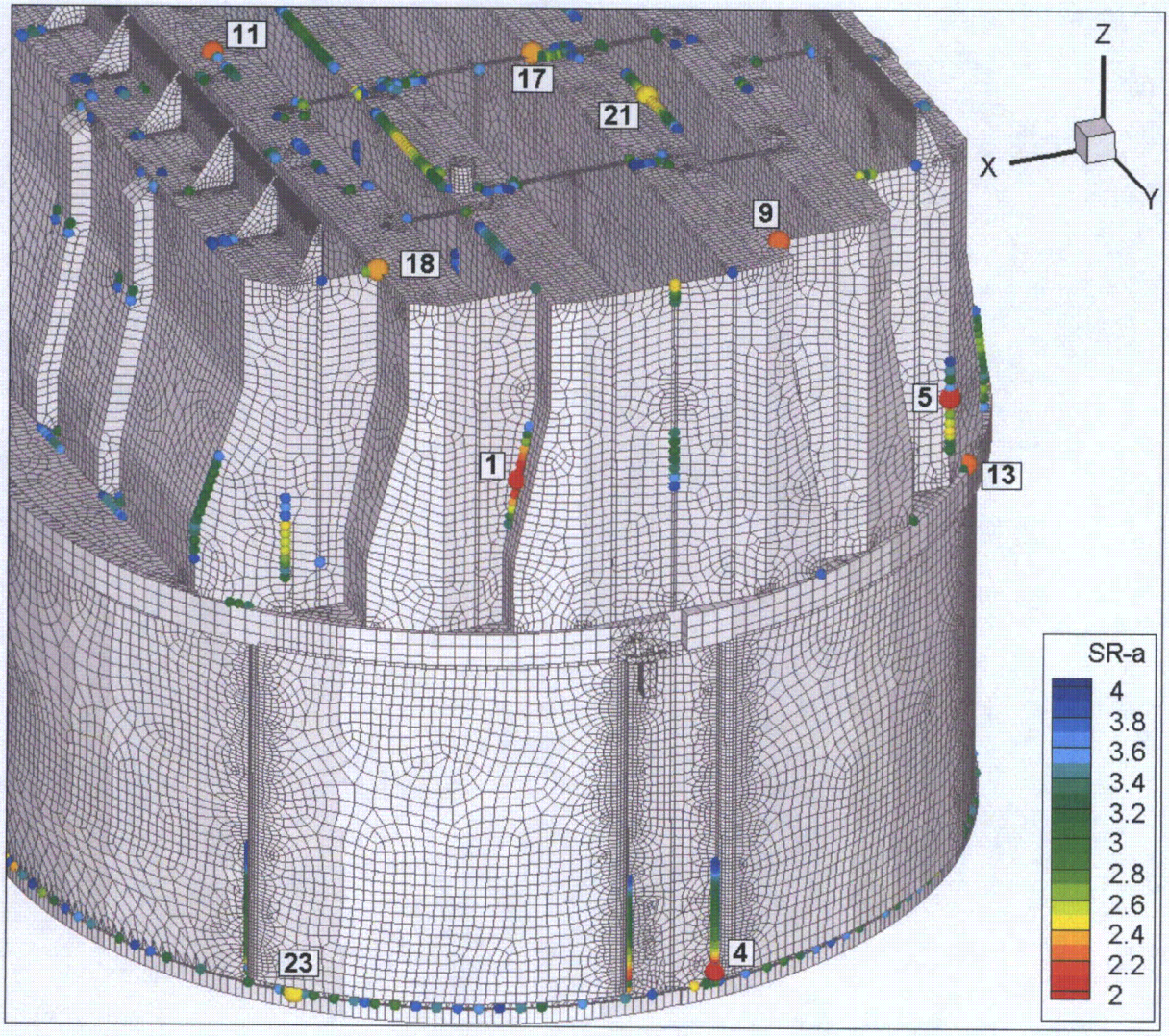

Figure 16g. Locations of minimum alternating stress ratios, SR-a≤4, at welds for EPU operation with frequency shifts. The recorded stress ratio at a node is the minimum value taken over all frequency shifts. Numbers refer to the enumerated locations for SR-a values at welds in Table 9b. This view shows locations 1, 4, 5, 9, 11, 13, 17, 18, 21 and 23.

Note that thinning of the inclined inner panel section outboard of location 1 is planned prior to EPU operation.

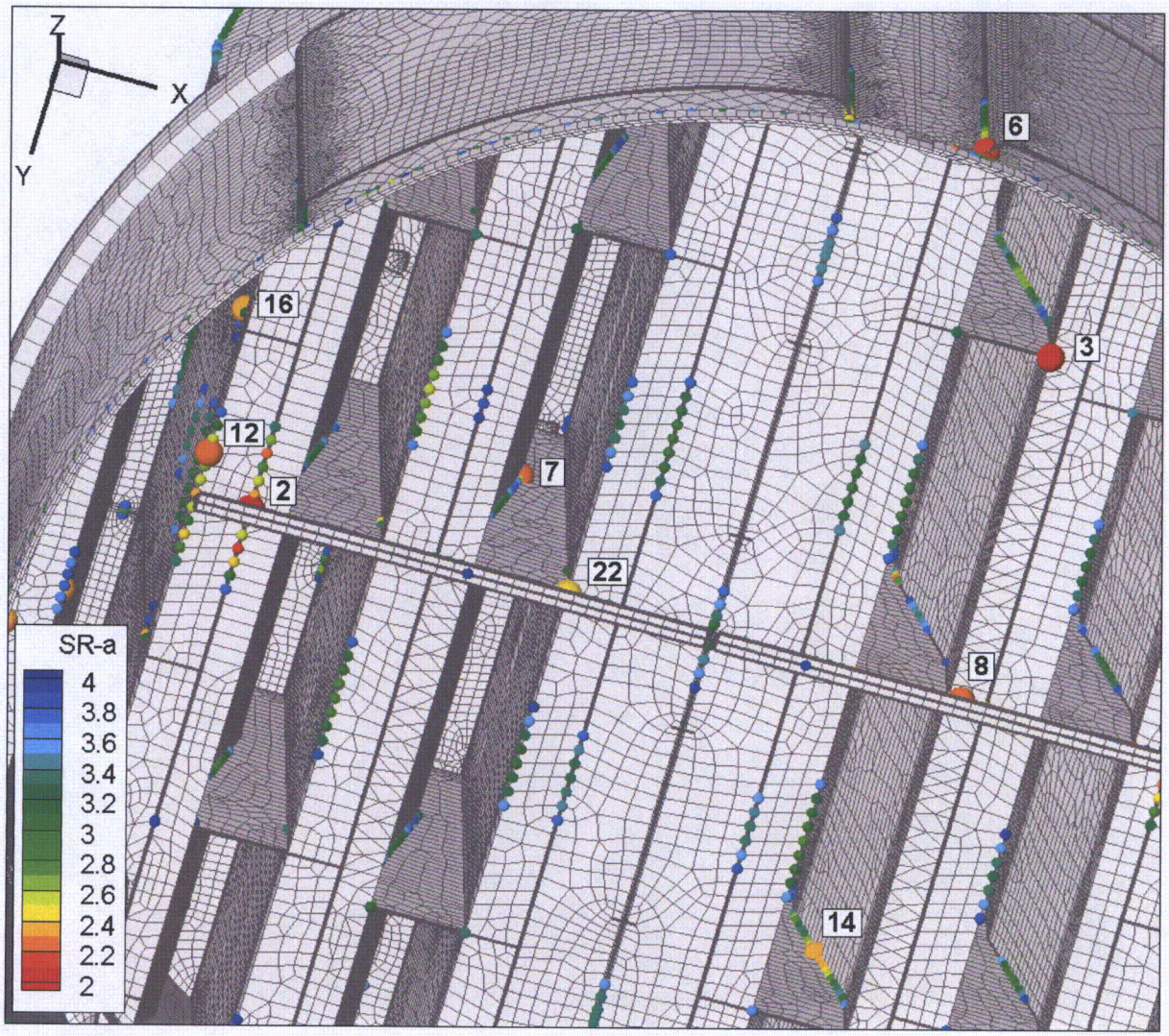

Figure 16h. Locations of minimum alternating stress ratios, SR-a≤4, at welds for EPU operation with frequency shifts. The recorded stress ratio at a node is the minimum value taken over all frequency shifts. Numbers refer to the enumerated locations for SR-a values at welds in Table 9b. This view shows locations 2, 3, 6-8, 12, 14, 16 and 22.

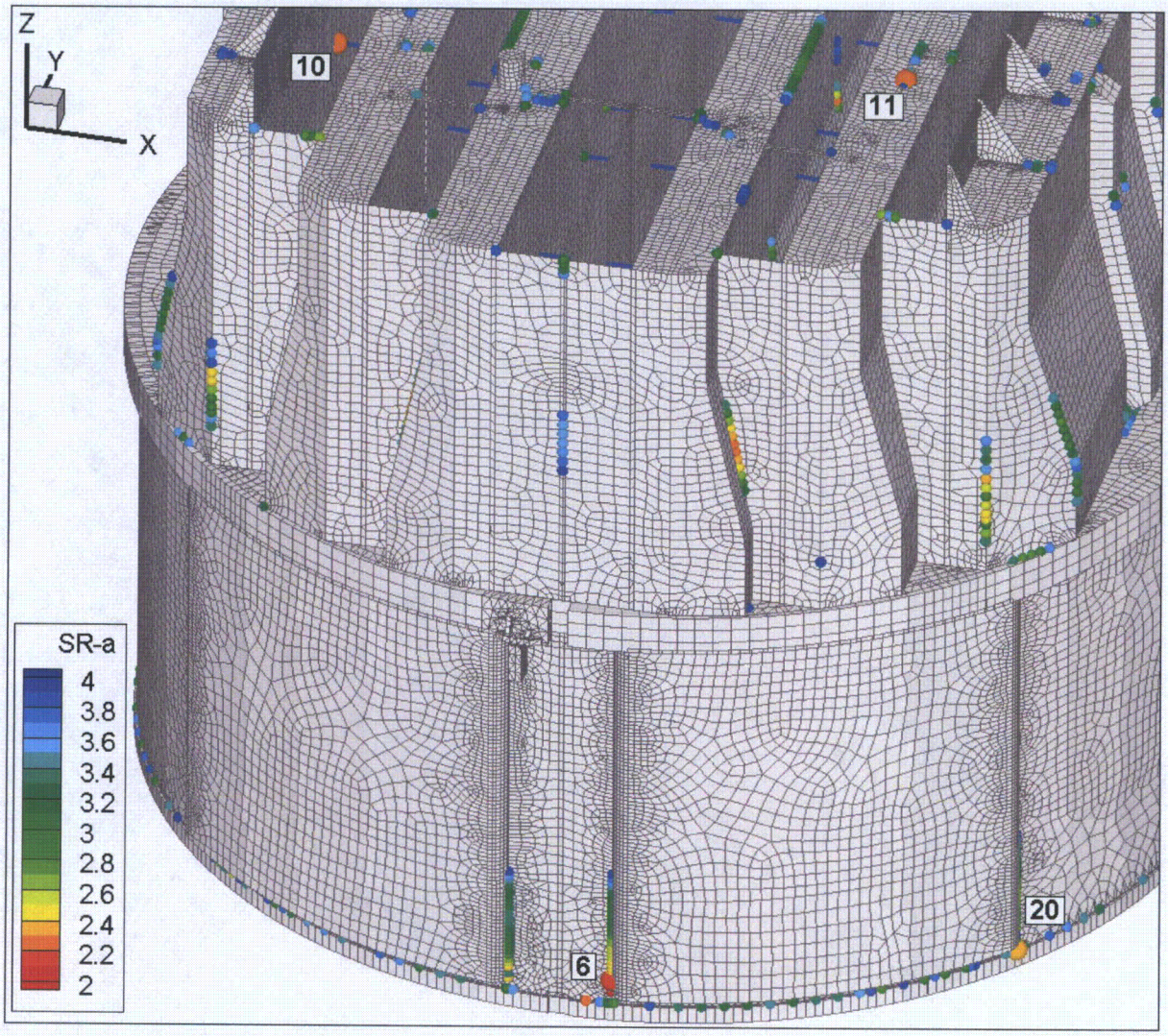

Figure 16i. Locations of minimum alternating stress ratios, SR-a≤4, at welds for EPU operation with frequency shifts. The recorded stress ratio at a node is the minimum value taken over all frequency shifts. Numbers refer to the enumerated locations for SR-a values at welds in Table 9b. This view shows locations 6, 10, 11 and 20.

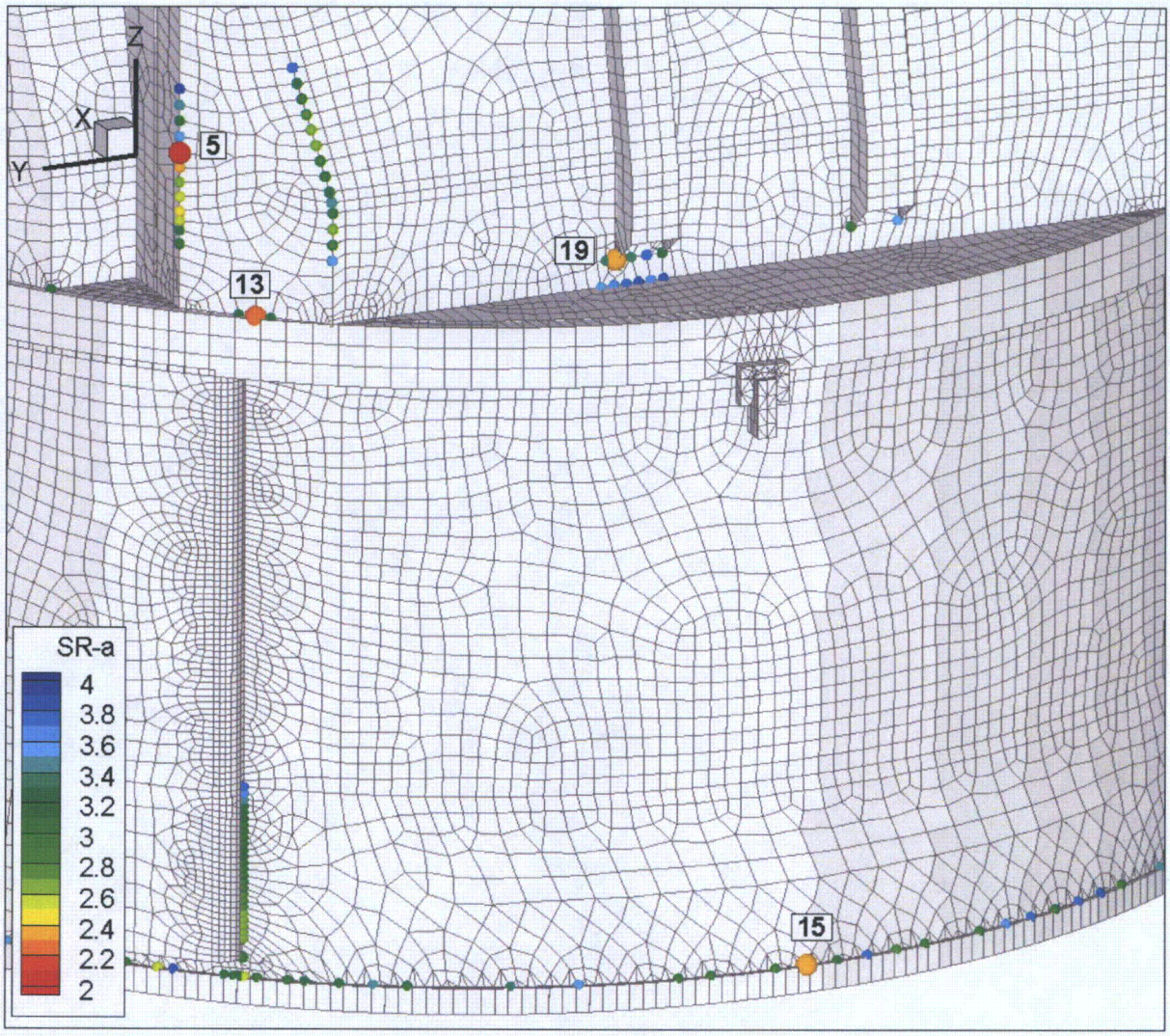

Figure 16j. Locations of minimum alternating stress ratios, SR-a≤4, at welds for EPU operation with frequency shifts. The recorded stress ratio at a node is the minimum value taken over all frequency shifts. Numbers refer to the enumerated locations for SR-a values at welds in Table 9b. This view shows locations 5, 13, 15 and 19.

5.4 Frequency Content

The frequency contribution to the stresses can be investigated by examining the power spectral density (PSD) curves and accumulative PSDs for selected nodes having low alternating stress ratios. The accumulative PSDs are computed directly from the Fourier coefficients as

$$\Sigma(\omega_n) = \sqrt{\sum_{k=1}^{n} |\tilde{\sigma}(\omega_k)|^2}$$

where $\tilde{\sigma}(\omega_k)$ is the complex stress harmonic at frequency, ω_k. Accumulative PSD plots are useful for determining the frequency components and frequency ranges that make the largest contributions to the fluctuating stress. Unlike PSD plots, no "binning" or smoothing of frequency components is needed to obtain smooth curves. Steep step-like rises in $\Sigma(\omega)$ indicate the presence of a strong component at a discrete frequency whereas gradual increases in the curve imply significant content over a broader frequency range. From Parsival's theorem, equality between $\Sigma(\omega_N)$ (where N is the total number of frequency components) and the RMS of the stress signal in the time domain is established.

The selected nodes are the five having the lowest alternating stress ratios (at a weld) in Table 9b. These are:

Node 113478 - located on the inner hood/closure plate weld. The associated PSDs are shown in Figure 17a.
Node 129283 –. located on the common junction between the middle base plate, vane bank and T-bar. The associated PSDs are shown in Figure 17b.
Node 108329 – located on the common junction between the middle base plate, inner hood and hood stiffener. The associated PSDs are shown in Figure 17c.
Node 109919 – located at the bottom of the drain channel/skirt weld. The associated PSDs are shown in Figure 17d.
Node 108484 –. located on the outer vane bank on a weld joining the vane bank plate, bottom perforated plate and end plate. The associated PSDs are shown in Figure 17e.

In each case, since there are six stress components and up to three different section locations for shells (the top, mid and bottom surfaces), there is a total of 18 stress histories per component. Moreover, at junctions there are at least two components that meet at the junction. The particular stress component that is plotted is chosen as follows. First, the component and section location (top/mid/bottom) is taken as the one that has the highest alternating stress. This narrows the selection to six components. Of these, the component having the highest Root Mean Square (RMS) is selected.

For the limiting node the dominant frequency in the stress PSD is 59.35 Hz, which, after compensating for the -2.5% frequency shift, corresponds to 60.9 Hz in the applied signal. The same peak appears in all of the stress PSDs plotted in Figure 17 and is dominant in all but the last node. This frequency lies in the 60-70 Hz range that reflects a high bias and uncertainty relative to the adjacent frequency bands. Note that the frequency lies outside the range (100-120 Hz)

where the loads are increased by bump-up factors. The 59.35 Hz frequency closely matches the natural frequency of a low order mode involving the outermost panel of the inner hood. This appears to explain why this part of the dryer exhibits high stresses. For the last node higher frequency contributions dominate. For node 108239 a significant frequency peak occurs at 49.1 Hz at the +10% frequency shift (44.6 Hz in the unshifted signal).

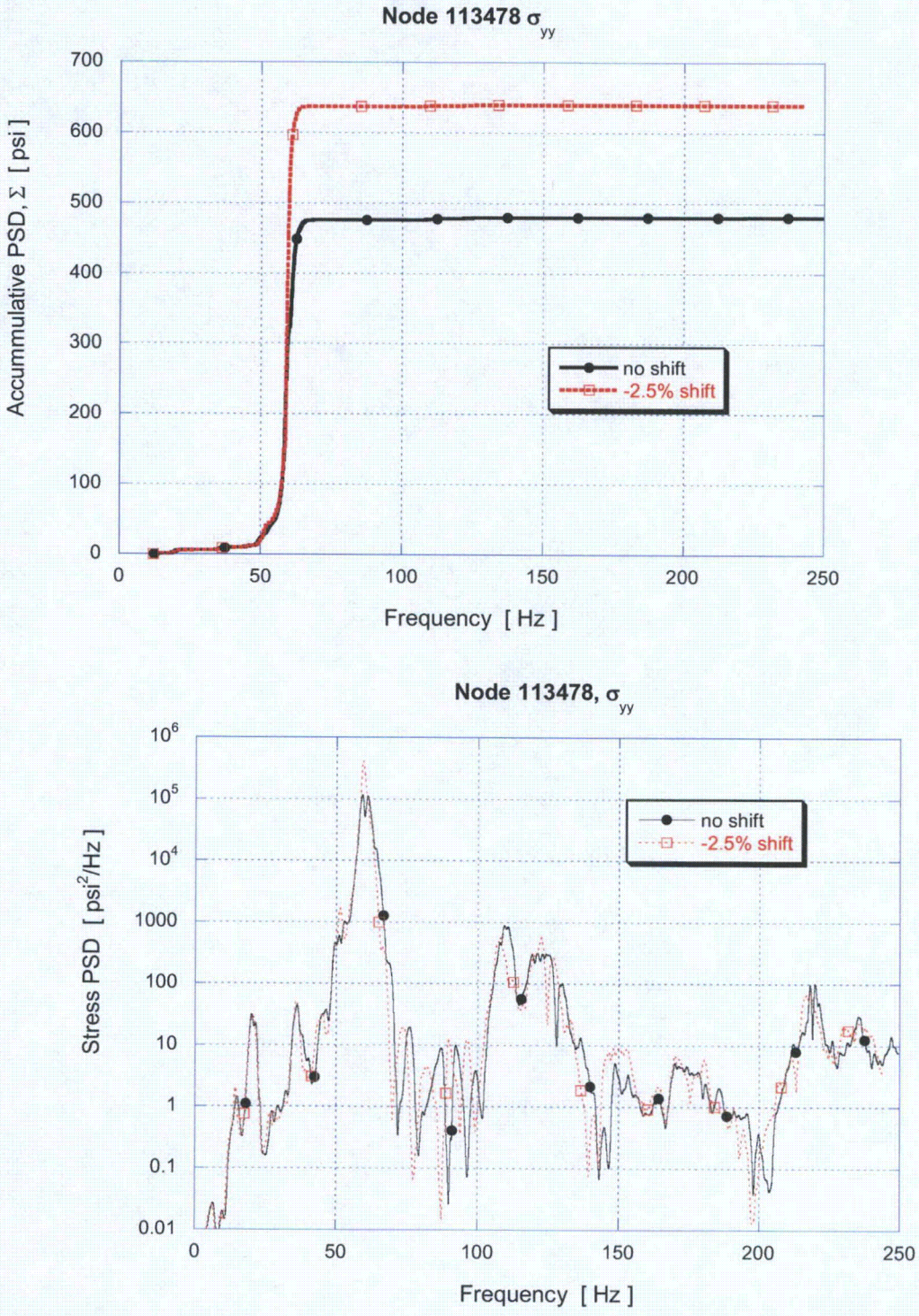

Figure 17a. Accumulative PSD and PSD of the σ_{yy} stress response at node 113478.

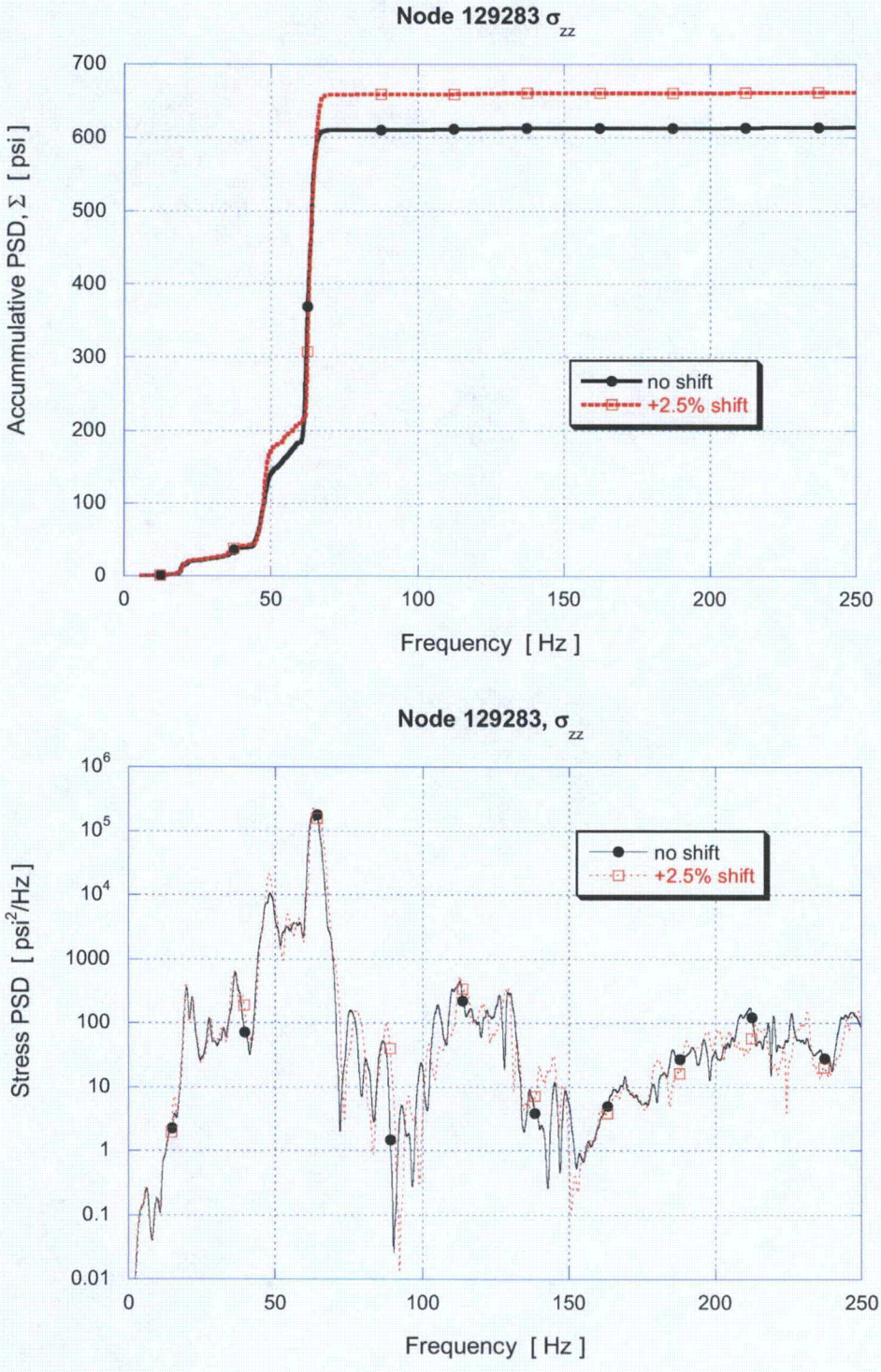

Figure 17b. Accumulative PSD and PSD of the σ_{zz} stress response at node 129283.

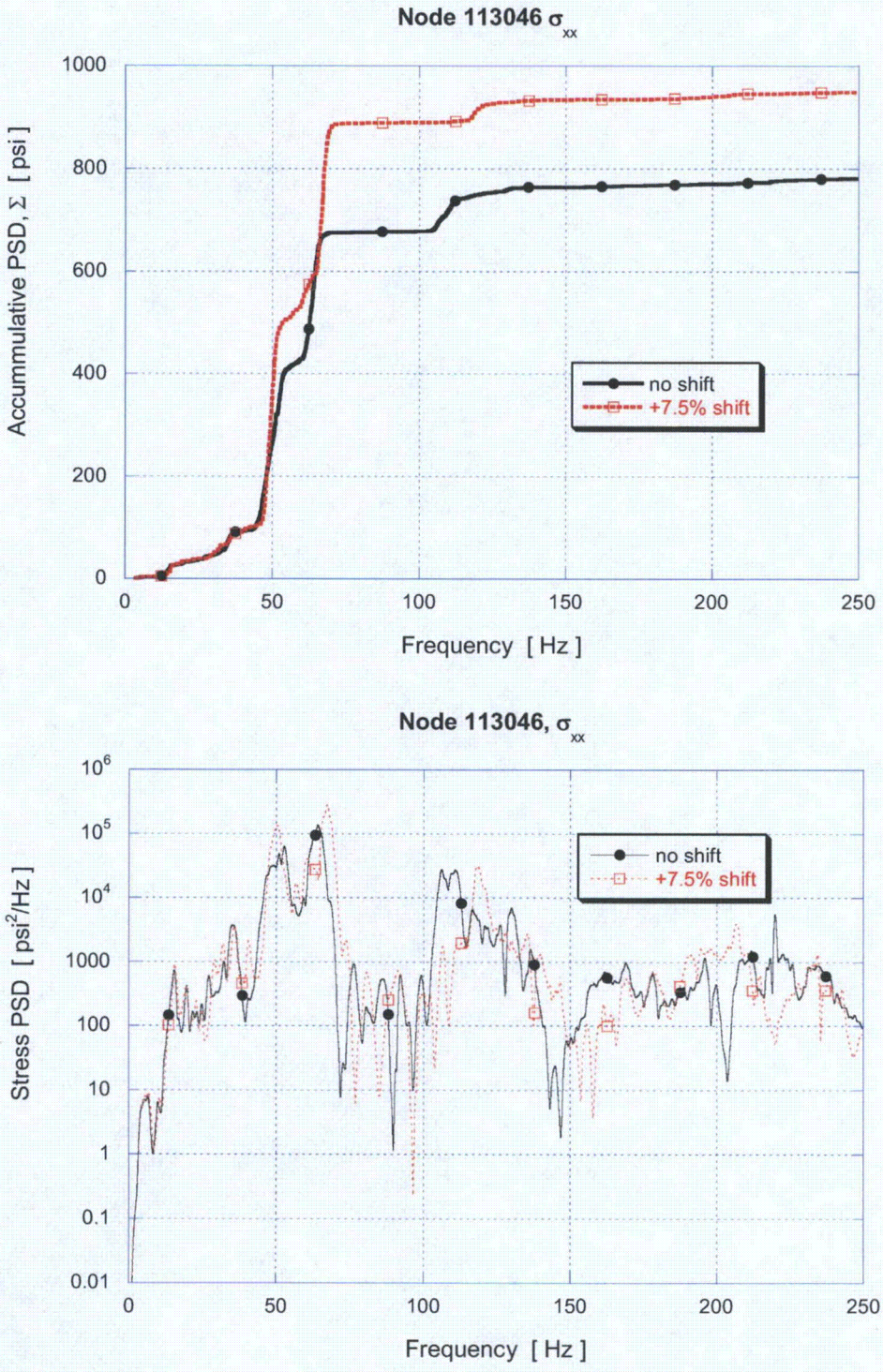

Figure 17c. Accumulative PSD and PSD of the σ_{XX} stress response at node 113046.

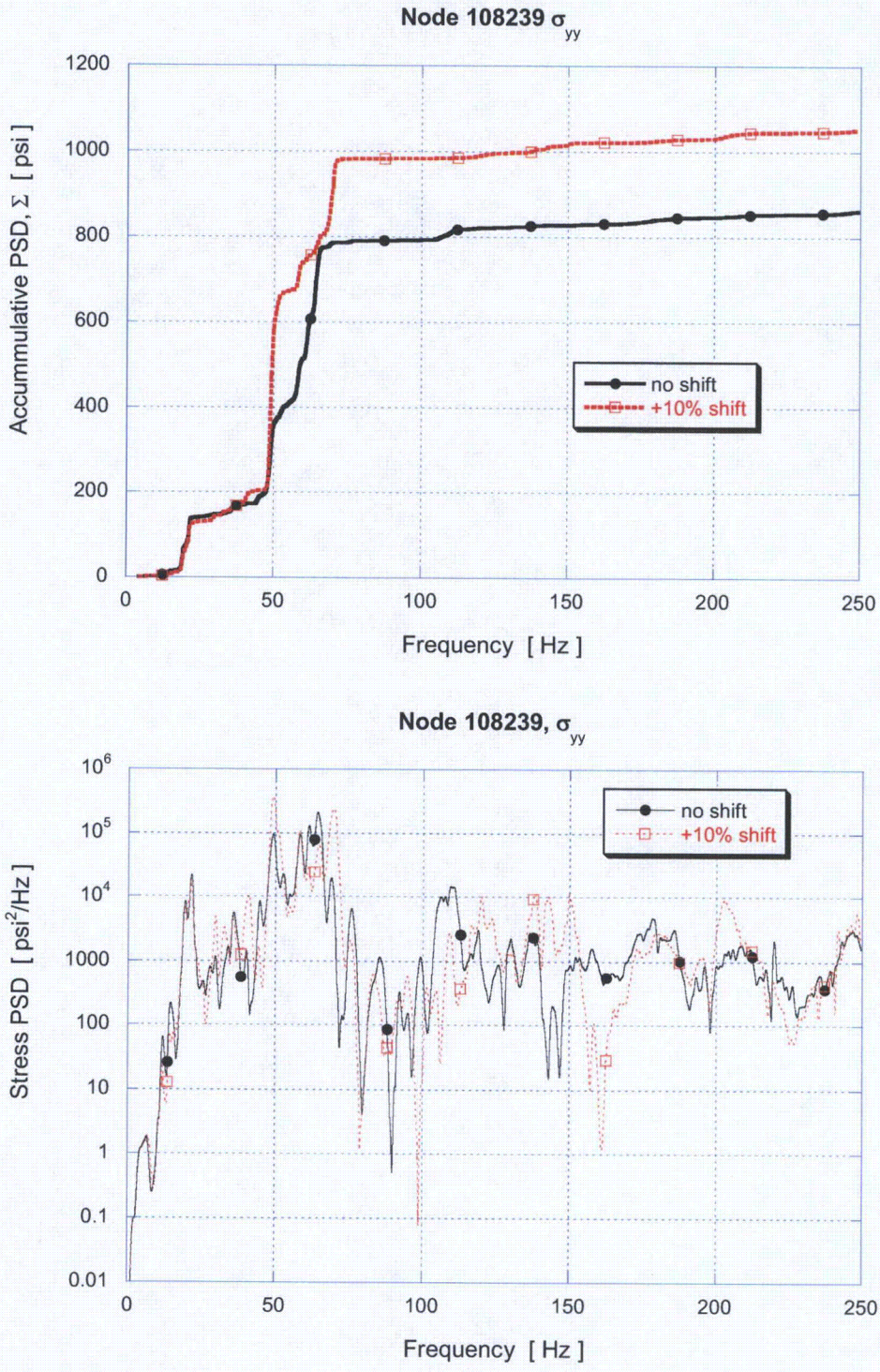

Figure 17d. Accumulative PSD and PSD of the σ_{yy} stress response at node 108329.

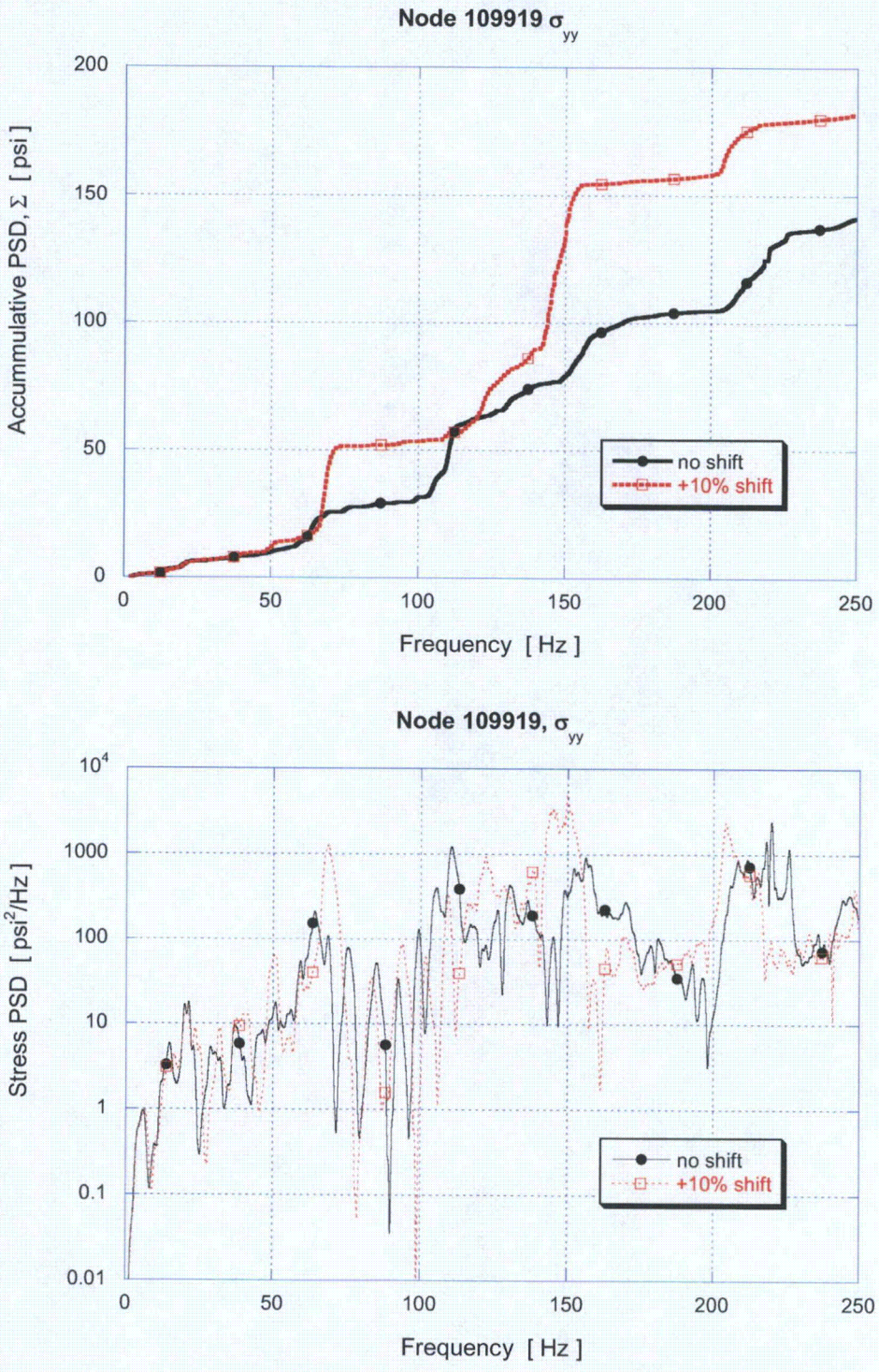

Figure 17e. Accumulative PSD and PSD of the σ_{yy} stress response at node 109919.

6. Conclusions

A frequency-based steam dryer stress analysis has been used to calculate high stress locations and calculated / allowable stress ratios for the Browns Ferry Unit 1 steam dryer at EPU load conditions. A detailed description of the frequency-based methodology and the finite element model for the BFN1 steam dryer is presented. The CLTP loads obtained in a separate acoustic circuit model [2], including end-to-end bias and uncertainty for both the ACM [4] and FEA, were applied to a finite element model of the steam dryer consisting mainly of the ANSYS Shell 63 elements, brick continuum elements, and beam elements. The resulting stress histories were analyzed to obtain maximum and alternating stresses at all nodes for comparison against allowable levels.

For added conservatism, no low power-based signal filtering is attempted in the current analysis. The EPU stresses are estimated using two methods. The first scales the CLTP stresses by the square of the steam flow velocity ratio, $(U_{110}/U_{CLTP})^2=1.35$. At CLTP the limiting alternating stress ratio is SR-a=2.77. Hence, using the first method the limiting alternating stress ratio at EPU is SR-a=2.77/1.35=2.05. The second method utilizes the bump up factors developed in [27] over the 100-120 Hz frequency interval and the velocity scaling (1.35) at all other frequencies. The stress ratios resulting from the application of EPU loads to the steam dryer are tabulated in Table 9 of this report. Using the second method the limiting alternating stress ratio is found to be SR-a=2.03. In both cases the alternating stress ratio remains above 2.0, thus qualifying the steam dryer for EPU operation with regard to stress evaluation.

On the basis of these CLTP plant loads, the dynamic analysis of the steam dryer shows that the combined acoustic, hydrodynamic, and gravity loads produces the following minimum stress ratios (with the T-bar excluded).

Frequency Shift	Minimum Stress Ratio at EPU	
	Max. Stress, SR-P	Alternating Stress, SR-a
0% (nominal)	1.40	2.18
-10%	1.41	2.38
-7.5%	1.39	2.40
-5%	1.37	2.09
-2.5%	1.37	2.03
+2.5%	1.40	2.05
+5%	1.34	2.19
+7.5%	1.27	2.05
+10%	1.31	2.06
All shifts	1.27- 1.41	2.03 – 2.40
Limiting	**1.27**	**2.03**

7. References

1. Continuum Dynamics, Inc. (2005), *Methodology to Determine Unsteady Pressure Loading on Components in Reactor Steam Domes (Rev. 6)*, C.D.I. Report No. 04-09 (Proprietary).
2. Continuum Dynamics, Inc. (2009), *Acoustic and Low Frequency Hydrodynamic Loads at CLTP Power Level to 120% OLTP Power Level on Browns Ferry Nuclear Unit 1 Steam Dryer to 250 Hz, Rev. 0*, C.D.I. Report No. 09-23P (Proprietary).
3. *ASME Boiler and Pressure Vessel Code, Section III, Subsection NG (2007).*
4. Continuum Dynamics, Inc. (2007), *Methodology to Predict Full Scale Steam Dryer Loads from In-Plant Measurements, with the Inclusion of a Low Frequency Hydrodynamic Contribution*, C.D.I. Report No. 07-09P (Proprietary).
5. Continuum Dynamics, Inc. (2009), *Stress Assessment of Browns Ferry Nuclear Unit 1 Steam Dryer with Tie-Bar Modifications, Rev. 3*, C.D.I. Report No. 08-15P (Proprietary), March.
6. Structural Integrity Associates, Inc. (2008), *Main Steam Line 100% CLTP Strain Data Transmission*, Email from R. Horvath dated 06-03-2008 and data supplied from ibackup.com.
7. ANSYS URL: http://www.ansys.com, *ANSYS Release 10.0 Complete User's Manual Set.*
8. Continuum Dynamics, Inc. (2007), *Response to NRC Request for Additional Information on the Hope Creek Generating Station, Extended Power Uprate*, RAI No. 14.110.
9. Continuum Dynamics, Inc. (2008), *Stress Assessment of Browns Ferry Nuclear Unit 1 Steam Dryer, Rev. 0*, C.D.I. Report No. 08-06P (Proprietary).
10. Press, W.H., et al., *Numerical Recipes*. 2 ed. 1992: Cambridge University Press.
11. O'Donnell, W.J., *Effective Elastic Constants For the Bending of Thin Perforated Plates With Triangular and Square Penetration Patterns.* ASME Journal of Engineering for Industry, 1973. **95**: p. 121-128.
12. de Santo, D.F., *Added Mass and Hydrodynamic Damping of Perforated Plates Vibrating In Water.* Journal of Pressure Vessel Technology, 1981. **103**: p. 175-182.
13. Idel'chik, I E. and E. Fried, *Flow Resistance, a Design Guide for Engineers*. 1989, Washington D.C.: Taylor & Francis. pg. 260.
14. Continuum Dynamics, Inc. (2007), *Dynamics of BWR Steam Dryer Components*, C.D.I. Report No. 07-11P.
15. U.S. Nuclear Regulatory Commission (2007), *Comprehensive Vibration Assessment Program for Reactor Internals During Preoperational and Initial Startup Testing*, Regulatory Guide 1.20, March.
16. Weld Research Council (1998), *Fatigue Strength Reduction and Stress Concentration Factors For Welds In Pressure Vessels and Piping*, WRC Bulletin 432.
17. Pilkey, W.D., *Peterson's Stress Concentration Factors, 2nd ed.* 1997, New York: John Wiley. pg. 139.
18. Lawrence, F.V., N.-J. Ho, and P.K. Mazumdar, *Predicting the Fatigue Resistance of Welds.* Ann. Rev. Mater. Sci., 1981. **11**: p. 401-425.
19. General Electric (GE) Nuclear Energy, *Supplement 1 to Service Information Letter (SIL) 644, "BWR/3 Steam Dryer Failure," September 5*. 2003.
20. Tecplot, Inc. (2004), URL: http://www.tecplot.com, *Documentation: Tecplot User's Manual Version 10 Tecplot, Inc.*, October.

21. Structural Integrity Associates, Inc. (2008), *Shell and Solid Sub-Model Finite Element Stress Comparison, Rev. 2*, Calculation Package, 0006982.301, Oct. 17.
22. Continuum Dynamics, Inc. (2008), *Stress Assessment of Browns Ferry Nuclear Unit 2 Steam Dryer with Outer Hood and Tie-Bar Reinforcements, Rev. 0*, C.D.I. Report No. 08-20P (Proprietary).
23. Structural Integrity Associates, Inc. (2009), *Comparison Study of Substructure and Submodel Analysis using ANSYS*, Calculation Package, 0006982.304, Rev. 2, January 8.
24. Continuum Dynamics, Inc. (2009), *Response to NRC Round 23 RAI EMCB 201/162 part c*, January.
25. Structural Integrity Associates, Inc. (2009), *Steam Dryer Hood Stiffener Stress Relief Modification Stress Reduction Factor (SRF) Computation*, SIA Calculation Package 0900833.302, Revision 0, August 19.
26. Structural Integrity Associates, Inc. (2008), *Comparison Study of Substructure and Submodel Analysis using ANSYS*, Calculation Package, 0006982.304, December.
27. Continuum Dynamics, Inc. (2008), *Flow-Induced Vibration in the Main Steam Lines at Browns Ferry Nuclear Units 1 and 2, With and Without Acoustic Side Branches, and Resulting Steam Dryer Loads*, C.D.I. Report No. 08-14P (Proprietary).
28. Continuum Dynamics, Inc. (2009), *Part Retention Analysis of T-Bar in the BFN1 Steam Dryer*, Letter Transmittal to TVA dated 03-10-2009.